...ct Engineering

Journal of Research

of the

National Bureau of Standards

DECEMBER 1953

VOLUME 51 NUMBER 6

U. S. DEPARTMENT OF COMMERCE
Sinclair Weeks, Secretary
NATIONAL BUREAU OF STANDARDS
A. V. Astin, Director

DECEMBER • 1953
VOLUME • 51
NUMBER • 6

JOURNAL OF RESEARCH

of the

NATIONAL BUREAU OF STANDARDS

PERIODICALS OF THE NATIONAL BUREAU OF STANDARDS

The National Bureau of Standards is engaged in fundamental and applied research in physics, chemistry, mathematics, and engineering. Projects are conducted in thirteen fields: electricity, optics and metrology, heat and power, atomic and radiation physics, chemistry, mechanics, organic and fibrous materials, metallurgy, mineral products, building technology, applied mathematics, electronics, and radio propagation. The Bureau has custody of the national standards of measurement and conducts research leading to the improvement of scientific and engineering standards and of techniques and methods of measurement. Testing methods and instruments are developed; physical constants and properties of materials are determined; and technical processes are investigated.

JOURNAL OF RESEARCH

Internationally known as a leading scientific periodical, the Journal presents research papers by authorities in the specialized fields of physics, mathematics, chemistry, and engineering. Complete details of the work are presented, including laboratory data, experimental procedures, and theoretical and mathematical analyses. Annual subscription: domestic, $5.50; foreign, $6.75.

TECHNICAL NEWS BULLETIN

Summaries of current research at the National Bureau of Standards are published each month in the Technical News Bulletin. The articles are brief, with emphasis on the results of research, chosen on the basis of their scientific or technologic importance. Lists of all Bureau publications during the preceding month are given, including Research Papers, Handbooks, Applied Mathematics Series, Building Materials and Structures Reports, and Circulars. Each issue contains 12 or more two-column pages; illustrated. Annual subscription: domestic, $1.00; foreign, $1.35.

BASIC RADIO PROPAGATION PREDICTIONS

The Predictions provide the information necessary for calculating the best frequencies for communication between any two points in the world at any time during the given month. The data are important to all users of long-range radio communications and navigation, including broadcasting, airline, steamship, and wireless services, as well as to investigators of radio propagation and ionosphere. Each issue, covering a period of one month, is released three months in advance and contains 16 large pages, including pertinent charts, drawings, and tables. Annual subscription: domestic, $1.00; foreign, $1.25.

Order all publications from the Superintendent of Documents
U. S. Government Printing Office, Washington 25, D. C.

The printing of this publication has been approved by the Director of the Bureau of the Budget, May 12, 1952.

Journal of Research of the National Bureau of Standards Vol. 51, No. 6, December 1953 Research Paper 2458

Preparation of D-Arabinose-1-C^{14} and D-Ribose-1-C^{14} [1]

Harriet L. Frush and Horace S. Isbell

By application of the cyanohydrin synthesis to D-erythrose, D-arabinose-1-C^{14} and D-ribose-1-C^{14} have been prepared in overall radiochemical yields of 30 and 8.5 percent, respectively. General acid catalysts in the cyanohydrin reaction appear to favor formation of the arabonic epimer. The epimeric acids resulting from the reaction of labeled cyanide and D-erythrose, and subsequent hydrolysis, were separated as crystalline potassium D-arabonate-1-C^{14} and cadmium D-ribonate-1-C^{14}, respectively. The salts were converted to the corresponding lactones, and these were reduced to the sugars by use of sodium amalgam in the presence of sodium acid oxalate.

1. Introduction

As part of a program to make position-labeled sugars available for research workers in other laboratories, methods have been developed at the National Bureau of Standards for the preparation of D-glucose-1-C^{14}, D-mannose-1-C^{14}, D-mannitol-1-C^{14}, D-fructose-1,6-C^{14}, lactose-1-C^{14}, and D-arabinose-5-C^{14} [1, 2, 3, 4, 5, 6].[2] The present report gives methods for the preparation of D-arabinose-1-C^{14} and D-ribose-1-C^{14}. D-Arabinose-1-C^{14} was required as an intermediate in the preparation of D-glucose-2-C^{14}, and both D-arabinose-1-C^{14} and D-ribose-1-C^{14} were needed for studies of the transformation of pentoses in biological systems. Rappoport and Hassid [7] obtained L-arabinose-1-C^{14} by application of the Sowden-Fischer nitromethane synthesis [8] to L-erythrose. The L-arabinose-1-C^{14} was separated in 3-percent yield by partition chromatography.

In light of prior work at the Bureau, it seemed desirable to attempt the synthesis of both D-arabinose-1-C^{14} and D-ribose-1-C^{14} by the cyanohydrin method, beginning with D-erythrose. It was found that in the reaction of cyanide with D-erythrose the presence of a general acid catalyst, such as bicarbonate or ammonium ion, favors formation of the arabonic epimer. The epimeric products of reaction were separated by the following steps: (1) Hydrolysis of the nitriles with aqueous sodium carbonate, (2) passage of the solution over a cation exchange resin to give the free acids, (3) neutralization of the acids with potassium hydroxide, and separation of labeled D-arabonic acid as crystalline potassium D-arabonate, (4) conversion of the potassium salts in the mother liquor to cadmium salts by passage of the solution over a cation exchange resin, and neutralization of the acid with cadmium hydroxide, and (5) separation of the labeled D-ribonic acid in the form of crystalline cadmium D-ribonate.

This procedure gave labeled potassium D-arabonate and cadmium D-ribonate in radiochemical yields of 50 and 23 percent, respectively. The potassium D-arabonate-1-C^{14} was converted to D-arabono-γ-lactone-1-C^{14}, and this was reduced with sodium amalgam in the presence of sodium acid oxalate.[3] A 56-percent yield of the crystalline D-arabinose-1-C^{14} was separated without carrier; by use of carrier, the radiochemical yield was increased to 60 percent. As potassium D-arabonate-1-C^{14} was produced in 50-percent yield, the over-all radiochemical yield of D-arabinose-1-C^{14} was 30 percent, based on the cyanide originally used.

The cadmium D-ribonate-1-C^{14}, prepared from the mother liquors of the potassium D-arabonate-1-C^{14}, was converted to D-ribono-γ-lactone-1-C^{14}, which was brought to crystallization by nucleation.[4] The lactone was reduced with sodium amalgam and gave D-ribose-1-C^{14} in 37-percent yield. Inasmuch as 23 percent of the activity of the cyanide had been obtained as cadmium D-ribonate-1-C^{14}, the over-all radiochemical yield of D-ribose-1-C^{14} was 8.5 percent. Work still in progress will undoubtedly raise the yields of both cadmium D-ribonate and D-ribose-1-C^{14}.

2. Experimental Procedures

2.1 Preparation of D-Erythrose

For the preparation of sirupy D-erythrose, Sowden's method of periodate oxidation of a 4,6-substituted glucose [9] was applied to 4,6-ethylidene-D-glucose essentially as described by Rappoport and Hassid [7], but with certain convenient modifications. A mixture of 5.64 g of 4,6-ethylidene-D-glucose, mp 180° to 181° C [10] and 4.6 g of sodium bicarbonate was dissolved in an ice-cold solution containing 11.7 g of sodium metaperiodate in 150 ml of water. The solution was kept in an ice bath for a few minutes, and finally at room temperature for 2.5 hr; it was then freeze-dried. The fluffy residue was extracted with a total of 150 ml of hot ethyl acetate in 3 portions. The extract was filtered through a bed of decolorizing

[1] The work described in this paper was sponsored by the Atomic Energy Commission, given in AEC Report NBS-2309.

[2] Figures in brackets indicate the literature references at the end of this paper.

[3] In previous work at the Bureau, an equimolecular mixture of sodium oxalate and oxalic acid was used as an internal neutralizing agent. Crystalline sodium acid oxalate is a more convenient reagent, and is readily prepared, although apparently not commercially available. Use of the acid salt has resulted in somewhat higher yields of the sugar, possibly through closer pH control.

[4] We are indebted to N. K. Richtmyer, of the National Institutes of Health, for seed crystals of D-ribono-γ-lactone.

carbon and diatomaceous earth, and the solvent was removed by distillation under reduced pressure. The residue, amorphous 2,4-ethylidene-D-erythrose, was hydrolyzed by refluxing for 1 hr with 60 ml of 0.1-*N* sulfuric acid; the hydrolyzate was cooled, and deionized by passage through a column of mixed cation [5] and anion [6] exchange resins. The resulting solution was concentrated under reduced pressure to about 50 ml, and was then freeze-dried. The colorless sirup weighed 2.91 g and had a specific rotation, $[\alpha]_D^{20}$, of $-17.3°$. The cyanide-combining power of the sirup was about 90 percent of the theoretical, and consequently it was assumed that the residue contained 90 percent of D-erythrose. It was used without further purification for the cyanohydrin synthesis described in the following sections.

2.2. Effect of General Acid Catalysts in the Cyanohydrin Synthesis on the Yield of the D-Arabonic Epimer

Several cyanohydrin syntheses employing C^{14}-labeled cyanide and sirupy D-erythrose were carried out on a semimicro scale under the conditions described below. After hydrolysis of the cyanohydrins, each mixture was treated with a large excess of nonradioactive potassium D-arabonate. From the radioactivity of the recrystallized potassium salt, the proportion of D-arabonic acid was calculated.

The mixtures, two of which are listed in table 1 as experiments 1 and 2, were frozen, and the tubes were sealed and allowed to stand at room temperature for 72 hr. They were then opened and heated on a water bath at 80° C for 7 hr in the presence of a stream of air. A few drops of water were added from time to time, but at the end of the hydrolysis period the solutions were allowed to evaporate to dryness. The residue in each tube was dissolved in 5 ml of water, and 500 mg of potassium D-arabonate was added. The mixture was warmed slightly to dissolve the salt, and the solution was filtered with the aid of a small amount of decolorizing carbon, and treated with 3 volumes of ethanol. Potassium D-arabonate crystallized freely from all preparations. After storage for 18 hr in a refrigerator, the mother liquor was removed from the crystals, which were washed in place with cold, aqueous ethanol (1:4). The samples were recrystallized once from water and ethanol, dried in a vacuum desiccator, and assayed. Experiments 1 and 2 reported in table 1 indicate that ammonium carbonate favors production of D-arabonic nitrile. A large-scale preparation reported in section 2.3, and also listed as experiment 3 in table 1, shows that sodium bicarbonate likewise favors production of the arabonic epimer. The results are in accord with the prior observation that general acid catalysts alter the proportion of the epimeric nitriles [3, 5].

[5] Amberlite IR-100, analytical grade, Resinous Products Division of Rohm & Haas Co., Philadelphia, Pa.
[6] Duolite A-4, Chemical Process Co., Redwood City, Calif.

TABLE 1. *Effect of a general acid catalyst on the yield of the arabonic epimer obtained by the addition of cyanide to D-erythrose*

Experiment	Reaction mixture [a]	Activity found in carrier potassium D-arabonate [b]	Arabonic epimer formed
	Millimoles		
1	[c] 0.0267 D-erythrose .0134 Na_2CO_3 [c] .0267 NaCN	μc [d] 9.90	% 37.1
2	[c] .0267 D-erythrose .134 $(NH_4)_2CO_3$ [c] .0267 NaCN	[d] 14.80	55.6
3	[e] 4.0 D-erythrose 10.0 $NaHCO_3$ [e] 3.1 NaCN	[f] 6,950	49.6

[a] Total volume was 1 ml in experiments 1 and 2, and 20 ml in experiment 3.
[b] Activities determined by means of a vibrating-reed electrometer after a modified Van Slyke-Folch wet oxidation procedure (see [11]).
[c] Assuming 90-percent purity of the erythrose sirup.
[d] Calculated for entire 500 mg of carrier added.
[e] Contained 26.7 μc of carbon 14.
[f] Radioactivity recovered in several crops.
[g] Contained 14 mc of carbon 14.

2.3. Preparation of Potassium D-Arabonate-1-C^{14} from D-Erythrose by the Cyanohydrin Synthesis in the Presence of Sodium Bicarbonate

Ten milliliters of an aqueous solution containing 3.1 millimoles of sodium cyanide (14.0 mc of carbon 14) and 5 millimoles of sodium hydroxide was frozen on the sides of a small glass-stoppered tube. A small lump of solid carbon dioxide was added, and then a solution containing 5 millimoles of sodium bicarbonate and approximately 4 millimoles of D-erythrose in 10 ml of water. The loosely stoppered flask was placed in an ice bath, shaken until the contents had dissolved, and then kept in the bath for 1 day, and at room temperature for 5 days. The nitriles were hydrolyzed by heating on a steam bath for 7 hr, and the resulting ammonia was removed by evaporation of the solution to dryness in a stream of air. The residue was taken up in water and passed over a column containing 10 ml of cation exchange resin [7] to remove sodium ions. The column was washed until the activity of the effluent was negligible, and the effluent was concentrated under reduced pressure to about 25 ml and neutralized with potassium hydroxide. Two grams of nonradioactive potassium D-arabonate was dissolved in the sirup and evaporation was continued to a volume of about 4 ml; the solution was then saturated with methanol. After 18 hr, a crop of potassium D-arabonate-1-C^{14} was obtained, which, when recrystallized and dried, weighed 2.23 g and had an activity of 5,980 μc. By the further addition of 2.5 g of carrier potassium D-arabonate in 3 portions, 970 μc of activity was obtained. Hence the total radiochemical yield of potassium D-arabonate-1-C^{14} was 6,950 μc, or 50 percent of the activity of the original cyanide. The residual sirup was used for the preparation of cadmium D-ribonate-1-C^{14} (see sec. 2.6).

[7] Amberlite IR-120, analytical grade, Resinous Products Division of Rohm & Haas Co., Philadelphia, Pa.

2.4. Preparation of Potassium D-Arabonate-1-C^{14} from D-Erythrose by the Cyanohydrin Synthesis in the Presence of Ammonium Carbonate

In another preparation of D-arabinose-1-C^{14}, the ammonium carbonate method was employed. Five milliliters of a solution containing 0.7 millimole of sodium hydroxide and about 0.7 millimole of sodium cyanide with 5.4 mc of carbon 14 was frozen on the walls of a small glass-stoppered tube. Five milliliters of approximately 1 *M* ammonium carbonate was then frozen in the tube, and finally 1 ml of a solution containing 1 millimole of D-erythrose[8] was added. The mixture was allowed to thaw in an ice bath and was then kept at room temperature for 3 days. It was treated essentially in the manner described in section 2.3, except that a crop of potassium D-arabonate-1-C^{14} (52 mg, containing 2,030 μc)[9] was separated without the addition of carrier. The total radiochemical yield (2,446 μc, or 45 percent) was slightly less than that of the former preparation. However, as greater mechanical loss was incurred in this preparation because of the higher level of activity, it is believed that the two methods are equally satisfactory in the synthesis of potassium D-arabonate-1-C^{14}.

2.5. Preparation of D-Arabono-γ-Lactone-1-C^{14} and Reduction to D-Arabinose-1-C^{14}

An aqueous solution containing 446 mg (2.19 millimoles) of potassium D-arabonate with 1,190 μc of activity was passed through a column of cation exchange resin (see footnote 7). The column was thoroughly washed, and the effluent was evaporated at 60° C substantially to dryness. The residue, dissolved in a few milliliters of methanol, was transferred to a reduction tube such as that described previously [3]. Briefly, it consists of a test tube 2.8 by 20 cm fitted with a stirrer reaching to the bottom of the tube and with a sidearm for the introduction of the amalgam. The solution in the tube was concentrated in an air stream and seeded with D-arabono-γ-lactone.[10] The tube was finally stored in a desiccator, and the contents was moistened from time to time with methanol. When lactonization was complete, as indicated by the disappearance of any sirupy phase (1 or 2 weeks), the material was reduced with sodium amalgam by the procedure described later.

The lactonization described above required considerable time. In order to avoid this delay, the following rapid procedure was developed: Two millimoles of potassium D-arabonate-1-C^{14} was passed through a column of cation-exchange resin, and the effluent was concentrated under reduced pressure to a sirup, which was transferred with a few drops of water to a reduction tube. Five milliliters of glacial acetic acid was added, and the tube was placed in a boiling-water bath and heated in a stream of air for 5 hr. After 1 hr of this period, 1 ml of water and 5 ml of acetic acid were added. At three 1-hr intervals thereafter, the material was treated with 5 ml of acetic acid only. At the end of the heating period, the pale-yellow residue was dissolved in 3 or 4 drops of methanol, seeded with D-arabono-γ-lactone, and placed in a desiccator over calcium chloride. It crystallized well within 24 hr.

When samples of nonradioactive D-arabonic acid were subjected to this procedure, the optical rotations, $[\alpha]_D^{20}$, 24 and 72 hr after the sirups were seeded with the crystalline lactone were, respectively, +66.0° and +67.6° (based on the weight of the lactone). These values correspond approximately to conversion of 91 and 94 percent, respectively, of the D-arabonic acid to the lactone.

Prior to the preparation of the labeled sugar, a series of sodium amalgam reductions was carried out on the nonradioactive lactone in order to determine optimum conditions. Sodium acid oxalate was employed as a neutralizing agent [6], and after removal of the salts in the manner described below, the reduction product was analyzed for reducing sugars by the modified Scales method [13]. It was found that a maximum yield of sugar (85 percent) is obtained with 4.6 g of 5-percent sodium amalgam per millimole of lactone.

In a typical reduction of the labeled lactone to the sugar, the reduction tube, containing 6.4 g of crystalline sodium acid oxalate and the lactone prepared from 446 mg of potassium D-arabonate-1-C^{14}, having 1,190 μc of activity, was placed in an ice bath. After the addition of 20 ml of ice water, the stirrer was adjusted to produce vigorous stirring at the bottom of the tube, and 9.2 g of 5-percent sodium amalgam pellets[11] was added through the side arm. Stirring was continued for 3 hr, at the end of which time the mercury was removed, and the aqueous mixture was diluted with 5 volumes of methanol. The crystalline salts were separated, washed with methanol, and discarded, after it was ascertained that they were inactive. Phenolphthalein indicator was added to the mother liquor, previously cooled in ice water, and then aqueous sodium hydroxide until a faint but permanent pink color was obtained. The solution was concentrated under reduced pressure to about 10 ml, and treated with 5 volumes of methanol; the precipitated salts were separated, washed with methanol, tested for radioactivity, and discarded. The solution was concentrated to remove the alcohol, and passed over a column containing 25 ml of mixed anion and cation exchange resins (see footnotes 5 and 6); the resins were washed until the activity of the washings was negligible. The effluent was con-

[8] Because of uncertainty in the concentration of the cyanide solution, the erythrose was in larger excess than would ordinarily be added.

[9] Except for the analyses in table 1, all assays of carbon 14 were made in formamide solution [12]. Details of the analysis of this crop of potassium D-arabonate-1-C^{14} are illustrative: The material was dissolved in water and the volume was adjusted to 10 ml. A 50-λ aliquot was diluted to 1 ml with water in a micromixing pipette. A 20-λ aliquot of this was diluted to 1 ml with formamide, and the solution gave 74.9 counts per second in a 2-π proportional counter in which 1 count per second is equivalent to 0.00271 μc.

[10] The free acid may crystallize from the freshly prepared sirup at this point. Conversion of the acid to the lactone at room temperature requires at least a week.

[11] The amalgam was prepared in small pellets by pouring it in molten condition through a heated alundum thimble, having a small hole in the bottom, into a 2-ft "shot tower" of mineral oil. The pellets were stored under mineral oil, and just before use, were blotted dry, weighed, and rinsed with benzene.

centrated under reduced pressure and at a temperature less than 40° C to about 10 ml; at this stage the solution was filtered into a round-bottomed flask through a microfilter containing a small bed of decolorizing carbon,[12] and the combined solution and washings were freeze-dried in a 50-ml flask. The residue in the flask was dissolved in a few drops of methanol, and 2-propanol was added to incipient turbidity. Crystallization began immediately after nucleation. At the end of 2 days, the mother liquor was separated, and the crystals were washed in place with a few drops of a methanol-2-propanol mixture (2:1). For recrystallization, the crude material, dissolved in a few drops of water, was transferred to a standard-taper test tube, and the water was removed under reduced pressure. The thick sirup was dissolved in a few drops of methanol, and 2-propanol was cautiously added, until saturation was approached. The crystals that formed in 24 hr weighed 185 mg and contained 672 μc of activity. With the aid of 100 mg of nonradioactive D-arabinose as carrier, an additional 39 μc of activity was obtained from the mother liquor. The yield of D-arabinose-1-C^{14} (711 μc) from potassium D-arabonate-1-C^{14} was thus 60 percent.[13]

2.6. Separation of Cadmium D-Ribonate-1-C^{14}

The mother liquor from the preparation of potassium D-arabonate-1-C^{14}, described in section 2.3, was evaporated to remove the alcohol present. The residue was dissolved in water and passed over a column of cation exchange resin (see footnote 7). The effluent, containing 6,900 μc of activity, was then neutralized with cadmium hydroxide to the end point of phenolphthalein. After the addition of 1 g of nonradioactive cadmium D-ribonate, the solution was filtered with the aid of decolorizing carbon, and the filtrate was evaporated under reduced pressure to a thin sirup. Nucleation of the sirup with crystalline cadmium D-ribonate and careful addition of aqueous methanol resulted in a voluminous crystallization. The crystals were separated by filtration, and recrystallized by dissolving in 4 ml of hot water and adding successively 5 ml of methanol and water (1:1) and 2 ml of methanol and water (2:1). The hot solution was then saturated with methanol and allowed to cool slowly. The first crop of recrystallized cadmium D-ribonate-1-C^{14} weighed 678.6 mg and had an activity of 1,796 μc. After successive additions of two 1-g quantities of nonradioactive cadmium D-ribonate as carrier, and recrystallization of the resulting crops of salt, an additional quantity of cadmium D-ribonate-1-C^{14} containing 1,416 μc was recovered. The total yield of cadmium D-ribonate-1-C^{14} was thus 3,212 μc, corresponding to 23 percent of the C^{14}-labeled cyanide used.

[12] This step removes a trace of oil that may be introduced with the sodium amalgam.

[13] In other preparations, radiochemical yields up to 70 percent have been obtained.

2.7. Preparation of D-Ribono-γ-lactone-1-C^{14} and Reduction to D-Ribose-1-C^{14}

A solution containing 679 mg of cadmium D-ribonate-1-C^{14}, with an activity of 1,800 μc, was passed over a column of cation exchange resin (see footnote 7), and the effluent was concentrated under reduced pressure to a sirup. The sirup was transferred by use of water to three reduction tubes and evaporated to dryness by heating on a steam bath under a stream of dry air. The residue in each tube was dissolved in a few drops of water and the solution, after the addition of 5 ml of methyl cellosolve, was evaporated again. This process was repeated 4 times over a period of 2 days. Each residue was then dissolved in 2 ml of methyl cellosolve, and the solution was seeded with crystalline D-ribono-γ-lactone and stored in a desiccator over calcium chloride. From time to time the residues were moistened with methyl cellosolve. Crystallization occurred slowly, but ultimately all sirup disappeared, and the residues appeared to be entirely crystalline.

A series of reductions on nonradioactive D-ribono-γ-lactone showed that a maximum yield of sugar (70 percent) was obtained when 9.2 g of 5-percent amalgam and excess sodium acid oxalate were employed for the reduction of 1 millimole of lactone. Each of the three samples of lactone mentioned above was dissolved in 20 ml of ice water and reduced by use of the above quantities of amalgam and oxalate. The product from the three reductions was combined, the mercury was separated, and the mixture was diluted with 5 volumes of methanol. The resulting crystalline salts were separated by filtration, washed with methanol, and discarded after a test showed negligible radioactivity. The filtrate was concentrated under reduced pressure to a volume of about 15 ml and diluted with 75 ml of methanol; the sodium salts that separated were removed by filtration and washed with methanol. As a test showed that this second crop of salts likewise contained no appreciable radioactivity, it was discarded. The alcoholic filtrate was concentrated to about 10 ml, neutralized with aqueous sodium hydroxide in the presence of phenolphthalein until a permanent pink color was obtained, and immediately deionized by passage over a column of mixed cation and anion exchange resins (see footnotes 5 and 6). The effluent and wash liquor were combined and concentrated under reduced pressure to a volume of 6 ml; 750 mg of carrier D-ribose was dissolved in the sirup, and the solution was filtered through 1 ml of a mixture of decolorizing carbon and diatomaceous earth. The filtered solution was freeze-dried, and the residue was dissolved in 0.5 ml of ethanol. A mixture of ethanol and isoamyl alcohol was added to the point of incipient turbidity, and the solution was seeded with D-ribose and stored in a refrigerator. When crystal growth seemed complete (5 days), the mother liquor was removed with a capillary pipette, and the crystals were carefully washed, in place, with ethanol and dried over calcium

chloride. The crude product (768 mg) had an activity of 667 μc, or 37 percent of the activity of the cadmium D-ribonate–1–C^{14} used.

For recrystallization, the product was dissolved in a few drops of water, a drop of acetic acid was added, and the solution was filtered through decolorizing carbon. The filtrate was concentrated under reduced pressure to a thick sirup. The residue was dissolved in ethanol, and the solution was concentrated again under reduced pressure. The residue was dissolved in 0.5 ml of ethanol, and after addition of isoamyl alcohol to incipient turbidity, the solution was seeded and stored, first at room temperature and finally in a refrigerator. After 5 days, the product was separated, washed in place with a few drops of ethanol, and dried. The recrystallized D-ribose-1-C^{14} (540 mg) contained 465 μc of carbon 14. By use of carriers on the mother liquor from the recrystallization, nearly all of the radioactivity of the crude D-ribose-1-C^{14} was reclaimed.

3. References

[1] H. S. Isbell, J. V. Karabinos, H. L. Frush, N. B. Holt, A. Schwebel, and T. T. Galkowski, J. Research NBS **48,**163 (1952) RP2301.

[2] H. S. Isbell, and J. V. Karabinos, J. Research NBS **48,** 2334 (1952) RP2335.

[3] H. L. Frush and H. S. Isbell, J. Research NBS **50,** 133 (1953) RP2400.

[4] H. L. Frush and H. S. Isbell, U. S. Atomic Energy Commission Report No. NBS–2308 (1953); J. Research NBS **51,** 167 (1953) RP2446.

[5] H. S. Isbell, U. S. Patent 2606918, August 1952.

[6] H. S. Isbell, U. S. Patent 2632005, March 1953.

[7] D. A. Rappoport and W. Z. Hassid, J. Am. Chem. Soc. **73,** 5524 (1951).

[8] J. C. Sowden and H. O. L. Fischer, J. Am. Chem. Soc. **69,** 1963 (1947).

[9] J. C. Sowden, J. Am Chem. Soc. **72,** 808 (1950).

[10] R. C. Hockett, D. V. Collins, and A. Scattergood, J. Am. Chem. Soc. **73,** 599 (1951).

[11] M. Calvin, C. Heidelberger, J. C. Reid, B. M. Tolbert, and P. F. Yankwich, Isotopic carbon, p. 92 (J. Wiley & Sons, Inc., New York, N. Y., 1949).

[12] A. Schwebel, H. S. Isbell, and J. V. Karabinos, Science **113,** 465 (1951).

[13] H. S. Isbell, W. W. Pigman, and H. L. Frush, J. Research NBS **24,** 241 (1940) RP1282.

WASHINGTON, September 1, 1953.

Journal of Research of the National Bureau of Standards Vol. 51, No. 6, December 1953 Research Paper 2459

Corrosion of Nickel Cast Irons in Soils

Irving A. Denison and Melvin Romanoff

The results of measurements of the corrosion and of the strength of nickel cast irons after exposure to different soil conditions for a maximum of 14 years are reported. The magnitude and progress of corrosion, as determined by weight-loss and pit-depth measurements, are correlated with the composition of the materials and the nature of the environmental conditions to which the specimens were exposed. The residual strength of the corroded cast iron that had been removed from the more corrosive soils was evaluated by subjecting the pipe specimens to hydraulic pressures up to 500 lb/in².

1. Introduction

Corrosion of cast iron in soils is characterized by the development of an adherent layer of corrosion products that increases in thickness as corrosion progresses. The thickening of this layer is due in part to electrochemical action between the ferritic and graphitic constituents of cast iron and partly to differences in potential that arise from contact of the cast metal with the soil, as, for example, by differential aeration. To the extent that corrosion of cast iron is caused by differences in potential within the metal itself, improved corrosion resistance would be expected to result from improvement in the quality of the casting. Wesley, Copson, and LaQue [1][1] have shown that the addition of small amounts of nickel and nickel plus chromium alters the structure of cast iron in such manner that galvanic action between the different constituents is reduced considerably. Larger additions of these alloying elements in amounts sufficient to produce an austenitic structure were shown to be considerably more effective in reducing corrosion under the experimental conditions because of the ennobling effect of nickel and chromium on the potential of iron.

In order to evaluate the effect of additions of nickel and of nickel plus chromium on the corrosion of cast iron in soils, samples of alloy cast irons were included in an extensive series of exposure tests of materials for underground construction. In 1932, samples of a high-alloy austenitic cast-iron pipe were buried at 15 test sites, and in 1941 samples of several low-alloy cast irons were buried at 13 of the same test sites, and at 1 other site. In a previous report [2], corrosion data were reported for five periods of exposure for the samples of high-alloy cast iron and for a single period for the samples of low-alloy cast irons. With the completion of the exposure tests in 1952, data for the latter materials became available for four periods of exposure, with a maximum exposure of 11 years.

After removal of the samples from the test sites, the procedure followed during the early periods of the exposure program was to clean the samples of all corrosion products preparatory to measuring the weight losses and the depths of the deepest pits. This procedure was later modified by subjecting those samples in the form of pipe to hydraulic pressure before removal of the corrosion products. This modification was introduced in order to evaluate the strength of the corrosion products remaining in the pits of the samples that had been perforated by corrosion. The methods used for cleaning the corroded samples and for measuring the depth of pitting have been previously described [3].

[1] Figures in brackets refer to literature references at the end of this paper.

2. Properties of the Soils at the Test Sites

The location of the test sites, the identification of the soil types, and the properties of the soils that are associated with corrosion are given in table 1. The retentiveness of the soils for water is indicated by the values for moisture equivalent, which is the quantity of water retained by a previously saturated soil against a centrifugal force of 1,000 times gravity. Because the real specific gravities of rock-forming minerals lie within a narrow range, values for apparent specific gravity are an index of the relative compactness or porosity of inorganic soils.

3. Description of the Materials

The forms, dimensions, and compositions of the specimens are given in table 2. The ends of the pipes were closed with cast-iron screw caps of the same composition as the specimens in order to exclude moisture from the interior. As an extra precaution against internal corrosion, the interior surface of the specimens was coated with heavy grease.

4. Weight Losses and Maximum Pitting

The data of table 3 indicate that the high-alloy cast iron E was considerably more resistant to corrosion, as measured by both weight loss and maximum pitting, than either the plain cast iron A or the low-alloy cast irons B, C, D, NC, and N. It is noteworthy that, except in cinders, the deepest pit measured on the specimens of material E in more than 14 years of exposure was only 74 mils.

The effect of composition on the corrosion of the low-alloy cast irons can be observed to somewhat better advantage by calculating the weight losses of

these specimens on a relative basis. This would have the effect of eliminating the differences in corrosivity of the soils due to differential aeration and emphasizing the effect of graphitic corrosion. In table 4 the weight losses of materials B, C, and D are shown for each soil and for each period of exposure relative to the plain cast iron A. Except for the well-drained soils of high resistivity (soils 53, 55, and 62), and soil 66, in which accelerated corrosion of the alloy cast irons occurred, the relative weight losses of the specimens during the initial period of exposure is seen to have decreased with increasing content of nickel. For example, during the first period of 5 years' duration the weight losses of material D in soils 58 and 63 were only 20 and 16 percent, respectively, of the weight losses of plain cast iron in the same soils for the same period. However, this initial advantage from the addition of nickel was usually not maintained, with the result that the weight losses of the alloy cast irons exposed for the maximum period usually did not differ greatly from the losses of plain cast iron. Hence, it would appear that the rates of corrosion of the alloys containing the higher amounts of nickel decrease less with time than do the rates for the alloys containing the lower amounts of nickel and plain cast iron.

5. Strength of Corroded Cast-Iron Pipe

Corrosion of cast iron in soils is characterized by the conversion of the metal into a layer consisting chiefly of oxides of iron and graphite. Although the original shape and appearance of the metal are retained, visual observation gives no indication of the extent of corrosion (fig. 1). It is generally recognized that corroded cast iron retains some of its original strength, but the extent to which cast-iron pipe may corrode underground and still retain sufficient strength to withstand the pressures commonly used in water- and gas-distribution systems has not previously been estimated.

In order to evaluate the residual strength of corroded cast-iron pipe, the samples of pipe that had been removed from the more corrosive soils after the longer periods of exposure were subjected to hydraulic pressures. The screwcap on one end of each sample was replaced by a similar cap in which a fitting had been inserted and the pipe section connected by copper tubing to a hand pump of suitable capacity. The pressure was increased at the rate of approximately 10 (lb/in.^{2})/sec until failure of the pipe occurred or the maximum pressure of 500 lb/in.^{2} was attained. After the application of hydraulic pressure, the corrosion products were removed, and the condition of the specimens was evaluated in the usual manner. The hydraulic pressures applied to the samples and the number of perforations in the samples after being cleaned are given in table 5.

The data in table 5 show that most of the specimens withstood a maximum presssure of 500 lb/in.^{2}, although removal of the corrosion products revealed numerous holes of various diameters. The few low values of bursting pressure given in the table probably should not be taken as accurately measuring the strength of the corroded pipe because of oxidation and probable damage to the pipe in handling and shipping. Hence it is reasonable to conclude that cast-iron pipe in an advanced stage of graphitic corrosion is able to withstand the minimum pressure required of class 150 pipe.

In considering the data of table 5, it is important to note that the pipe samples were subjected to hydraulic pressure from 6 months to a year after removal from the test sites. Inspection of the samples showed that during this interval some oxidation of the corrosion products occurred, as was indicated by slight increase in the volume of the corrosion products. Because oxidation is associated with loss in strength, it is reasonable to assume that if the samples had not been removed from the test sites, they would have withstood the applied pressure, even if they had been in a more advanced stage of corrosion. Instances of the loss in strength of graphitized cast-iron objects on exposure to air have been cited by Speller [4].

In order to evaluate the strength of the corrosion products of cast-iron pipe undisturbed by removal from the test sites, 3-ft sections of 6-in. cast-iron pipe, closed at both ends, were buried at 4 of the Bureau test sites. The investigation was undertaken with the cooperation of the Cast Iron Pipe Research Association. Provision was made for applying hydraulic pressure to the pipe sections by means of a fitting inserted in the closure at one end of the pipe. According to the plan of the test, a pressure of 400 lb/in.^{2} is applied to the pipe sections at approximately 2-year intervals until rupture occurs, at which time the section will be removed and the extent of corrosion evaluated. As none of the pipe sections has failed as yet to withstand the applied pressure, the test is necessarily incomplete. However, the data obtained to date in certain of the soils provide significant information on the strength of corroded cast-iron pipe under normal conditions of exposure.

In table 6 are shown the number of years during which the pipe sections have withstood the applied pressure. For comparison, the condition of similarly exposed specimens of cast-iron pipe, as indicated by the maximum and average penetration, is also shown. The data reported for site 70 is especially significant. Although 1 of the control specimens was perforated within 6 years, the 3-ft section has withstood the applied pressure for 24 years, during which time it would be expected to be converted almost entirely to corrosion products. Similarly, the development of a pit 302 mils in depth in 6 years on the control specimens in soil 118 indicates that the 3-ft section, which withstood the applied pressure after 24 years of exposure, should also be in an advanced stage of corrosion.

6. Summary

This report contains the results of measurements of weight loss, maximum depth of pitting, and of

hydraulic bursting pressure made on samples of nickel cast irons after exposure to different soil conditions. Additions of nickel up to 3 percent significantly reduced the initial corrosion of cast iron in poorly drained soils of low resistivity, but this advantage was not maintained for the duration of the exposure tests. Samples of austenitic cast iron containing 15 percent of nickel, together with chromium and copper, showed good resistance to corrosion in most of the soils, especially with respect to maximum depth of pitting.

With some exceptions, samples of severely corroded plain and low-alloy cast-iron pipe withstood a maximum hydraulic pressure of 500 lb/in.^{2} after exposure at the test sites for periods up to 11 years and storage in the laboratory for approximately 1 year. Because the effect of oxidation in the air is to weaken the layer of corrosion products, the observed values for hydraulic bursting pressure are probably to be considered minimum values. The results of incomplete field tests of the bursting pressure of undisturbed sections of plain cast-iron pipe are in good agreement with the results of the measurements made on the stored samples.

The direction of this program by Mr. K. H. Logan prior to his retirement in 1946 is acknowledged.

7. References

[1] W. A. Wesley, H. R. Copson, and F. L. LaQue, Metals & Alloys **7**, 325 (1936).

[2] Irving A. Denison and Melvin Romanoff, J. Research NBS **44**, 47 (1950) RP2057.

[3] Kirk H. Logan, Underground corrosion. NBS Circular 450 (1945).

[4] F. N. Speller, Corrosion, causes and prevention (McGraw-Hill Book Co., New York, N. Y., 1951).

TABLE 1. *Properties of the soils at the test sites*

Test sites			Aeration [a]	Moisture equivalent	Apparent specific gravity	Resistivity at 60° F (15.6° C)	pH	Total acidity [b] (milligram equivalent per 100 g of soil)	Composition of water extract (milligram equivalent per 100 g of soil)						
Environment and soil type	Soil	Location							Na+K as Na	Ca	Mg	CO_3	HCO_3	Cl	SO_4
				Percent		*Ohm-cm*									
INORGANIC OXIDIZING SOILS															
Cecil clay loam	53	Atlanta, Ga	G	33.7	1.60	17,800	4.8	5.1	----	----	----	----	----	----	----
Hagerstown loam	55	Loch Raven, Md	G	32.0	1.49	5,210	5.8	10.9	----	----	----	----	----	----	----
Susquehanna clay	62	Meridian, Miss	F	34.6	1.79	6,920	4.5	12.0	----	----	----	----	----	----	----
Chino silt loam	65	Wilmington, Calif	G	26.4	1.41	148	8.0	A	7.65	12.40	2.20	0.00	1.30	6.05	16.90
Mohave fine gravelly loam	66	Phoenix, Ariz	F	16.5 [c]	1.79	232	8.0	A	6.55	0.51	0.18	.00	0.73	2.77	2.97
INORGANIC REDUCING SOILS															
Sharkey clay	61	New Orleans, La	P	30.8	1.78	943	6.8	4.9	0.73	0.68	0.33	0.00	0.71	0.10	0.91
Ducas clay	64	Cholame, Calif	F	41.1	1.88	62	7.5	A	28.10	2.29	.76	.00	.89	28.80	.26
Lake Charles clay	56	El Vista, Tex	VP	28.7	2.03	406	7.1	5.1	3.12	0.69	.47	.00	.80	1.59	3.04
Merced silt loam	70	Buttonwillow, Calif	F	24.7	1.69	278	9.4	A	8.38	.38	.22	.02	1.87	1.12	5.57
ORGANIC REDUCING SOILS															
Carlisle muck	59	Kalamazoo, Mich	VP	43.6	....	1,660	5.6	12.6	1.03	3.08	2.70	0.00	0.00	3.47	1.04
Muck	58	New Orleans, La	P	57.8	1.43	712	4.8	15.0	2.03	2.23	1.29	.00	.00	0.47	2.54
Rifle peat	60	Plymouth, Ohio	P	43.4	1.28	218	2.6	297.4	2.91	10.95	2.86	.00	.00	.00	56.70
Tidal marsh	63	Charleston, S. C	VP	46.7	1.47	84	6.9	14.6	33.60	6.85	4.00	.00	.00	12.70	36.60
CINDERS															
Cinders	67	Milwaukee, Wis	VP	....	....	455	7.6	A	0.77	3.03	0.53	.00	.55	0.08	2.89

[a] G, good; F, fair; P, poor, VP, very poor.
[b] A, alkaline reaction.

TABLE 2. *Composition of the materials*

Material	Identification	Form	Nominal Width or Diameter	Length	Thickness	C (total)	Si	Mn	S	Cr	Ni	Cu
			in.	*in.*	*in.*	%	%	%	%	%	%	%
Plain cast iron	A	Pipe	1.5	13	0.250	3.22	2.19	0.91	0.12	....	....	....
Low-alloy cast iron	B	....do	1.5	13	.250	3.28	2.09	.83	.12	....	1.27	0.32
Do	C	....do	1.5	13	.250	3.24	2.08	.80	.12	....	1.71	.98
Do	NC	Plate	2.5	14	.5	2.80	2.03	....	....	....	2.08	1.10
Do	N	....do	2.5	14	.5	2.75	2.00	....	....	....	3.10	....
Do	D	Pipe	1.5	13	.250	3.21	2.11	.72	.12	....	3.32	....
High-alloy cast iron	E	....do	1.5	10	.250	2.98	2.13	1.00	....	2.61	15.00	6.58

TABLE 3. *Losses in weight and maximum pitting of plain and alloy cast irons*

Number	Type	Exposure: For all materials except E [z]	Exposure: For material E only [y]	Loss in weight: Cast-iron pipe: Plain cast iron A	1.27 Ni 0.32 Cu B	1.17 Ni 0.98 Cu C	3.32 Ni D	15.0 Ni 6.6 Cu 2.6 Cr E	Loss in weight: Cast-iron plate: 2.08 Ni 1.10 Cu NC	3.10 Ni N	Maximum penetration: Cast-iron pipe: Plain cast iron A	1.27 Ni 0.32 Cu B	1.71 Ni 0.98 Cu C	3.32 Ni D	15.0 Ni 6.6 Cu 2.6 Cr E	Maximum penetration: Cast-iron plate: 2.08 Ni 1.10 Cu NC	3.10 Ni N
		Years	*Years*	*oz/ft²*	*oz/ft²*	*oz/ft²*	*oz/ft²*	*oz/ft²*	*oz/ft²*	*oz/ft²*	*Mils*	*Mils*	*Mils*	*Mils*	*Mils*	*Mils*	*Mils*
INORGANIC-OXIDIZING SOILS																	
53	Cecil clay loam	4.9	2.0	3.2	3.9	3.5	3.5	1.2	3.3	2.0	r 179+	124	144	136	30	133	120
		7.2	5.4	5.1	4.2	4.9	4.6	0.7	4.1	3.2	131	131	122	120	36	138	131
		8.6	7.4	6.0	6.3	5.7	5.9	.7	4.4	3.4	194+	129	215+	139	51	148	144
		10.8	9.3	5.9	4.7	5.5	5.1	1.4	3.2	3.7	145	136	132	120	23	149	163
			14.3					1.2							44		
55	Hagerstown loam	5.1	2.0	2.2	2.5	2.6	2.6	0.8	1.6	2.1	110	114	123	96	30	110	113
		7.0	5.4	3.8	3.5	3.8	4.2	.6	2.8	3.1	108	118	114	115	37	123	119
		8.7	7.4	5.1	4.8	4.8	4.5	.7	3.4	3.1	116	115	117	126	41	148	140
		11.1	9.3	3.5	3.8	4.1	4.3	4.3	3.8	4.1	132	158	114	157	34	147	171
			14.3					1.1							51		
62	Susquehanna clay	4.9	1.0	3.6	3.5	3.8	2.6	1.7	3.1	2.5	53	77	112	104	43	94	76
		7.2	5.4	6.7	5.1	4.9	5.1	1.1	1.8	4.5	76	89	122	135	49	89	84
		8.7	7.4	8.7	9.0	7.7	8.5	1.0	5.8	5.9	74	110	120	175+	37	143	139
		10.9	9.3	5.6	6.5	6.7	5.4	2.7	4.9	5.2	117	199+	180+	223+	53	152	144
			14.3					2.3							60		
65	Chino silt loam	5.0	2.0	.86	7.7	9.9	7.0	1.5	7.9	8.2	113	148	129	157	26	149	100
		7.2	5.4	5.6	3.1	3.4	2.3	3.0	4.9	4.2	109	114	123	107	42	110	102
		8.8	7.4	11.9	6.6	5.5	6.0	2.0	8.6	9.7	121	117	154	197+	42	163	152
		10.9	9.3	3.4	3.0	2.6	3.7	2.6	7.4	8.6	111	114	112	185+	35	154	158
			14.3					3.1							59		
66	Mohave fine gravelly loam	5.0	2.0	6.2	8.2	9.3	8.3	3.1	6.6	z 10.2	67	80	80	80	26	88	z 80
		7.2	5.4	29.6	27.5	27.8	28.6	3.0	29.9	27.7	209+	227+	250+	250+	36	237	221
		8.8	7.4	25.6	28.5	D	D	3.5	21.7	22.4	189+	141	250+	250+	38	218	230
		11.0	9.3	5.3	6.8	9.5	9.4	3.3	9.0	8.6	160+	142	143	115	40	153	147
			14.3					7.6							54		
INORGANIC-REDUCING SOILS																	
56	Lake Charles clay	4.9	2.0	6.5	2.9	4.1	2.9	3.3	4.8	7.3	124	96	64	50	42	110	120
		7.2	5.4	19.4	20.5	20 9	16.3	4.6	18.8	16.2	202+	210+	188	179	32	198	183
		8.7	7.4	19.4	18.3	20.8	20.7	9.4	15.7	15.6	188+	250+	208+	250+	53	220	231
		10.9	9.3	19.3	21.7	20.3	19.4	14.6	26.6	27.2	250+	250+	213+	192+	58	216	248
			14.3					17.3							72		
61	Sharkey clay	4.9	2.0	6.8	5.7	5.6	5.2	0.3	3.4	5.4	78	122	112	104	36	84	90
		7.2	5.4	6.6	5.4	5.3	5.1	1.8	5.0	4.7	93	108	110	116	39	11	10
		8.7	7.4	7.9	7.8	5.6	6.2	1.7	4.9	4.1	96	136	135	122	30	121	138
		10.9	9.3	4.9	3.7	3.4	2.5	2.3	3.4	3.5	96	120	120	120	30	120	120
			14.3					2.3							39		

61	Sharkey clay	4.9	2.0	6.8	5.7	5.6	5.2	0.3	3.4	3.4	78	122	112	104	36	84	90
		7.2	5.4	6.6	5.4	5.3	5.1	1.8	5.6	4.7	93	108	110	116	39	111	105
		8.7	7.4	7.9	7.8	5.6	6.2	1.7	4.9	4.1	96	136	133	122	50	121	128
		10.9	9.3	4.0	3.7	3.4	3.5	2.3	3.1	2.9	85	172	122	132	36	139	104
			14.3					5.2							58		
64	Docas clay	5.0	2.0	19.7	20.4	18.7	14.4	4.4	15.5	15.8	151	187+	210+	226+	28	138	138
		7.2	5.4	22.1	20.4	17.2	9.5	3.1	23.4	23.1	242+	237+	229+	175+	27	206	191
		8.8	7.4	24.2	24.7	14.5	15.0	5.8	37.5	35.7	240+	185+	161	189+	40	220	218
		11.0	9.3	25.1	14.8	23.6	21.1	12.8	26.5	25.0	214+	213+	205+	250+	74	178	195
			14.3					4.8							34		
70	Merced silt loam	5.0	2.0	7.5	4.8	4.2	3.7		7.0	7.6	104	106	90	93		101	107
		7.2	5.4	35.3	34.4	31.4	D		26.8	26.1	250+	250+	250+	250+		254	240
		8.8	7.4	34.4	D	D	D		25.4	25.5	217	250+	250+	250+		268+	255+
		11.0	9.3	D	D	D	D		37.2	38.1	250+	250+	250+	250+		268+	265+
			14.3														
[a]																	
	ORGANIC-REDUCING SOILS																
58	Muck	4.9	2.0	6.8	4.4	3.5	1.4	0.8	3.6	3.2	106	140	019	144	50	118	119
		7.2	5.4	6.4	4.8	4.2	6.1	4.9	4.8	5.1	160+	171+	168+	168+	34	148	139
		8.7	7.4	6.8	7.6	5.8	6.0	8.6	5.2	5.5	116	121	82	100	58	123	118
		10.9	9.3	5.4	4.3	4.5	3.7	9.9	5.3	6.7	151+	190+	168+	136	53	206	143
			14.3					10.0							54		
59	Carlisle muck	5.1	2.0	14.4	13.3	11.1	7.6		5.4	5.4	89	89	111	87		78	80
		7.1	5.4	10.3	8.3	8.7	9.1	0.4	8.7	8.5	81	84	78	76	14	82	89
		8.7	7.4	15.6	11.3	13.2	11.1	.6	9.0	9.0	76	80	86	86	28	93	92
		11.1	9.3	16.0	15.5	15.6	15.4	.7	16.0	16.4	107	107	103	106	26	113	128
			14.3					1.2							36		
60	Rifle peat	5.1	2.0	6.5	2.0	1.9	3.5	4.2	4.4	3.6	52	39	32	94	24	56	66
		7.1	5.4	13.6	12.1	10.8	11.8	4.9	10.4	9.7	71	69	72	75	80	74	78
		8.7	7.4	14.2	13.8	12.8	14.9	z 1.3	11.7	11.7	66	64	54	60	z 22	68	65
		11.1	9.3	10.1	16.8	6.2	7.3	10.0	8.0	9.7	71	61	65	56	45	81	79
			14.3					11.6							72		
63	Tidal marsh	4.9	2.0	3.8	2.4	2.3	0.6	0.6	z 4.3	z 3.5	99	102	86	24	22	z 110	z 106
		7.2	5.4	5.9	3.9	4.8	6.2	.6	5.3	4.6	111	97	104	015	16	114	121
		8.6	7.4	4.5	6.1	4.6	4.2	.7	3.9	3.7	55	58	58	42	55	62	58
		10.8	9.3	4.3	4.8	3.6	2.0	1.6	8.0	6.4	92	152+	124+	55	32	187	226
			14.3					1.5							30		
	CINDERS																
67	Cinders	5.1	2.0	D	D	D	D	17.6	D	D	250+	250+	250+	250+	94	250+	250+
		7.1	5.4	D	D	D	D	38.4	D	D	250+	250+	250+	250+	250+	250+	250+
		8.7	7.4	D	D	D	D	24.3	D	D	250+	250+	250+	250+	250+	250+	250+
		11.1	9.3	D	D	D	D	D	D	D	250+	250+	250+	250+	250+	250+	250+
			14.3					D							250+	250+	250+

[a] Average of 2 specimens removed at each of the 5- and 9-year periods. Average of 3 specimens removed at each of the 7- and 11-year periods.
[b] Average of 2 specimens removed from each site at each period.
[c] + indicates that 1 or more specimens contained holes due to corrosion.
[d] Data for 1 specimen only. The other specimen was missing.
[e] D, Specimens destroyed by corrosion.
[f] Data for 4 specimens.

TABLE 4. *Weight losses of pipe specimens of low-alloy cast irons on a relative basis*

[Relative to weight loss of plain cast iron A = 100]

Soil	Exposure	1.27 Ni 0.32 Cu Pipe B	1.71 Ni 0.98 Cu Pipe C	3.32 Ni Pipe D
INORGANIC-OXIDIZING SOILS				
	Years			
53	5	122	109	109
	7	82	96	90
	9	105	95	98
	11	80	93	86
55	5	114	118	118
	7	92	100	110
	9	94	94	88
	11	84	91	96
62	5	97	106	72
	7	76	73	76
	9	103	88	98
	11	116	120	96
65	5	90	115	81
	7	55	61	41
	9	55	46	50
	11	88	76	109
INORGANIC-REDUCING SOILS				
66	5	132	150	134
	7	93	94	97
	9	111	136	136
	11	117	179	177
56	5	60	63	45
	7	106	108	84
	9	94	107	107
	11	112	105	101
61	5	84	82	76
	7	82	80	77
	9	98	71	78
	11	92	85	88
64	5	104	95	73
	7	92	78	43
	9	102	60	62
	11	99	94	84
ORGANIC-REDUCING SOILS				
58	5	65	48	20
	7	75	66	95
	9	112	85	88
	11	80	83	68
59	5	92	77	53
	7	81	84	87
	9	72	85	71
	11	97	98	96
60	5	31	29	54
	7	89	79	87
	9	97	90	105
	11	67	61	72
63	5	63	61	16
	7	66	81	105
	9	136	102	93
	11	112	84	46

TABLE 5. *Hyaraulic bursting pressures and number of perforations of pipe samples*

Soil	Exposure	Sample	Pipe A		Pipe B		Pipe C		Pipe D	
			Bursting pressure	Number of holes	Bursting pressure	Number of holes	Bursting pressure	Number of holes	Bursting pressure	Number of holes
	Years		*lb/in.²*		*lb/in.²*		*lb/in.²*		*lb/in.²*	
56	7.2	a	350	2	500+	1				
		b	500+	1	500+	1				
	8.7	a	500+	3	500+	1	500+	3	500+	2
		b			500+	1			500+	1
	10.9	a	500+	1	500+	1				
		b	500+	5	500+	10	500+	6	500+	8
58	7.2	a	500+	1	500+	1	500+	1	500+	1
	10.9	a	500+	1	500+	1	500+	2		
64	7.2	a	500+	6	0	7	50	10	500+	3
		b	500+	5	200	5	150	6		
	8.8	a	425	4	500+	4			500+	1
	11.0	a	500+	2	500+	3	375	4	500+	2
		b	500+	10			225	6	500+	3
		c							350	7
66	7.2	a	450	5			500+	3		
		b	500+	2			0	6	0	7
	8.8	a	500+	1			500+	6	275	3
	11.0	b					350	4	500+	5
		a	500+	1						
70	7.2	a	500+	5	0	14	500+	6	500+	7
		b	500+	4	0	11	0	12	0	14
	8.8	a			500+	6	0	12	0	12
		b			425	8	500+	7	300	9
	11.0	a	500+	12	175	18			500+	9
		b	50	16	500+	6				
		c	500+	11						

TABLE 6. *Condition of cast-iron pipe withstanding a maximum hydraulic pressure of 400 lb/in.²*

Soil		Specimens exposed for measurement of weight loss and pitting				Specimens exposed for application of hydraulic pressure of 400 lb/in.²	
Number	Type	Exposure	Wall thickness	Maximum pit depth	Average penetration	Maximum period of exposure	Wall thickness
		Years	*Mils*	*Mils*	*Mils*	*Years*	*Mils*
[1]15	Houston black clay.	17.6	450	226	14.9	24	450
64	Docas clay	5.0	250	250+	30.4	12.5	450
70 (23)	Merced silt loam	6.2	450	450+	58.4	24	450
[1]118	Niland gravelly sand.	5.9	450	302	49.3	24	450

[1] See references [2 and 3] for properties of the soils.

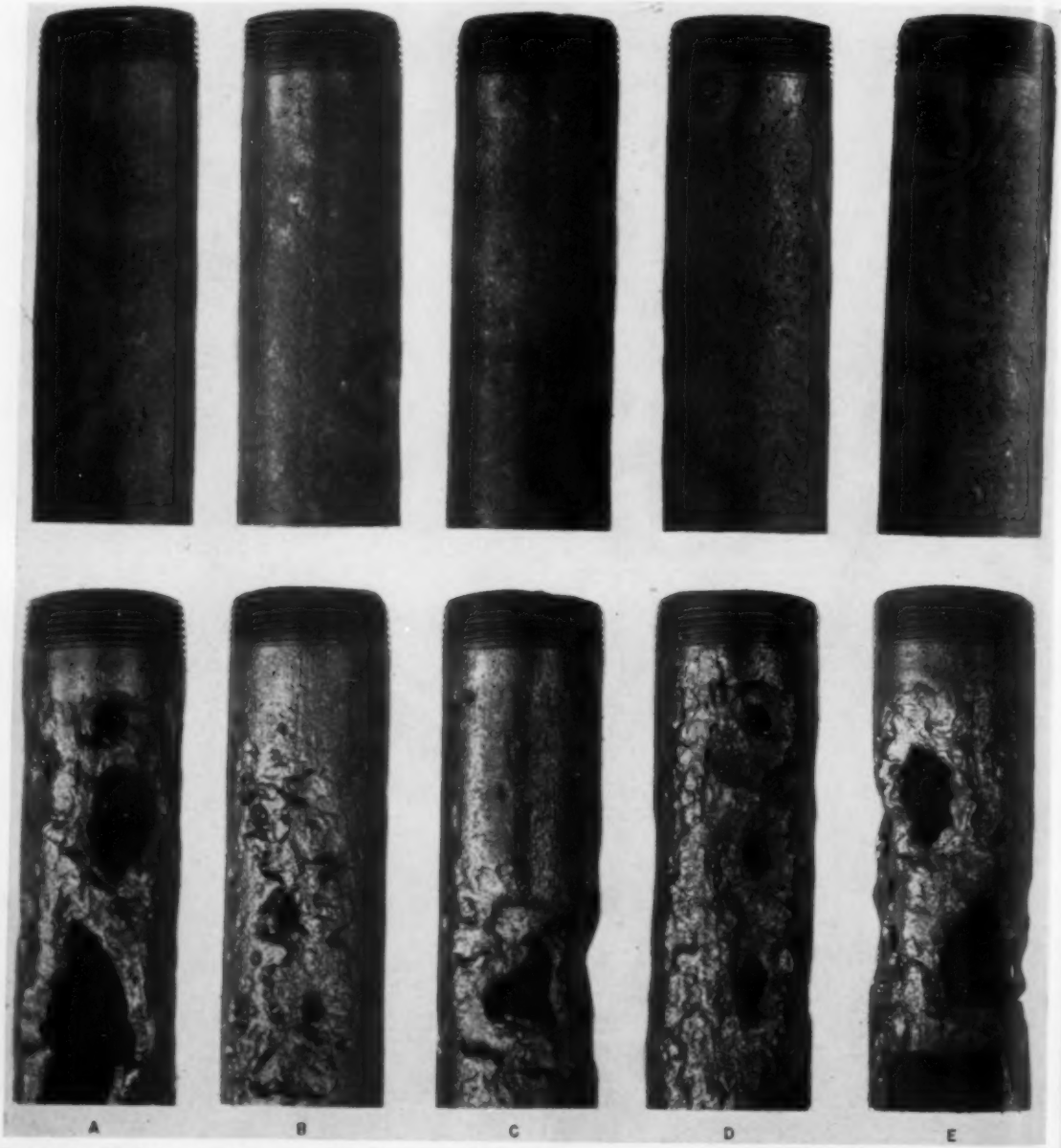

FIGURE 1. *Condition of cast iron exposed to highly corrosive soils before (top row) and after (bottom row) removal of the corrosion products.*

Exposure 11 years, approximately. A, Lake Charles clay at El Vista, Tex.; B, Muck, at New Orleans, La.; C, Tidal marsh at Charleston, S. C.; D, Docas clay at Cholame, Calif.; E, Merced silt loam at Buttonwillow, Calif.

WASHINGTON, August 28, 1953.

Journal of Research of the National Bureau of Standards Vol. 51, No. 6, December 1953 Research Paper 2460

Calorimetric Properties of 41° and 122° F Polybutadienes[1]

George T. Furukawa and Robert E. McCoskey

The heat capacity of 41° and 122° F polybutadienes was measured from 15° to 330° K. The 41° F polybutadiene was found to have a higher (195° K) glass-transformation temperature than the 122° F polymer (187° K). Also, the 41° F polymer exhibited a higher degree of crystallizability than the 122° F polymer. The crystallization temperature range of the 41° F polymer was found to be 200° to 295° K and that of the 122° F polymer 200° to 270° K. The data were used to construct a smoothed table of heat capacity, enthalpy, and entropy from 0° to 330° K.

1. Introduction

Calorimetric investigations of the thermal properties of 41° and 122° F butadiene-styrene copolymers containing 8.58 weight percent of bound styrene are described in a previous paper [1].[2] The properties studied included heat capacity, enthalpy, entropy, glass transformation, and crystallization. The two copolymers, which were prepared at two different temperatures, exhibited wide differences in thermal properties. For example, the glass-transformation temperature of the 41° F copolymer was found to be 200° K and of the 122° F copolymer, 193° K. Also, the 41° F copolymer exhibited crystallization from 210° to 285° K, whereas the 122° F copolymer showed no such crystallization effects. This paper deals with similar calorimetric studies with 41° and 122° F polybutadienes, both of which have been found to undergo crystallization. The effect of the degree of crystallinity upon the heat capacity of the two polymers was investigated, and the degrees of crystallizability of the two polymers were compared. The heat-capacity measurements were made from about 16° to 330° K. The results were used to compute a smoothed table of heat capacity, enthalpy, and entropy from 0° to 330° K.

2. Apparatus and Method

The details of the calorimetric apparatus and method used have been described [1, 2]. The polymer sample was sealed in a copper container within an adiabatic calorimetric system. The container was provided with a platinum resistance thermometer, a heater, and a vane system for rapid distribution of heat. To thermally isolate the container during the calorimetric experiments, the temperature of the shield system surrounding the container was maintained the same as that of the container surface by means of differential thermocouples and shield heaters. The space surrounding the container was evacuated, and the container and the adjacent shield surfaces were polished. The electric power input was measured by using a Wenner potentiometer, and the length of the heating periods was measured by means of a timer operated on standard 60 cycles. The temperature measurements above 90° K are in accordance with the 1948 International Temperature Scale [3]; between 10° and 90° K they are on a provisional scale [4], which consists of a set of platinum resistance thermometers calibrated with a helium-gas thermometer.

The polymers were subjected to two generally different rates of cooling prior to the heat-capacity experiments in order to study in what way their heat capacity and crystallinity were dependent upon the thermal history. In one series of experiments, the polymers were cooled as rapidly as possible by immersing the calorimeter in liquid nitrogen with helium gas in the space surrounding the container. By this procedure the polymers were cooled to about 90° K in 30 min and to 80° K in an additional 30 min, and a portion of the polymer molecules was expected to be "frozen" in the higher energy states. In the second series of measurements, the polymers were cooled slowly in order to obtain as high a degree of crystallinity as practicable. By maintaining a high vacuum in the space surrounding the container, and by using different refrigerants successively, the cooling process was prolonged from a few days to 12 days.

3. Samples

The two polybutadiene samples were obtained through the courtesy of the University of Akron Government Laboratories, Synthetic Rubber Research. The 41° F polybutadiene designated MS–1045 was prepared using a low-sugar cumene hydroperoxide-redox recipe [5], and the 122° F polymer designated GL–657 was prepared by using a recipe [6] generally used for GR–S type polymers. The polymerization formulas are given in table 1.

The polymers were purified by M. Tryon, of the Rubber Section of the Bureau, by a procedure previously outlined [1]. The analysis of the samples is given in table 2. The samples were pressed into sheets ⅛ to ¼ in. thick and cut to fit between the vanes of the calorimeter containers. Before sealing the containers, the polymers were pumped at high vacuum for 3 days to remove moisture, air, and benzene. The mass of the MS–1045 sample investigated was 42.706 g, and that of the GL–657 was 47.081 g. A small quantity of helium gas was sealed with the polymers to enhance thermal equilibrium during heat-capacity experiments.

[1] The work discussed herein was performed as a part of the research project sponsored by the Reconstruction Finance Corporation, Office of Synthetic Rubber, in connection with the Government synthetic rubber program.

[2] Figures in brackets indicate the literature references at the end of this paper.

TABLE 1. *Polymerization formulas*[a]

	Polymer	
	MS–1045[b]	GL–657[c]
Polymerization temperature °F	41	122
Ingredients (parts by weight):		
Butadiene	100	100
Dodecylmercaptan	0.30	1.06
Sulfole B–8		4.3
S. F. Flakes	4.5	
Dresinate 214	0.5	
$Na_3PO_4 \cdot 12H_2O$		0.096
NaOH	0.1	
Daxad 11		0.23
$K_2S_2O_8$	0.10	
Cumene hydroperoxide	168	180
Water		
Activator (parts by weight):		
$FeSO_4 \cdot 7H_2O$	0.12	
$K_4P_2O_7$	0.17	
Dextrose	1.00	
Water	12.0	
Shortshopping agents (parts by weight):		
Hydroquinone	0.1	0.2
$NaNO_2$	0.04	
Ditertiary butylhydroquinone	0.3	
Dresinate 214	0.07	
Methanol	3.00	
Water	8.0	5.0
Final conversion %	61.4	72.6
Viscosity, ML–4	36	50

[a] The polymerization formulas were taken directly from the reports cited in footnotes b and c.
[b] Private communication from W. K. Taft, the University of Akron-Government Laboratories, to L. A. Wood, National Bureau of Standards.
[c] R. W. Laundrie, Butadiene-styrene copolymers for refractive index studies, Project P 109.74, AU–725.

TABLE 2. *Composition of the polybutadienes*[a]

	Percentage by weight	
	MS–1045	GL–657
Carbon	88.47	88.66
Hydrogen	11.160	11.180
Sulfur	0.083	0.150
Oxygen	.12	.145
Ash	.34	.057
Phenylbetanaphthylamine[b]	.10	.12

[a] Analysis by R. A. Paulson.
[b] Added after the analysis.

4. Results

4.1. 41° F Polybutadiene, MS–1045

The experimental details of heat treatment, temperature range of the measurements, and temperature drifts with the 41° F polybutadiene are summarized in table 3. The observed heat capacities are given in table 4, and the general behavior of these results are shown in the plot of figure 1. The measurements of run 1 were made after shock-cooling the polymer from room temperature to 77° K. During the course of the heat-capacity measurements, upward temperature drifts were observed from 177° to 283° K as the polymer molecules slowly transformed into states of lower energy [1]. During the shock-cooling process a certain portion of the polymer molecules failed to undergo transition to states of lower energy. When the temperature was raised to a certain range during the heat-capacity

TABLE 3. *Heat treatments and the observations with the 41° F polybutadiene, MS–1045*

Run	Treatment of samples	Temperature range of measurements	Temperature drift observations
		°K	
1	Cooled rapidly from room temperature to 77° K.	77 to 298	Upward drift from 177° to 283° K.
2	Left at room temperature for 1 day	303 to 334	No drift.
3	Cooled slowly from room temperature to 77° K over 2 days.	77 to 301	Upward drift from 180° to 280° K.
4	Cooled slowly from room temperature to 77° and then to 15° K.	15 to 88	No drift.
5	Cooled slowly from room temperature to 77° and then to 53° K.	53 to 90	Do.

TABLE 4. *Observed heat capacities with 41° F polybutadiene, MS–1045*

T	*C*	*T*	*C*
Run 1		Run 3—Continued	
°K	*abs j* ° $K^{-1}g^{-1}$	°K	*abs j* ° $K^{-1}g^{-1}$
82.40	0.5654	174.98	1.074
91.56	.6174	182.82	1.121
101.24	.6692	188.69	1.187
111.76	.7273	194.24	1.374
121.83	.7830	199.15	1.529
132.07	.8404	209.11	1.736
142.64	.8989	225.17	1.924
153.39	.9581	241.36	2.184
164.22	1.016	256.19	2.379
171.19	1.060	271.61	2.510
175.52	1.082	287.52	2.133
180.47	1.111	298.40	1.969
186.02	1.150		
191.31	1.293	Run 4	
196.37	1.416		
201.41	1.397	15.58	0.0707
209.19	1.511	17.51	.0872
219.97	1.718	19.88	.1068
233.65	1.903	21.79	.1240
249.20	2.200	23.44	.1387
263.10	2.612	25.79	.1605
276.16	2.557	28.86	.1882
290.28	2.083	32.18	.2188
		35.82	.2495
Run 2		39.18	.2782
		42.79	.3045
307.46	1.992	47.02	.3380
315.26	2.017	76.30	.5274
322.98	2.043	81.39	.5589
330.62	2.069	86.19	.5883
Run 3		Run 5	
80.14	0.5505	55.01	0.3910
87.24	.5928	59.00	.4182
96.11	.6409	64.54	.4547
105.52	.6918	70.06	.4882
115.73	.7479	74.35	.5145
126.23	.8056	78.86	.5422
136.90	.8641	83.11	.5687
147.71	.9226	87.55	.5958
158.70	.9821		
166.03	1.024		

experiments, these molecules acquired sufficient thermal energy for transition to lower energy states with the consequent liberation of heat. Prior to run 3, the polymer was cooled slowly from room temperature to 77° K over 2 days, and the results showed upward temperature drifts from 180° to 280° K. Below the glass-transformation temperature (195° K), the heat-capacity results of run 3 (polymer slowly cooled) were slightly lower than run

TABLE 5. *Heat capacity, enthalpy, and entropy of 41° F. polybutadiene, MS–1045*

T	C	$(H_T-H_{0°K})$	$(S_T-S_{0°K})$
° K	abs j ° K^{-1}g^{-1}	abs j g^{-1}	abs j ° K^{-1}g^{-1}
0	0	0	0
5	0.0034	0.0042	0.0011
10	.0256	.0662	.0089
15	.0655	.2923	.0266
20	.1081	.7280	.0514
25	.1534	1.381	.0804
30	.1983	2.261	.1123
35	.2419	3.362	.1462
40	.2829	4.675	.1812
45	.3211	6.187	.2168
50	.3570	7.882	.2524
55	.3916	9.754	.2881
60	.4247	11.80	.3236
65	.4567	14.00	.3589
70	.4881	16.36	.3939
75	.5191	18.88	.4286
80	.5499	21.55	.4631
85	.5798	24.38	.4973
90	.6083	27.35	.5313
95	.6356	30.46	.5649
100	.6624	33.70	.5982
105	.6894	37.08	.6311
110	.7169	40.60	.6639
115	.7448	44.25	.6963
120	.7725	48.05	.7286
125	.8001	51.98	.7607
130	.8276	56.05	.7926
135	.8552	60.25	.8244
140	.8830	64.60	.8560
145	.9109	69.08	.8875
150	.9379	73.71	.9188
155	.9646	78.46	.9500
160	.9922	83.35	.9810
165	1.021	88.39	1.012
170	1.050	93.56	1.043
175	1.079	98.89	1.074
180	1.108	104.4	1.105
185	1.14	----------	----------
190	1.21	----------	----------
195	1.31	----------	----------
200	1.50	----------	----------
205	1.65	----------	----------
210	1.68	----------	----------
215	1.70	----------	----------
220	1.72	----------	----------
225	1.73	----------	----------
230	1.75	----------	----------
235	1.76	----------	----------
240	1.78	----------	----------
245	1.80	----------	----------
250	1.81	----------	----------
255	1.83	----------	----------
260	1.84	----------	----------
265	1.86	----------	----------
270	1.87	----------	----------
275	1.89	----------	----------
280	1.91	----------	----------
285	1.92	----------	----------
290	1.94	----------	----------
295	1.95	----------	----------
300	1.97	----------	----------
305	1.985	352.2	2.123
310	2.000	362.2	2.156
315	2.016	372.2	2.188
320	2.033	382.3	2.220
325	2.050	392.5	2.251
330	2.067	402.8	2.283

1 (polymer rapidly cooled), with the difference increasing with temperature to a maximum of about 1 percent near the glass-transformation temperature. The upward temperature drifts from about 200° to 285° K are attributed to slow crystallization of the polymer molecules. Except for a few heat-capacity points of run 1, all experimental points in the crystallization interval were above the broken line of figure

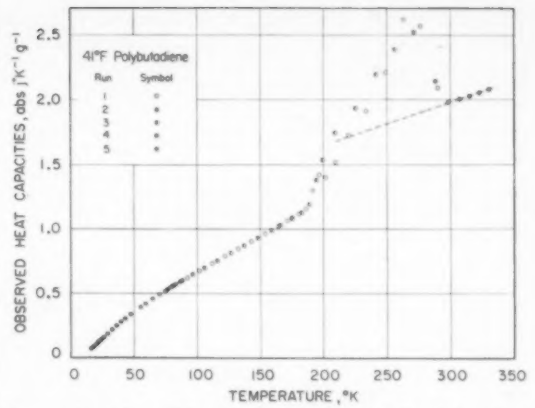

FIGURE 1. *Observed heat capacities of the 41° F polybutadiene, MS–1045.*

1. This indicates more melting than crystallization; consequently, the upward drifts observed are probably the result of the formation of new crystals and of the recrystallization of polymer near the heater, where the temperature was higher during the heating period. The broken line of figure 1 is the heat capacity of hypothetical amorphous polymer and was obtained by linearly extrapolating the heat capacity in the range 295° to 330° K to the glass-transformation temperature. This linear extrapolation of the amorphous portion of the heat capacity was made on consideration that the heat capacity of HyCar O. R.–15 [7], which does not crystallize, could be represented within 0.2 percent from 250° (just above the glass-transformation temperature) to 340° K by a linear equation. Similarly, in another noncrystallizing synthetic rubber, GR–S [8], the heat capacity from about 225° to 330° K could be represented by a quadratic equation to 0.1 percent or by a linear equation to about 0.3 percent or better.

The data of table 4 were used to construct the heat-capacity values of table 5, spaced at equal temperature intervals. The heat capacities given were based on the results with the polymer slowly cooled. From 180° to 305° K the heat-capacity values of table 5 were obtained from a large-scale plot of the observed heat capacities. In the crystallization interval (200° to 295° K) the results from the broken line were tabulated. Below 180° K and above 305° K the deviations of the observed heat capacities from empirical equations were first plotted, then the deviation curves and the empirical equations were used to obtain heat capacities at even temperatures. The heat capacities below the lower limit (15° K) of the measurements were obtained by fitting a Debye function to the observed values in the temperature range 15° to 30° K. The function used is [3]

$$C=0.2425D(88.7/T). \quad (1)$$

[3] The equation has no significance other than for extrapolation of the heat capacity.

The glass-transformation temperature of this particular sample of 41° F polybutadiene was found to be about 195° K. Above 295° K the polymer is believed to be completely amorphous.

The enthalpy and entropy of the 41° F polybutadiene were obtained by evaluating the thermodynamic relations

$$(H_T - H_{0°K} = \int_0^T C dT \qquad (2)$$

and

$$(S_T - S_{0°K} = \int_0^T C dT/T, \qquad (3)$$

respectively, where $(H_T - H_{0°K})$ and $(S_T - S_{0°K})$ are the enthalpy and entropy of the polymer relative to the absolute zero of temperature. The other symbols have their usual significance. Except below 15° K and between 180° and 305° K, eq (2) and (3) were evaluated by tabular integration, using four-point Lagrangian integration coefficients [9]. Below 15° K the Debye function (eq 1) was evaluated analytically. Between 180° and 305° K the enthalpy was obtained directly from the experimental measurements [1] by summing the energy input of run 3 (polymer was cooled slowly), in which the experiments were made continuously from 180.0093° to 301.6183° K. When corrected to the even temperature interval (180° to 305° K), the enthalpy change amounted to 247.84 abs j g^{-1}. The entropy change was obtained by summing similarly the various $C\Delta T/T_m$'s of run 3, where $C\Delta T$ is the enthalpy change of the heating interval and T_m is the midtemperature of the interval. After correcting to the temperature interval 180° to 305° K, the entropy change amounted to 1.018 abs j $°K^{-1}g^{-1}$.

4.2. 122° F Polybutadiene, GL–657

The experimental results with the 122° F polybutadiene are summarized in tables 6 and 7. Table 6 shows details of the heat treatments, temperature range of the measurements, and the drift observations. The observed heat-capacity values are given in table 7 and plotted in figure 2. When the polymer was cooled rapidly, the subsequent heat-capacity experiments (run 3) showed upward temperature drifts from 148° to 253° K. However, when the polymer was cooled slowly, the heat-capacity results (run 2) showed downward temperature drifts from 186° to 189° K and upward drifts from 220° to 265° K. These results show that in the experiments with the polymer rapidly cooled, the upward temperature drifts set in about 40 deg below the temperature at which the downward drifts began with the polymer slowly cooled. In the experiments with the 41° F polybutadiene slowly cooled over 2 days, no downward temperature drifts were observed below the glass-transformation temperature. Only upward temperature drifts were observed. Probably 2 days were not sufficient for much of the 41° F polymer to transform to lower energy states at temperatures below the glass-transformation temperature.

TABLE 6. *Heat treatments and the observations with the 122° F polybutadiene, GL–657*

Run	Treatment of sample	Temperature range of measurements	Temperature drift observations
		° K	
1	Cooled slowly from room temperature to 115° K over 3 days; then rapidly to 55° K.	55 to 90	No drift.
2	Cooled slowly from room temperature to 78° K over 12 days.	82 to 289	Downward drift from 186° to 189° K; upward from 220° to 265° K.
3	Cooled rapidly from room temperature to 79° K.	79 to 292	Upward drift from 148° to 253° K.
4	Left at room temperature for 5 days and cooled to 273° K.	274 to 336	No drift.
5	Cooled slowly to 78° K; then rapidly to 15° K.	15 to 63	Do.
6	Cooled slowly to 150° K	Heated continuously from 173 to 282 K.	Do.

TABLE 7. *Observed heat capacities of 122° F polybutadiene, GL–657*

T	C	T	C
Run 1		Run 3—Continued	
° K	*abs j ° K⁻¹g⁻¹*	° K	*abs j ° K⁻¹g⁻¹*
55.61	0.3985	164.34	1.028
57.32	.4093	175.01	1.082
59.75	.4256	181.40	1.122
62.83	.4461	185.10	1.318
65.75	.4641	189.07	1.658
68.55	.4803	192.72	1.679
72.52	.5036	196.36	1.669
77.61	.5338	200.07	1.585
82.38	.5611	211.86	1.364
87.93	.5930	229.89	1.836
		245.42	2.089
Run 2		260.48	1.973
		276.00	1.884
88.26	0.5953	287.73	1.917
99.80	.6593		
110.33	.7174	Run 4	
120.24	.7717		
130.20	.8258	277.33	1.884
140.13	.8793	282.23	1.901
150.63	.9353	287.05	1.916
161.53	.9949	291.78	1.935
171.96	1.058	296.56	1.946
180.35	1.124	301.59	1.962
185.11	1.220	306.76	1.979
188.04	1.434	312.54	1.996
190.94	1.567	318.71	2.017
194.37	1.611	324.83	2.040
198.17	1.643	331.91	2.063
201.92	1.673		
212.26	1.771	Run 5	
228.17	2.124		
242.93	2.140	16.70	0.0864
257.37	1.986	18.61	.1033
273.62	1.883	20.39	.1175
285.48	1.912	22.24	.1353
		24.47	.1560
Run 3		27.21	.1802
		29.88	.2040
83.47	0.5725	33.46	.2351
93.41	.6273	37.77	.2701
104.36	.6867	41.81	.3011
114.46	.7427	46.39	.3360
123.90	.7963	51.38	.3718
133.47	.8513	56.14	.4023
143.21	.9071	60.76	.4331
153.21	.9641		

The upward temperature drifts from 200° to 270° K are considered to arise from slow crystallization of the rubber polymer in a manner similar to the 41° F polymer described earlier. Also, the relatively high heat capacity above the broken line indicates

TABLE 8. *Heat capacity, enthalpy, and entropy of 122° polybutadiene, GL–657*

T	C	$(H_T-H_{0°K})$	$(S_T-S_{0°K})$
° K	*abs j °K⁻¹g⁻¹*	*abs j g⁻¹*	*abs j °K⁻¹g⁻¹*
0	0	0	0
5	0.0036	0.0045	0.0012
10	.0271	.0701	.0094
15	.0707	.3107	.0283
20	.1154	.7777	.0548
25	.1502	1.440	.0844
30	.2045	2.325	.1164
35	.2477	3.459	.1513
40	.2878	4.798	.1890
45	.3257	6.333	.2231
50	.3615	8.052	.2593
55	.3955	9.945	.2954
60	.4279	12.00	.3312
65	.4590	14.22	.3667
70	.4891	17.59	.4018
75	.5185	19.11	.4366
80	.5474	21.78	.4709
85	.5760	24.58	.5050
90	.6043	27.54	.5387
95	.6323	30.63	.5721
100	.6601	33.86	.6053
105	.6877	37.23	.6382
110	.7153	40.74	.6708
115	.7428	44.38	.7032
120	.7702	48.16	.7354
125	.7976	52.08	.7674
130	.8248	56.14	.7992
135	.8520	60.33	.8308
140	.8791	64.66	.8623
145	.9061	69.12	.8936
150	.9330	73.72	.9248
155	.9600	78.45	.9558
160	.9874	83.32	.9867
165	1.0153	88.33	1.018
170	1.0453	93.48	1.048
175	1.0798	98.79	1.079
180	1.12	.....	.....
185	1.24	.....	.....
190	1.54	.....	.....
195	1.63	.....	.....
200	1.66	.....	.....
205	1.68	.....	.....
210	1.70	.....	.....
215	1.71	.....	.....
220	1.73	.....	.....
225	1.74	.....	.....
230	1.76	.....	.....
235	1.77	.....	.....
240	1.78	.....	.....
245	1.80	.....	.....
250	1.81	.....	.....
255	1.83	.....	.....
260	1.84	.....	.....
265	1.86	.....	.....
270	1.87	.....	.....
275	1.886	280.4	1.885
280	1.900	289.8	1.919
285	1.915	299.4	1.953
290	1.929	309.0	1.986
295	1.944	318.7	2.019
298.16	1.953	324.8	2.040
300	1.958	328.4	2.052
305	1.973	338.3	2.084
310	1.987	348.2	2.117
315	2.004	358.1	2.149
320	2.021	368.2	2.180
325	2.039	378.3	2.212
330	2.058	388.6	2.243

more melting than crystallization. In the experiments with the polymer slowly cooled (run 2) all the points were above the broken line. However, with the polymer rapidly cooled (run 3) a low point was observed, which gave a γ-like shape to the heat

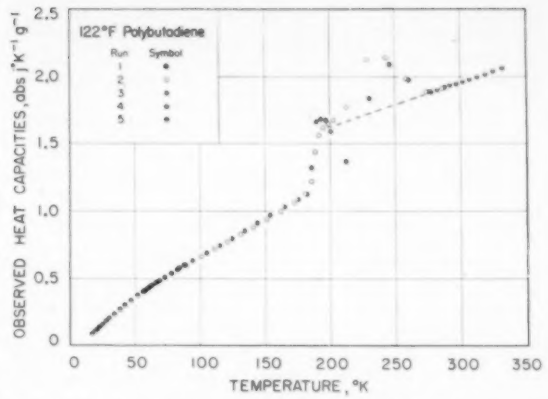

FIGURE 2. *Observed heat capacities of the 122° F polybutadiene, GL–657.*

capacity (see fig. 2). A large amount of crystallization has caused the apparent heat capacity to be relatively low.

The results of these measurements were used to compute a table of heat capacities at equally spaced temperature intervals (see table 8). The results used were those from the experiments with the polymer slowly cooled, and the procedure used in obtaining the smoothed heat capacities, including those in the crystallization interval, was similar to that with the 41° F polymer. The Debye function for the extrapolation of the data below 15° K was

$$C=0.2631D(89.5/T). \quad (4)$$

The glass-transformation temperature of this material was found to be 187° K. The crystallization range was 200° to 270° K, which is about 25 deg narrower than the 41° F polybutadiene (200° to 295° K). Above 270° K, where the heat capacity is smooth, the polymer is believed to be amorphous.

The enthalpy and entropy of the 122° F polybutadiene were evaluated by a procedure similar to the 41° F polymer. The values are given in table 8.

4.3. Reliability of the Results

The reliability of the heat-capacity measurements with these polymers is difficult to evaluate because of the nonreproducibility of the physical state from experiment to experiment. The heat-capacity measurements made previously with normal materials of low molecular weight are believed to be accurate to 0.2 percent [10]. The results with these polymers show considerable scattering in the temperature range where temperature drifts occur, as the results are dependent upon how long temperature equilibrium is awaited. In the experiments where temperature drifts occurred, although no attempt was made to wait until complete temperature equilibrium was

reached, the general nature of the heat capacity is believed to be preserved. In the temperature range where no temperature drift occurred, the heat-capacity results obtained for a given heat treatment are believed to be accurate within 0.2 to 0.3 percent.

The enthalpy and entropy values given in tables 5 and 8 are believed to be generally accurate to 0.5 percent.

5. Discussion

The results of these experiments show that by changing the polymerization temperature of polybutadiene from 41° to 122° F the glass-transformation temperature was lowered from 195° to 187° K. This behavior is similar to that observed with 41° and 122° F butadiene-styrene copolymers containing 8.58 weight percent of bound-styrene [1] previously reported. Also, the temperature range of crystallization has become narrower in the 122° F polymer (200° to 270° K). The crystallization temperature range of 41° F polymer was found to be from 200° to 295° K. In the butadiene-styrene copolymers [1], crystallization took place in the 41° F copolymer but was absent in the 122° F copolymer.

In table 9 the enthalpy changes from 175° to 305° K are given for both polymers. The results listed are from experiments in which the polymers were given various prior heat treatments, as described earlier. Slight adjustments have been made in the original experimental enthalpy in order that the temperature range be the same in both polymers. In the 41° F polymer the enthalpy changes between shock-cooled and annealed differ by only 5.51 abs j g^{-1}. In the case of the 122° F polybutadiene, the difference is 12.07 abs j g^{-1}. The enthalpy changes obtained for the 41° F polybutadiene for this temperature interval are much greater than that of the 122° F polybutadiene. These results seem to indicate that the 41° F polymer has a higher crystallizability than the 122° F polymer. The integrated enthalpy change was obtained by tabular integration of the heat capacity given by the hypothetical amorphous curve. The comparison of the enthalpy change in the 122° F polymer when shock-cooled with the integrated value indicates that the amorphous condition was practically frozen-in. On the other hand, a similar comparison of the 41° F polymer would indicate that even upon shock-cooling considerable crystallization took place.

TABLE 9. *Comparison of the enthalpy changes of 41° and 122° F polybutadienes from 175° to 305° K*

	Polybutadiene	
	41° F	122° F
	abs j g^{-1}	*abs j g^{-1}*
Shock-cooled	247.79	227.59
Annealed	253.30	239.66
Integrated (amorphous)	220.80	225.58
Annealed minus integrated	32.50	13.88

In the investigation of the 41° F butadiene-styrene copolymer [1] of 8.58 weight percent of bound styrene the enthalpy change difference of the annealed and integrated results amounted to about 16 to 19 abs j g^{-1}. In this investigation the 41° and 122° F polybutadienes gave 33 and 14 abs j g^{-1}, respectively. Bekkedahl and Matheson [11] reported 16.71 abs j g^{-1} for the heat of fusion of natural rubber, which indicates that 41° F polybutadiene has a higher crystallizability than natural rubber.

The authors are indebted to W. Bruenner, G. J. King, and M. L. Reilly for assisting with some of the experimental work and computation, to M. Tryon for purifying the samples, and to R. A. Paulson for the analysis.

6. References

[1] G. T. Furukawa, R. E. McCoskey, and G. J. King, J. Research NBS **50,** 357 (1953) RP2425.
[2] R. B. Scott, C. H. Meyers, R. D. Rands, Jr., F. G. Brickwedde, and N. Bekkedahl, J. Research NBS **35,** 39 (1945) RP1661.
[3] H. F. Stimson, J. Research NBS **42,** 209 (1949) RP1962.
[4] H. J. Hoge and F. G. Brickwedde, J. Research NBS **22,** 351 (1939) RP1188.
[5] Private communication from W. K. Taft, The University of Akron-Government Laboratories, to L. A. Wood, National Bureau of Standards.
[6] R. W. Laundrie, Butadiene-styrene copolymers for refractive index studies, Project P 100.74, AU–725.
[7] N. Bekkedahl and R. B. Scott, J. Research NBS **29,** 87 (1942) RP1487.
[8] R. D. Rands, Jr., W. J. Ferguson, and J. L. Prather, J. Research NBS **33,** 63 (1944) RP1595.
[9] Tables of Lagrangian Interpolation Coefficients (Columbia University Press, New York, N. Y., 1944).
[10] G. T. Furukawa, D. C. Ginnings, R. E. McCoskey, and R. A. Nelson, J. Research NBS **46,** 195 (1951) RP2191.
[11] N. Bekkedahl and H. Matheson, J. Research NBS **15,** 503 (1935) RP844.

WASHINGTON, July 30, 1953

Thermal Degradation of Tetrafluoroethylene and Hydrofluoroethylene Polymers in a Vacuum[1]

S. L. Madorsky, V. E. Hart, S. Straus, and V. A. Sedlak *

Teflon and tetrafluoroethylene photopolymers, on pyrolysis in a vacuum at 423.5° to 513.0° C, yield almost 100 percent of monomer. The rate of formation of monomer at any given temperature follows a first-order reaction and is independent of the method of preparation of polymer or its initial average molecular weight. The activation energy was determined by a pressure method and a weight method, and a value of 80.5 kcal was found by both methods. A preliminary heating of Teflon in air at 400° to 470° C did not change appreciably its rate of degradation into monomer when it was subsequently heated in a vacuum. Polyvinyl fluoride, 1,1-polyvinylidene fluoride, and polytrifluoroethylene were pyrolyzed in the range 372° to 500° C. The volatiles consisted in all cases of HF and a wax-like material consisting of chain fragments of low volatility. Polyvinyl fluoride and polytrifluoroethylene degrade to complete volatilization, whereas 1,1-polyvinylidene fluoride becomes stabilized at about 70-percent loss of weight. The rate-of-volatilization curves indicate a first-order reaction for polyvinyl fluoride, a zero-order reaction for trifluoroethylene, and an undetermined order for 1,1-polyvinylidene fluoride. The order of thermal stability for these polymers, as compared with polymethylene, is as follows: Polyvinyl fluoride < polymethylene < polytrifluoroethylene < 1,1-polyvinylidene fluoride < polytetrafluoroethylene.

1. Introduction

There is very little in the literature on the thermal degradation of fluorocarbons, in general, or on fluorocarbon polymers, in particular. Swarts [1],[2] Rogers and Cady [2], and Steunenberg and Cady [3] pyrolyzed a number of low molecular weight fluorocarbons in the presence of a glowing platinum filament. Lewis and Naylor [4] pyrolyzed polytetrafluoroethylene at 600° and 700° C and at pressures varying from 5 to 760 mm Hg. The volatiles consisted of C_2F_4, C_3F_6, and C_4F_8. In this work a study was made of the thermal degradation of a series of fluoropolymers to determine their relative thermal stability, the nature and relative amounts of the volatiles given off, and the rates of thermal degradation. This series includes polytetrafluoroethylene (Teflon) $[—C_2F_4—]_n$, polyvinyl fluoride $[—C_2H_2F—]_n$, 1,1-polyvinylidene fluoride $[—C_2H_2F_2—]_n$, and polytrifluoroethylene $[—C_2HF_3—]_n$.

2. Materials Used

The polytetrafluoroethylene was a commercial Teflon tape, 0.07 mm thick. The polyvinyl fluoride and the polyvinylidene fluoride were prepared by E. I. du Pont de Nemours & Co. The polytrifluoroethylene was prepared from the monomer by photopolymerization at −20° C in the presence of di-*tert*-butyl peroxide and then heated overnight at 105° C.[3] Analyses for C, H, and F in the hydrofluorocarbon polymers are given in table 1.

TABLE 1. *Chemical analysis of hydrofluorocarbon polymers*

Polymer	Analysis						Total found
	Carbon		Hydrogen		Fluorine		
	Theoretical	Found	Theoretical	Found	Theoretical	Found	
	%	%	%	%	%	%	%
Polyvinyl fluoride	52.2	52.0	6.6	6.5	41.2	41.0	99.5
Polyvinylidene fluoride	37.5	37.4	3.2	3.2	59.3	58.5	99.1
Polytrifluoro ethylene	29.0	29.7	1.5	1.5	69.5	68.0	99.2

3. Apparatus and Experimental Procedure

The investigation of thermal degradation of this series of polymers was carried out along two lines.

1. *Pyrolysis in a vacuum and fractionation and analysis of the volatile products.* This procedure was followed for all of the polymers, except Teflon, using a Dewar-like molecular still, which has been described in previous papers [6, 7]. A 20- to 30-mg sample, either in solution or in finely divided from, was spread on a platinum tray. Size of the sample was limited so as to prevent loss of material by spattering during pyrolysis. The sample was first subjected to a preliminary heating in a vacuum for 2 hr at about 150° C in order to eliminate the solvent and adsorbed gases. It was then brought to the temperature of pyrolysis by heating for 45 min, and this temperature was then maintained for 20 min. The following fractions were collected: I, residue; II, a waxlike material, nonvolatile in a vacuum at room temperature; III, a fraction volatile at room temperature; IV, a gaseous fraction noncondensable at the temperature of liquid nitrogen. Weights of all four fractions were determined, and, in the case of fractions III and IV, chemical composition was determined by means of the mass spectrometer. To facilitate mass-spectrometric analysis, fraction III was further subdivided by distillation into a light fraction, IIIA, and a heavy fraction IIIB. For Teflon, which requires a higher temperature of pyrolysis and which yields almost 100 percent of monomer, a different type of apparatus was used.

2. *Rate of volatilization of polymers in a vacuum.* This property was investigated in the case of all polymers by a weight method, and in the case of Teflon, also by a pressure

*Present address: U. S. Public Health, Atlanta, Ga.

[1] This work was performed as a part of the research project on high-temperature-resistant polymers sponsored by the Ordnance Corps, Department of the Army. The paper was presented at the 124th meeting of the American Chemical Society, Polymer Chemistry Division, September 1953.

[2] Figures in brackets indicate the literature references at the end of this paper.

[3] The monomer and polymer were prepared by R. E. Florin and D. W. Brown, of the Polymer Structure Section of the National Bureau of Standards. The monomer was prepared by the method of Park, Sharrah, and Lacher [5].

method. The spring-balance apparatus used in the weight method is described in a previous paper [8]. The sample was limited to 5 to 8 mg in order to avoid loss by spattering during the heating. It was placed in a platinum crucible, and the crucible was suspended by means of a 3-mil tungsten wire from a sensitive tungsten-spring balance, enclosed in a Pyrex housing, which could be evacuated to about 10^{-6} mm Hg. The crucible was heated externally, and loss of weight of the sample was determined by observing a crossline on an extension of the spring.

An apparatus for the study of rate of thermal degradation of Teflon by the pressure method is shown diagrammatically in figure 1. In this figure, A is a quartz tube, 3 cm long, 6-mm inside diameter, and 8-mm outside diameter, closed at one end. This tube fits into a larger quartz tube, B, closed at one end. Tube B is sealed to a Pyrex ground joint, C, by means of a graded seal. Samples weighing from 5 to 345 mg were used in this apparatus. If spattering occurred during pyrolysis, it would not result in loss of material in this apparatus. This apparatus was also used in the study of pyrolysis of Teflon.

A cylindrical electric heater, not shown in the figure, was designed to maintain a uniform temperature at its center for a distance of about 4 cm. This heater could be moved in a fixed horizontal position, so that tube A fitted approximately in the center of the heater muffle. An a-c 110-v current was fed to the heater through a voltage stabilizer and was controlled by variable resistances. The temperature was measured by means of a platinum versus platinum-10 percent rhodium thermocouple fixed permanently in the muffle of the heater, so that when the heater was moved in position for pyrolysis, the junction of the thermocouple came in contact with the closed end of tube B. The temperature inside of tube A was calibrated by means of an additional platinum versus platinum-10 percent rhodium thermocouple placed temporarily inside of this tube. There was no appreciable temperature gradient throughout the length of tube A. Temperature fluctuations of both thermocouples were within about ± 0.5 deg C.

Tube A, containing a weighed specimen of Teflon, was placed in tube B. The apparatus was evacuated to about 10^{-3} mm Hg by means of an oil pump, not shown in the figure, and a liquid-nitrogen trap, P. Preheating of a sample of Teflon in a vacuum at about 300° to 350° C for 48 hr resulted in no appreciable loss in weight. The heater, which had been maintained overnight at the operating temperature, was then moved into position around tube B. It took 3 to 5 min for the temperature of the sample to reach a constant value. At the termination of an experiment, the heater was removed quickly from the apparatus.

During pyrolysis the apparatus was cut off from the evacuation pump by means of stopcock D, while a mercury-diffusion pump, E, remained in operation. This pump was effective in removing the volatiles from the pyrolysis zone, against a back pressure of 25 mm. The volume between this pump and stopcock D was calibrated.

Rates of volatilization of Teflon were determined from the pressure developed in the calibrated volume. The pressure was measured at time intervals by means of a multiplying manometer, F, containing a low-vapor-pressure silicone oil in the left arm of the manometer on top of a mercury column. The manometer was calibrated by means of a three-scale McLeod gage, reading to 25 mm Hg, with a precision of 0.2 percent. The scale on the multiplying manometer could be read with a precision of 0.02 mm. Pressures up to 6 mm were measured.

A sample of the fraction noncondensable at the temperature of liquid nitrogen, corresponding to fraction IV when the Dewar-like apparatus is used for pyrolysis, was obtained in the following manner. Liquid nitrogen was placed around trap L. The condensable material, corresponding to fraction III, condensed in this trap, while fraction IV remained suspended in the space between pump E and stopcock D. Stopcock H over tube G was closed, and the tube was sealed off at K. The contents of tube G were analyzed in the mass spectrometer. The weight of fraction IV was determined from its pressure, total volume, and analysis.

To obtain a sample of fraction III for analysis, the system was evacuated while trap L was still immersed in liquid nitrogen. With stopcock D closed, fraction III was then allowed to expand into the apparatus by removing liquid nitrogen from around trap L. Fraction III was then sampled in tube G′ by closing stopcock H′ and placing liquid nitrogen around G′ while the sample tube was sealed off at K′. Weight of fraction III was determined from its pressure, total volume and analysis.

In some experiments it was found expedient to collect the entire fraction III and to weigh it. This was done by collecting it in one of the weighed tubes, M, provided with ground joints, O. Liquid nitrogen was placed around the lower part of M and held there until condensation was complete. The tube was then sealed at N, without melting it off, and subsequently weighed. Repeated experiments showed a good check between the two methods of determining total weight of fraction III.

The residue, fraction I, was weighed in tube A. A wax-like material, fraction II, appeared in some experiments as a deposit in the cold part of tube B, just outside the heater. The weight of this fraction was determined by subtracting the sum of weights of fractions III and IV from the total loss of weight of the sample. In cases where fraction II did not appear, there was a good balance between total weight of all fractions and original weight of sample.

4. Pyrolysis of Teflon

Results of pyrolysis of Teflon are shown in table 2. This table gives also, in the last column, the results of studies of rates of thermal degradation. The experiments were carried out in the pressure apparatus shown in figure 1 and are marked P in column 1 of

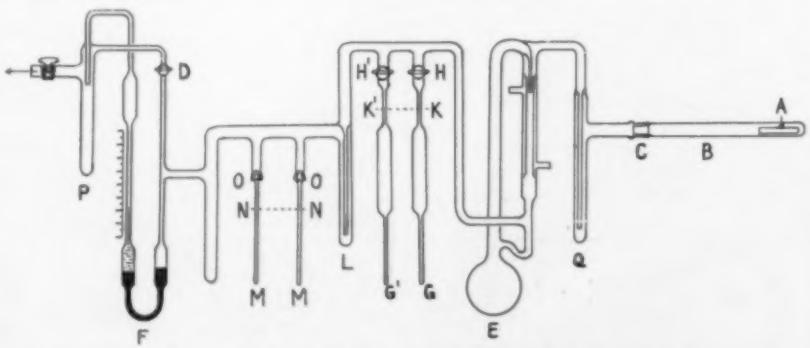

FIGURE 1. *Apparatus for the study of rates of thermal degradation of polymers by the pressure method.*

TABLE 2. *Experimental data on thermal degradation of Teflon by the pressure and weight methods*

Method employed *	Temperature	Duration	Weight of sample	Total loss in weight	Rate of volatilization
	° C	min	mg	%	%/min
P	423.5	337	305.7	0.5	0.00152
P	434.5	252	345.3	.9	.00368
P	450.0	332	99.7	4.4	.0136
P	454.0	108	210.5	1.8	.0170
P	474.5	82	57.4	6.4	.0806
W	480.0	420	6.45	46.7	.118
P	480.5	142	49.6	17.6	.1364
W	490.0	360	7.01	61.8	.240
P	496.5	56	140.3	19.6	.3887
P	499.0	220	7.73	63.4	.465
W	500.0	445	7.05	93.1	.490
W	510.0	230	6.93	91.5	.952
P	510.5	149.	5.53	76.0	.956
P	513.0	173	5.25	90.1	1.264

* P and W refer to experiments carried out by the pressure and weight methods, respectively.

table 2. There was no wax-like (fraction II) deposit in any of these experiments. Fraction IV, on the average, amounted to 0.1 mole percent of the total volatilized part and consisted of CO. Thus fraction III is practically equal to total loss in weight given in column 5 of table 2. Teflon retains its original shape until about 50 percent of volatilization. Beyond this point it softens and slumps.

A method of comparing the thermal stability of a number of polymers is described in previous papers [7, 9]. In this work the thermal stability of Teflon is shown in figure 2, compared with that of hydrofluorocarbon polymers and polymethylene. In the case of Teflon, the time required to heat a sample to the operating temperature was only 3 to 5 min as compared with 45 min for the other polymers that were pyrolyzed in the Dewar-like apparatus. In order to put the thermal-stability curve for Teflon on a comparable basis with the other curves, it was moved 15° C to the left. This adjustment was made on the basis of experiments with polystyrene and polytrifluoroethylene in the Dewar-like apparatus and the pressure apparatus.

In one experiment a sample of about 100 mg of Teflon was heated in four consecutive steps to almost complete volatilization. In view of the large size of the sample, the volatiles were condensed during pyrolysis in trap Q, figure 1, by means of liquid nitrogen to insure their complete removal from the hot zone. However, when collecting samples for weighing or for analysis, or when evacuating the apparatus between steps, trap Q was maintained at room temperature. After each step, samples from fractions III and IV were collected for analysis in tubes G and G′, respectively (fig. 1). Total weight of fraction III was obtained by collecting it in one of the tubes M and weighing. Allowance was made for the amount of fraction III collected in tube G. Results of the step-experiment are shown in table 3. Fraction II appears only in the last step, where the cumulative volatilization was 93.7 percent. In all the pressure experiments shown in table 2, except the last one, maximum volatilization was 76 percent; and fraction II was not observed in these experiments.

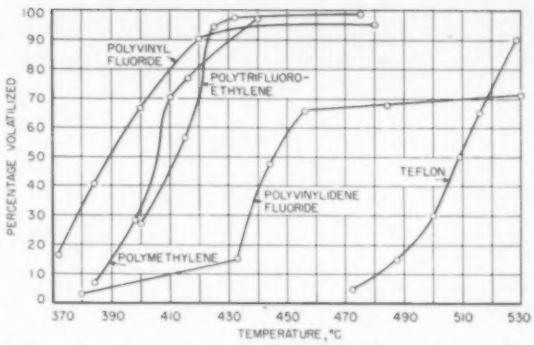

FIGURE 2. *Relative thermal stability of Teflon, polymethylene and hydrofluoroethylene polymers.*

TABLE 3. *Pyrolysis of Teflon in consecutive 60-minute steps, and mass-spectrometer analysis of the volatile products*

Temperature	Cumulative volatilization based on original sample	Fractions based on volatilized part for each step			Mass-spectrometer analysis of fractions III and IV combined, for each step				
		II	III	IV	C_2F_4	C_3F_6	SiF_4	CO_2	CO
° C	%	%	%	%	*Mole %*	*Mole %*	*Mole %*	*Mole %*	*Mole %*
504	23.2	0	99.97	0.03	96.8	2.9	0	0.2	0.11
509	47.9	0	99.98	.02	96.9	2.7	.1	.2	.07
517	71.4	0	99.95	.05	96.0	3.0	.4	.4	.18
538	93.7	8	91.73	.27	86.8	6.4	3.2	2.6	1.03

In the last experiment, at 513.0° C, where volatilization was 90.1 percent, the weight of the sample was small; and, if a fraction II appeared, it was too small to be detected.

Results of mass-spectrometer analysis are also shown in table 3. The CO shown in this table appeared as fraction IV, and the rest appeared as fraction III. As seen from this table, composition of the volatiles did not vary up to at least 71.4 percent of volatilization. The SiF_4, CO_2, and CO might have resulted from oxygen in the polymer or, most likely, from a reaction between Teflon and quartz [10].

5. Rates of Volatilization of Teflon

5.1. Determination by the weight method

Experimental data on rate experiments with Teflon tape in the spring-balance apparatus are shown in table 2. The weight experiments are marked W in the first column of this table. In figure 3 the rates are plotted in percentages of the original sample per minute against percentages volatilized. By extrapolating the straight lines to zero volatilized, the initial rates are obtained. These initial rates are shown in the last column of table 2 (for experiments marked W).

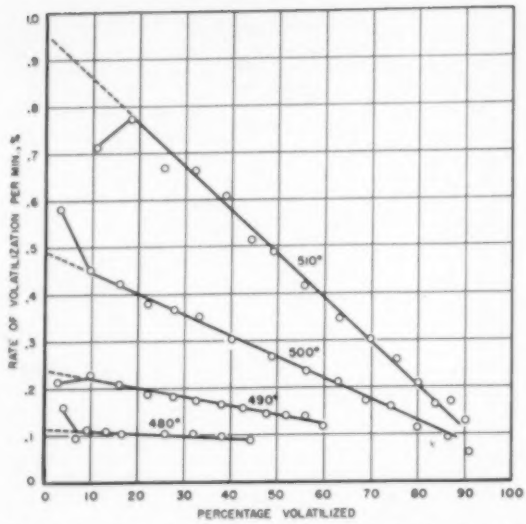

FIGURE 3. *Rate of thermal degradation of Teflon by the weight method, as a function of percentage of volatilization.*

5.2. Determination by the pressure method

Inasmuch as Teflon yields, on pyrolysis, mainly the monomer and a small percentage of other products, all in constant proportion and volatile at room temperature, the rate of volatilization can be obtained from a curve in which pressure of the gas in a fixed volume is plotted against time. Results of a series of rate experiments in the pressure apparatus are shown in the last column of table 2. An example of a pressure-time curve is shown by the curved line in figure 4 for a rate experiment made at 513° C. This experiment is shown in table 2 as the last experiment of the series.

The condition for a first-order reaction is that the plot of $\ln(a-x)$, where $(a-x)$ is the residue, against time, t, is a straight line [11]. In such a plot, rate of reaction, k, is the slope of the straight line, and can thus be evaluated. The straight line in figure 4 was obtained by plotting log of residue, calculated in terms of pressure, against time for the 513.0° experiment. Using such curves as shown in figure 4, the rates shown in the last column of table 2 were obtained for the experiments marked P.

To determine the effect of heating Teflon in air on rates of volatilization, samples were heated in air at 400°, 425°, and 450° C. The amounts volatilized were about the same as in a vacuum. When the samples were heated at 470°, the amount volatilized was slightly greater in air than in a vacuum. The residues from air-heated samples were pyrolyzed in a vacuum. The behavior of these residues, with regard to rate and products of volatilization, was about the same as for original Teflon.

The effect of thickness of the Teflon specimen on rate of volatilization in a vacuum was determined by

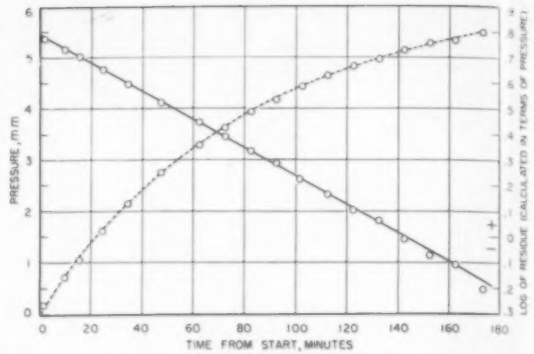

FIGURE 4. *Rate of thermal degradation of Teflon at 513.0° C by the pressure method.*

....., Time versus pressure plot; _____, time versus log of residue plot.

the following experiment. A 1.3-mm cube of Teflon was pyrolyzed at 514.5° for 133 min. Total volatilization was 78.3 percent, and the rate was the same as for tape Teflon pyrolyzed under similar conditions. In another experiment, a 1.9-mm cube of Teflon was pyrolyzed at 495°. Initially, the rate was slow, but it soon reached the value for tape Teflon.

Some photopolymers of tetrafluoroethylene were prepared [12] by irradiating the monomer with ultraviolet light in the presence of $(CF_3)_2Hg$, benzoyl peroxide, CF_3I, and di-*tert*-butyl peroxide as catalysts; also in the absence of a catalyst. On pyrolysis in a vacuum, these polymers had the same rates of volatilization as the tape Teflon.

The activation energy is obtained by plotting logarithms of rate versus inverse of absolute temperature. This plot is shown in figure 5 for the weight and the pressure experiments. All the points fall on a straight line. Multiplying the slope of this line by $2.303R$, where R is the gas constant, 1.987 cal/deg, a value of 80.5 kcal is obtained, which is the activation energy for the thermal degradation of Teflon. The frequency factor, A, as calculated by means of Arrhenius' equation, has a value of 4.7×10^{18}, when rates are expressed in fraction per second.

6. Pyrolysis of Polyvinyl Fluoride, Polyvinylidene Fluoride, and Polytrifluoroethylene

Pyrolysis of these polymers was carried out in the Dewar-like molecular still. Experimental details are shown in table 4. The gaseous fraction, IV, amounted in all cases to less than 0.1 percent of the total volatilized part. Mass-spectrometer analysis showed it to consist of hydrogen and carbon monoxide. The less volatile fraction, III, was found on mass-spectrometer analysis to consist, in the cases of polyvinyl and polyvinylidene fluorides, mainly of SiF_4, H_2O, and some unidentified hydrofluorocarbon fragments. In the case of polytrifluoroethylene, this fraction, in addition to SiF_4 and H_2O, contained some CO_2.

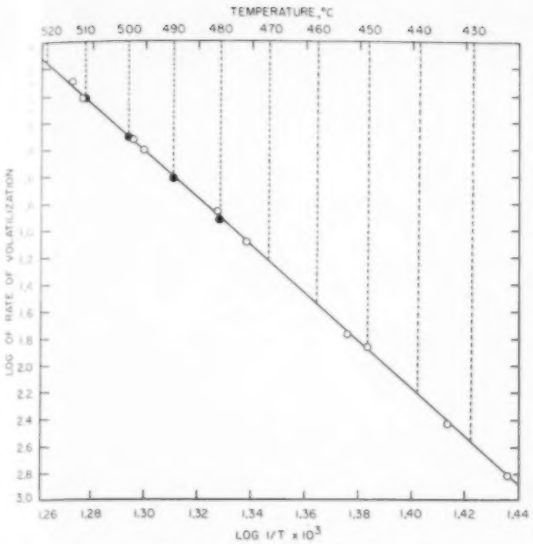

FIGURE 5. *Activation energy slope for the thermal degradation of Teflon.*

●, Weight method; ○, pressure method.

TABLE 4. *Pyrolysis of hydrofluorocarbon polymers* [a]

Experiment	Weight of sample	Temperature	Total volatilized part	Fraction III (HF)—	
				Based on volatilized part	Based on original sample
	mg	°C	%	%	%
Polyvinyl fluoride					
1	22.8	372	16.5	49.7	8.2
2	21.8	385	40.7	37.3	15.2
3	26.7	400	66.4	28.2	18.7
4	18.8	420	90.4	.....	.....
5	26.2	480	95.3	27.5	26.2
Polyvinylidene fluoride					
1	26.1	380	3.7	.....	.....
2	21.3	433	15.2	41.4	6.3
3	19.6	444	47.6	51.5	24.5
4	29.6	456	65.5	.....	.....
5	29.2	484	67.5	.....	.....
6	27.1	530	71.0	48.0	34.2
Polytrifluoroethylene					
1	23.7	400	27.4	8.0	9.0
2	25.5	415	56.5	5.3	12.3
3	17.1	425	94.4	.....	.....
4	23.5	432	97.7	5.7	23.0
5	34.8	475	98.7	.....	.....

[a] Duration of each experiment—45 minutes of heating to pyrolysis temperature, followed by 30 minutes of pyrolysis at this temperature.

The SiF_4 and H_2O are due to a reaction between HF, resulting from pyrolysis, and SiO_2 in the glass apparatus. This reaction can take place at room temperature in the presence of a trace of H_2O. Formation of H_2SiF_6 from HF and SiF_4 is possible, but, under conditions of vacuum and insufficient amount of H_2O, hydrofluorosilicic acid tends to decompose back into HF and SiF_4. Pyrex also contains some B_2O_3, which might react with HF, but there was no evidence in the mass-spectrometer analysis of the presence of BF_3. Aluminum oxide, ordinarily present in the glass, does not react appreciably with HF at room temperature.

The CO_2 found in fraction III from polytrifluoroethylene could not be explained on the basis of a reaction between fluorocarbon and SiO_2 of the glass. According to White and Rice [10] such a reaction takes place at elevated temperatures, and in this case the polymer was in contact during pyrolysis with platinum, and the polymer fragments were in contact with glass at low temperatures. It is possible that the polytrifluoroethylene contained some oxygen as a part of its structure. This oxygen, on reacting with the polymer, could give CO_2. No analysis for oxygen in the original polymer was made because of the difficulty involved in such analysis in the presence of fluorine. The fluorocarbon tends to react with the glass container at the elevated temperature employed in analysis, and CO_2 results from such a reaction. The CO detected in fraction IV from pyrolysis of hydrofluorocarbon polymers could come from oxygen as an impurity.

Fraction III was calculated in the case of all three polymers to HF on the basis of SiF_4 content in the volatiles. This fraction is shown in the last two columns of table 4 in weight percent of the total volatilized part and in weight percent of sample. Fraction II consisted of a nonvolatile light-brown wax-like deposit, soluble in acetone. Because fraction IV was only about 0.1 percent, fraction II, in percentage of total volatilized part, can be taken as the difference between 100 and the percentage of fraction III, in terms of volatilized part, given in table 4. Mass-spectrometer analysis of fraction III indicated the presence of hydrofluorocarbon molecules of molecular weight up to 150. However, in calculations of HF as fraction III, these hydrofluorocarbon fragments were included in fraction II because their nature could not be identified. Judging from results of pyrolysis of other polymers, in the temperature range of 370° to 430° C [7, 9], fraction II from the hydrofluoropolymers should have an average molecular weight of about 600 to 700. The residue, fraction I, from all three polymers appeared light brown during the early stages of degradation and dark brown toward the end. In the case of polyvinylidene fluoride, the residue, above 50 percent of volatilization, appeared black.

As can be seen from table 4, polyvinyl fluoride and polytrifluoro ethylene volatilize almost 100 percent. Polyvinylidene fluoride, however, seems to become stabilized at around 65 percent of volatilization. When the temperature of pyrolysis was raised from 456° to 530° C, the additional loss in weight was only 5.5 percent. In one experiment in the pressure apparatus a 69.3-mg sample of polyvinylidene fluoride was heated in a vacuum from room temperature to 650° C in 80 min. Total loss by volatilization was

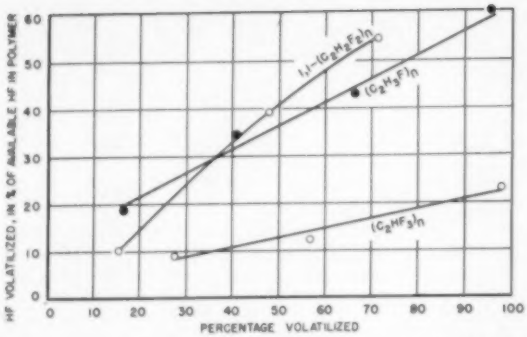

FIGURE 6. *Yield of* HF, *in percentage of total available* HF *in the polymer, as a function of total percentage of volatilization from the polymer.*

76.1 percent. The residue was further heated in the apparatus for 30 min by means of a Meker burner, applied to the outer tube B (fig. 1). Additional loss in weight was 1.5 percent of the original sample. The residue resembled coke in hardness and appearance. In another experiment a 78.9-mg sample of polyvinylidene fluoride was heated gradually in the same apparatus from room temperature to 500° during 2 hr and then kept at 500° for 1 hr. Loss of weight by volatilization was 70.3 percent. Chemical analysis showed that the residue still contained 1.7 percent of H and 12.6 percent of F by weight.

Relative thermal stability curves for the three hydrofluorocarbon polymers are shown in figure 2, in comparison with similar curves for Teflon and polymethylene. The polymethylene curve is based on pyrolysis experiments made in the Dewar-like apparatus at five temperatures. Experimental conditions were about the same as in the case of the hydrofluorocarbon polymers. The polymethylene was a nonbranched, high-molecular weight polymer of the same stock that was used by Mandelkern and associates [13] in their study of intrinsic viscosity.

Loss of HF from the three hydrofluorocarbon polymers during pyrolysis, in percentage of available HF in the polymer, is plotted against percentage of volatilization in figure 6.

7. Rates of Volatilization of Hydrofluorocarbon Polymers in a Vacuum

In view of the complex nature of the thermal degradation of polyvinyl fluoride, polyvinylidene fluoride, and polytrifluoroethylene, involving splitting off of HF, in addition to scissions of the chain, activation energies would be of little significance. However, the shape of the rate curves might be of interest as revealing details of the mechanism of thermal degradation. One rate curve for each of these polymers is shown in figure 7. The important aspect of these curves is not their relative rate, for this is shown in figure 2, but their shape. The polyvinyl-fluoride curve beyond 19 percent of volatilization resembles that of a first-order reaction, whereas the polytrifluoroethylene curve resembles that of a zero-order reaction, at least in the range 25 to 80 percent of volatilization. The rate curve for polyvinylidene fluoride is conditioned primarily by the stabilization effect, above 50 percent of volatilization.

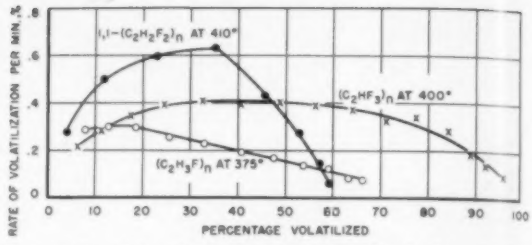

FIGURE 7. *Rates of thermal degradation of hydrofluoroethylene polymers, as a function of percentage of volatilization.*

8. Discussion of Results

8.1. Teflon

In considering the mechanism of thermal degradation of Teflon, the following experimental facts should be borne in mind: The monomer yield is almost 100 percent; the material softens and slumps above about 50 percent of volatilization; the reaction is of first order; and the rate of volatilization is very likely independent of chain length, because Teflon, tetrafluoroethylene photopolymers, and air-heated Teflon all had the same rates of volatilization and the same volatile products.

On the basis of these facts, a mechanism involving unzipping of monomer units at free-radical ends of chains is assumed. The absence of fraction II would seem to indicate that the kinetic chain length is very long, so that once unzipping is initiated, it continues in most cases to the end of the molecule. Initiation may take place when free radicals form either through breaking off of foreign elements, or groups of elements, at the chain ends, or when a break occurs in the chain due to thermal agitation. Such thermal breaks are more likely to occur in the long chains than in the short chains, and result in free-radical chain ends. The general trend during pyrolysis is for the average chain length to become shorter, as indicated by the fact that the residue softens at about 50 percent volatilization. On the other hand, the shorter the chains, the greater will be the tendency for their recombination at their free-radical ends.

8.2. Hydrofluorocarbon polymers

The substitution of one or more hydrogen atoms for fluorine on the chain changes radically the nature of the polymer. Unlike polytetrafluoroethylene, none of the hydrofluorocarbon polymers yield any appreciable amount of monomer. Instead of monomer, the volatiles consist of HF and chain fragments of

various sizes. The following mechanism is suggested. When HF breaks off, a double-bond forms in the chain at that point. A break in the chain may then occur at a C—C bond in β-position to this double bond. This break, as in polyethylene, results in one end of the break becoming saturated and the other end forming a double bond. In polyvinylidene fluoride, where there is more available HF, double bonds will form in the chain at an accelerated rate until they appear in conjugated position. This causes a lesser degree of chain scissions and the chain becomes stabilized. The yield of fraction III (HF), in percentage of volatilized part or in percentage of sample (table 4), is greater from polyvinylidene fluoride than from polyvinyl fluoride, which is to be expected. However, in percentage of total available HF on the chains, the yield of HF is about the same (fig. 6).

In the case of polytrifluoroethylene, the amount of HF liberated is small as compared with polyvinyl and polyvinylidene fluorides (fig. 6). It seems that an abundance of fluorine on the polymer chain is less favorable to splitting off of HF than a similar abundance of hydrogen. Discoloration of fraction II and of the residue in all three polymers is probably due to runs of conjugated double bonds, the same as was found in the pyrolysis of polyvinyl chloride [14]. Discoloration was found more pronounced in the case of polyvinylidene fluoride than in the cases of the other two hydrofluorocarbon polymers.

9. References

[1] F. Swarts, Bul. soc. chim. Belg. **42,** 114 (1933).
[2] G. C. Rogers and G. H. Cady, J. Am. Chem. Soc. **73,** 3513 (1952).
[3] R. K. Steunenberg and G. H. Cady, J. Am. Chem. Soc. **74,** 4165 (1952).
[4] E. E. Lewis and H. A. Naylor, J. Am. Chem. Soc. **69,** 1968 (1947).
[5] J. D. Park, M. L. Sharrah, and J. R. Lacher, J. Am. Chem. Soc. **71,** 2339 (1949).
[6] S. L. Madorsky and S. Straus, J. Research NBS **40,** 417 (1948) RP1886; Ind. Eng. Chem. **40,** 848 (1948).
[7] S. L. Madorsky, S. Straus, D. Thompson, and L. Williamson, J. Research NBS **42,** 499 (1949) RP1989; J. Polymer Sci. **4,** 639 (1949).
[8] S. L. Madorsky, J. Polymer Sci. **9,** 133 (1952).
[9] S. Straus and S. L. Madorsky, J. Research NBS **50,** 165 (1953) RP2405.
[10] L. White, Jr., and O. K. Rice, J. Am. Chem. Soc. **69,** 267 (1947).
[11] S. Glasstone, Textbook of physical chemistry, 2d ed., p. 1046 (D. Van Nostrand Co., New York, N. Y., 1946).
[12] R. E. Florin, L. A. Wall, D. W. Brown, and L. Hymo (paper in preparation).
[13] L. Mandelkern, M. Hellmann, D. W. Brown, D. E. Roberts, and F. A. Quinn, Jr., J. Am. Chem. Soc. **75,** 696 (1953).
[14] Donald Druesedow and C. F. Gibbs, Symposium on Polymer Degradation Mechanisms, National Bureau of Standards, 1953.

WASHINGTON, July 23, 1953.

Journal of Research of the National Bureau of Standards Vol. 51, No. 6, December 1953 Research Paper 2462

An Analogue Computer for the Solution of the Radio Refractive-Index Equation

Walter E. Johnson

The solution to the radio refractive-index equation provides information necessary to the research worker studying tropospheric radio propagation in the very high and ultrahigh regions. Present means of computation are either time consuming or of low accuracy. An analogue computer is developed to solve this equation by utilizing basic computation circuits incorporated into a null-balance bridge circuit. A unique feature of this computer is the modification of a linear 10-turn potentiometer so that its output to input voltage ratio versus rotation closely approximates the exponential-type curve of the saturated water-vapor term in the refractive-index equation.

This computer is now in use at the Central Radio Propagation Laboratory, of the National Bureau of Standards, Boulder, Colo., and has superseded other methods of calculating the radio refractive index.

1. Introductory Concepts

Analogue and digital computation devices are not only lightening the load of mathematicians and design engineers, but also are in many cases enabling the research worker to explore problems that have, in the past, been neglected because of the volume of calculations required prior to embarking on the analysis of the actual problem. Such a case exists in radio-propagation studies in the form of atmospheric refractive-index computations.

1.1. Development of the Basic Refractive-Index Equation

The two parts of the equation for the radio refractive index as developed by Debye [1][1] are: (a) a term proportional to density resulting from the induced polarization of the gas molecules in an external field; and (b) a term proportional to the permanent dipole moment of the molecules.

The latest microwave determinations of the constants of this equation yield the following expression [2]:

$$N=(n-1)10^6=\frac{77.6}{T}\left(p+\frac{4810e}{T}\right), \qquad (1)$$

where

N=refractivity of air,
n=refractive index of air,
T=absolute temperature in degrees Kelvin,
p=total pressure in millibars,
e=partial pressure of water vapor in millibars.

1.2. The Refractive Index in Radio-Wave-Propagation Studies

For low angles of elevation, the curvature of a radio ray is, to a high degree of approximation, equal to the gradient or change of refractive index with height. Consequently, the radio horizon fof VHF–UHF communications is determined solely by the refractive-index gradient. With an increase in the refractive-index gradient, the distance to the radio horizon frequently can increase fourfold and under extreme conditions may become theoretically infinite. Therefore, a knowledge of the refractive-index profile with height would suffice for refraction studies. If, however, one is concerned with reflection from elevated layers, then one needs the additional knowledge of the distribution of refractive index throughout the layer.

In radio surveying and navigation studies the absolute value of the refractive index is needed because of the fact that the velocity of electromagnetic waves in air is inversely proportional to the refractive index.

For a typical propagation study, at least two Weather Bureau radiosonde [2] stations are selected, one on each side of the radio-transmission path. Each radiosonde records data at between 15 and 20 different elevations. For 1 year's radio data, there would be at least 21,600 calculations of N to be made for the two radiosonde stations, taking observations twice each day. Therefore, it can be seen that a great deal of time is consumed in laborious calculations prior to making a radio-propagation study.

1.3. Present Methods of Calculating the Refractive Index

One of the most common means of reducing the calculating time is the utilization of nomograms. A recent example of the nomogram approach is that of Swingle [3], which utilizes a separate nomogram for each term in the refractive-index equation and has a maximum possible accuracy of ± 1 N unit. The solutions that utilize a single nomogram are never more precise than Swingle's method, and it is not uncommon to encounter errors of ± 5 N units.

Another approach to solving the equation is to use specially constructed slide rules. Weintraub [4] utilizes 2 slide rules, 1 for each term in the refractive-index equation, and attains an accuracy of $\pm \frac{1}{2}$ N unit.

[1] Figures in brackets indicate the literature references at the end of this paper.

[2] The radiosonde is a measuring system designed to measure the temperature, pressure, and relative humidity of the atmosphere at elevations from sea level to 100,000 ft above sea level.

A major factor to be considered is that both the nomogram and the slide-rule methods require the strict attention of the calculator, and, as such, fatigue and the human element restrict not only the average accuracy of the results, but also the number of consecutive computations possible at one time. The time necessary to compute the separate terms in the refractive index and the subsequent addition varies from approximately 30 sec, using slide rules, to from 30 to 45 sec, using nomograms.

The material to follow describes a relatively simple electric analogue computer that has been designed to solve this equation.

2. Computer Requirements

The general requirements that a computer designed to solve this equation must meet are much the same as those that would be placed on any computer. An ideal approach to the problem would be to make the computer as accurate, as fast, and as convenient as possible. However, it would be well to take a more realistic approach toward finding practical limits to each of these three requirements.

2.1. Accuracy

In general, the computer accuracy need be no greater than is consistent with the accuracy of the available data to be used. Striving for greater accuracy would only lead to greater expense and perhaps undue complications in the circuits. However, the possibility that the accuracy of the available data may at some future date be increased must be taken into account.

At present, the greater part of the available meteorological data has been obtained from radiosonde ascents. The accuracies associated with these data would dictate a computer accuracy of no greater than 1 or 2 N units of refractivity. However, future plans indicate that some of the data will be obtained from relatively accurate recording instruments placed at discrete elevations on specially located steel towers. To accurately solve the refractive-index equation, using data obtained in this manner, it will be necessary to specify an accuracy of $\pm\frac{1}{2}$ N unit.

2.2. Speed

A very obvious limitation on the overall time required to complete one computation is that the total time can be no less than the time required to supply information to the computer, which is proportional to the variables in the equation. This is commonly referred to as the "setup" time. In operation, the operator will be required to read data sheets, which have temperature, pressure, and relative humidity recorded as numerical values and introduce this information into the computer. Using either of the two more common media of dials or pushbuttons, it would appear well to allow at least 3 sec for each of these operations. Allowing another 3 sec to complete the solution would indicate a figure of approximately 12 sec to obtain one solution with the computer. This figure, if met by the computer, would be a considerable improvement over the speed obtained by either the nomogram or the slide rules.

2.3. Convenience

In designing a computer of this type, which must perform a large number of similar computations, too much stress cannot be laid on its convenience of operation. A machine that has been designed with this in mind not only speeds up the operational time for the operator, but also greatly reduces operational errors. Certain general features emerge from a careful consideration of the convenience requirement.

The dials or pushbuttons used to introduce the variables should be arranged in the same relative order as the data on the data sheets. Also they should be convenient to read and should be calibrated in the same units as the original data. The method of reading the answer should be such that the operator may read and record the result from the same convenient position as used to set up the computer.

With these general requirements in mind, let us next investigate the basic electric circuits that will be required in an electric analogue computer designed to solve the refractive-index equation.

3. Basic Computation Circuits

If the constants 77.6 and 4810 in eq. (1) are replaced by K_1 and K_2, respectively, and e by its equivalent, $e_s RH$, the saturated vapor pressure times the relative humidity, the equation will now appear as

$$N=\frac{K_1}{T}\left(p+K_2\frac{e_s}{T}RH\right). \tag{2}$$

It is to be noted that for the present e_s/T will be considered as a variable, as are T, p, and RH. The discussion to follow describes the method used to eliminate e_s/T as an independent variable and thus reduce to three the number of variables that must be introduced into the computer.

Inspection of the equation reveals that multiplication must be accomplished in obtaining the product $K_2\ (e_s/T)RH$. Addition is next used to add p to this product, and finally, division is utilized to divide this binomial by T/K_1. The circuits to follow indicate how each of these three mathematical operations may be duplicated electrically. In each of these circuits e_i represents a d-c voltage source, with zero internal impedance, and e_0 is the output voltage, as measured with an infinite impedance voltmeter. The variable-resistance symbols represent linear potentiometers so designed that the voltage as measured at the slider is equal to the percentage rotation times the voltage applied to the potentiometer. X is used to represent the percentage of total rotation as measured in the direction of the small arrow associated with X.

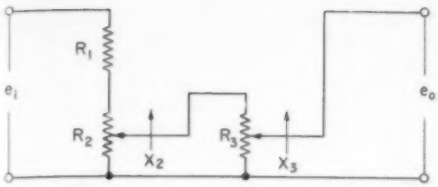

FIGURE 1. *Multiplication circuit.*

3.1. Multiplication

The circuit shown in figure 1 is presented as a method of multiplying two variables by a constant. The equation that expresses the ratio of output voltage to input voltage in this circuit is

$$\frac{e_0}{e_i}=\frac{\dfrac{X_2R_2R_3}{X_2R_2+R_3}}{R_1+(1-X_2)R_2+\dfrac{X_2R_2R_3}{X_2R_2+R_3}}X_3.$$

If $R_3 \gg R_2$, the equation [3] may be simplified as follows:

$$\frac{e_0}{e_i}=\frac{R_2}{R_1+R_2}X_2X_3. \tag{3}$$

This equation shows that when $R_2/(R_1+R_2)$ is made equal to the desired constant and X_2 and X_3 equal to the variables, the voltage ratio, e_0/e_i, will equal the product of the constant and the two variables.

3.2. Addition

The method of adding a constant, a variable, and a constant times a variable is shown below. R_{4a} and R_{4b} are identical potentiometers mounted on the same shaft. Their sliders are so phased that they both are on zero at the same time. X_4 may then be used to represent the percentage of rotation of either potentiometer. The subscripts chosen for the resistance values will prove to be convenient later when combining the basic circuits into the combined computation circuit.

The ratio of output to input voltage is given by

$$\frac{e_0}{e_i}=\frac{R_pR_2}{R_s(R_1+R_2)}X_2+\frac{R_{6a}+X_4R_{4a}}{R_s},$$

where

$$R_p=\frac{(R_1+R_2)(R_{4a}+R_8')}{R_1+R_2+R_{4a}+R_8'} \quad \text{and} \quad R_s=R_p+R_{4a}+R_{6a};$$

[3] When R_3 is 200 times R_2, the solution obtained by eq (3) shows a maximum error in e_0/e_i of 0.07 percent. This maximum error occurs at a value of X_2 equal to 66.7 percent.

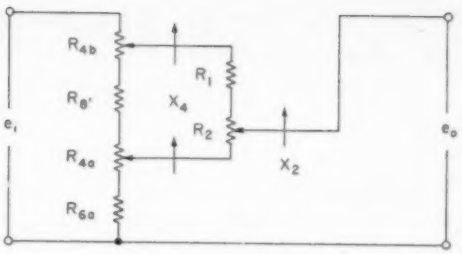

FIGURE 2. *Addition circuit.*

or, rewriting,

$$\frac{e_0}{e_i}=\frac{R_{4a}}{R_s}\left[\frac{R_{6a}}{R_{4a}}+X_4+\frac{R_pR_2}{R_{4a}(R_1+R_2)}X_2\right]. \tag{4}$$

If the correct values are chosen for the resistances, this circuit (fig. 2), as shown by eq (4), can be used to solve the addition of a constant, a variable, and a constant times a variable. It is to be noted that the resistance as measured at the input terminals is a constant and equal to R_s.

3.3. Division

A method must next be found to divide a constant by a constant plus a variable. The circuit shown in figure 3 accomplishes this electrically. Again, subscripts have been chosen as a convenience to later work.

The equation for the voltage ratio is

$$\frac{e_0}{e_i}=\frac{R_s}{R_s+R_7+X_5R_5}$$

or

$$\frac{e_0}{e_i}=\frac{R_s/R_5}{(R_s+R_7)/R_5+X_5} \tag{5}$$

Equation (5) is of the proper form to solve a division problem of the type encountered in the solution of the refractive-index equation, that is, a constant divided by a constant plus a variable.

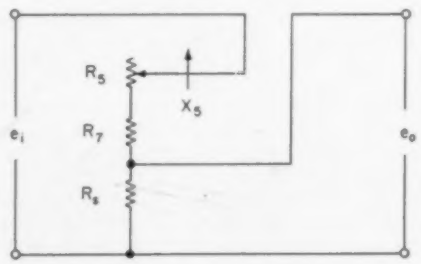

FIGURE 3. *Division circuit.*

4. A Circuit to Solve the Refractive-Index Equation

4.1. Limits on the Variables

Before proceeding to combine the three basic circuits, it will be well to investigate each variable separately in the equation and discover the limits that may be placed on each of them. In addition, the variables in the equation must be modified so that they may be interpreted as the X variables as used in the basic circuits. This requires that the maximum value of each variable be referred to a value of unity, and as such can be made equal to a percentage of rotation as expressed by the X variables. Consideration will also be given toward establishing limits on the variables such that standard dials graduated (or marked) with 10 major divisions to the revolution may be used.

The temperature, T, as found in the equation, represents the absolute temperature and may be written as $273+t$, where t is in degrees centigrade. Because the data obtained from the recording instruments are in terms of degrees centigrade, it will be more convenient to have the dial marked in these same units. Investigation of the data currently available disclosed that temperatures to be encountered will lie between $\pm 50°$ C. This range permits each revolution of a 10-turn potentiometer to represent a change of 10 deg, and the dial can be marked to read zero at its midscale position. With regard to the circuit, the temperature expression may be rewritten $T=100(2.23+X_T)$. As a check on the validity of this expression, consider the absolute temperature at 0° C. X_T, or the fractional rotation, would equal 0.5, and the expression would give an absolute temperature of 273° K, as was to be expected.

Initial investigation of the pressure variable indicated that a range of 0 to 1,000 millibars would be adequate to accommodate all the current and future data. However, closer checks revealed that a range of 100 to 1,100 millibars would be more suitable. This range still permits assigning 100 millibars to each revolution of a 10-turn potentiometer, but requires that a constant be added to the circuit to take account of the 100-millibar shift. The expression for p is written $p=1{,}000(0.1+X_p)$. Here again X_p is the percentage of dial rotation, with the dial calibrated from 100 to 1,100 millibars. As an example, with the dial set for 600 millibars, X_p would equal 0.5, and p would equal 600.

The relative-humidity variable lends itself admirably to expression as a percentage rotation. Because it varies from 0 to 100 percent in the same manner as the X variable, the dial may be graduated 0 to 100 and used directly. Investigation of the data disclosed that the complete range 0 to 100 would be required to accommodate all the data.

Although the e_s/T variable will later be eliminated as an independent variable, its limits will be considered at this time. Using the 1951 Smithsonian Meteorological Tables [5], e_s/T was found to vary from 0.0003 at $-50°$ C to 0.3820 at $+50°$ C. In order to use all the available rotation of a linear potentiometer, it will be necessary to express the variable as $0.3820\,X_{e_s/T}$ and use a specially marked dial to position the slider of the potentiometer.

4.2. The Basic Circuits Combined

With the above information in mind, eq (2) may be rewritten

$$N=\frac{K_1}{100(2.23+X_T)}\left[1000(0.1+X_p)+0.3820X_{(e_s/T)}X_{RH}\right]$$

or

$$N=\frac{10K_1}{2.23+X_T}\left[0.1+X_p+0.3820\frac{K_2}{1000}X_{(e_s/T)}X_{RH}\right]$$

The basic circuits will now be combined, and it will be shown that, by properly selecting the resistance values, the combined circuit can be used to solve the refractive-index equation in the form of eq (6).

Using the equations already established for the basic circuits, the equation for the combined circuit of figure 4 may now be written. The output voltage of the division circuit is applied as the input voltage to the addition circuit, and the variable X_3 is included in the last term of the equation for the addition circuit. Justification for this action is found by comparing the multiplication circuit of figure 1 with the right-hand portion of the addition circuit of figure 2.

The equation for the ratio of voltages in figure 4 is

$$\frac{e_0}{e_i}=\frac{\dfrac{R_{4a}}{R_5}}{\dfrac{R_4+R_7}{R_5}+X_5}\left[\frac{R_{6a}}{R_{4a}}+X_4+\frac{R_pR_2}{R_{4a}(R_1+R_2)}X_2X_3\right] \quad (7)$$

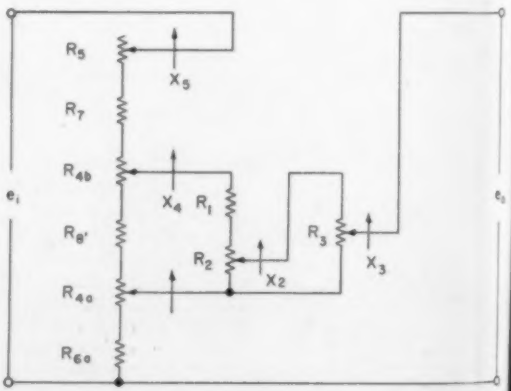

FIGURE 4. *Combined computation circuit.*

A comparison of eq (6) and (7) will show the similarity of the two equations. It is now only necessary to equate the resistance combinations in eq (7) to the constants in eq (6). The output to input voltage ratio is then equal to N.

5. Elimination of e_s/T as an Independent Variable

Up to this point e_s/T has been considered as a separate variable in the equation. The curve plotted in figure 5,[4] shows that e_s/T has explicit dependence on the temperature. This fact can be used to eliminate e_s/T as an independent variable and consequently reduce the setup time for the computer.

As discussed in section 4.1., if a linear potentiometer is to be used to introduce the e_s/T ratio, its dial must have a special marking. The same ratio may be established by using a linear dial and a potentiometer with an output function that matches the curve in figure 5. Unfortunately, the curve cannot be duplicated by any convenient mathematical expression. However, it is possible to approximate the curve by a series of straight lines connecting the circled points on figure 5. Although this approach does not yield a perfect solution at all points, the accuracy can be made as high as required by merely increasing the number of straight-line approximations.

A method known as resistance loading, or "padding", was used to alter the normally linear output of a 10-turn potentiometer. This linear relationship between resistance and shaft rotation can be altered by connecting padding resistors between tap points on the potentiometer coil so that the output will vary in a close approximation to the desired function. By properly choosing the resistance of the pads, the straight lines generated between the tap points can be made to cross the desired curve at two points. The number of tap points was chosen so that at no point would the series of straight lines deviate from the theoretical enough to contribute over $\frac{1}{4}N$ unit error to the final result.

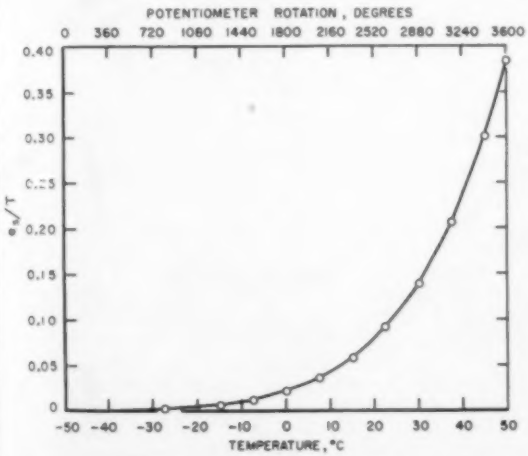

FIGURE 5. e_s/T *versus temperature.*

Theoretical curve shown by the solid line, actual output function shown by the circles. e_s is the saturation vapor pressure in millibars; T is absolute temperature.

[4] Data for this curve were taken from the 1951 Smithsonian Meteorological Tables [5].

Examination of the curve disclosed that taps located at the following degree positions would provide for the desired accuracy: 810, 1260, 1530, 1800, 2070, 2340, 2610, 2880, 3150, and 3420. A 2,000-ohm potentiometer was selected for this modification, as 2,000 ohms was the lowest resistance, commercially available, 10-turn potentiometer that could be obtained for this purpose. Approximate resistance values were calculated to pad the 2,000-ohm potentiometer to the desired points on the curve, and it was found possible to hold the total resistance after padding to 200 ohms. The exact values of the padding resistances were determined by the voltage-comparison method described below.

A 500-ohm 10-turn potentiometer was placed in series with the tapped potentiometer R_2. A voltage was applied to the series combination, and the output voltage at the slider was read, potentiometer type precision voltmeter. The ratio of slider voltage was calculated for each tap point, and, starting from the lowest tap point, the values of the padding resistors were adjusted to make the voltage ratio check exactly with the desired value of e_s/T. The 500-ohm potentiometer was adjusted after every change in padding resistance so as to keep the total series resistance constant and equal to 523.5 ohms. Because the maximum value of e_s/T was to be 0.3820, the 500-ohm potentiometer was replaced by a fixed resistance (R_1) of 323.5 ohms upon completion of the padding operation.

This method provided much greater accuracy than could have been obtained by calculating the values for the padding resistors. With the type of precision voltmeter used, it was possible to read the voltages to five-figure accuracy, and consequently the resistors could be changed to permit adjusting the voltage ratios at the tap points to an accuracy of 0.01 percent. Wire-wound resistors of the same temperature coefficient wire as that used in the potentiometer were specially constructed for this purpose.

Using the potentiometer just described, it is now possible to graduate its dial from $-50°$ C to $+50°$ C in exactly the same manner as the temperature dial. In fact, the dial can now be eliminated and the e_s/T potentiometer can be connected directly to the shaft of the temperature potentiometer. This has in effect eliminated the e_s/T variable, in that it now depends directly on the temperature dial for its setting.

6. Final Design Considerations

6.1. Choice of Solution Presentation

As shown by eq (7), the computation circuit as developed to this point will provide a solution to the refractive-index equation in the form of a voltage ratio. A more convenient and accurate method of presenting the solution is to combine the composite circuit of figure 4 into a bridge circuit and use a sensitive null indicator to detect the bridge balance. Figure 6 shows the complete computer circuit diagram. Potentiometer R_9 and the fixed resistance R_{10} constitute one arm of the bridge, and the combined computation circuit of figure 4 forms the other arm. R_9 is the same type 10-turn linear potentiometer as used to introduce the variables. A linearly calibrated dial attached to R_9 was used to read N directly. R_{10} is a wire-wound resistor, as are all the other fixed resistances.

The null indicator used is of a special design having a maximum sensitivity of ¼-in. motion per microampere at about the zero position. Its response falls off logarithmically on either side of zero and thus provides automatic protection against excessive currents caused by large unbalances in the bridge circuit.

6.2. Selection of Resistance Values

Referring to figure 6, the following expression for the voltage as measured at the slider of R_9 may be written:

$$\frac{e_0}{e_i}=\frac{X_9R_9}{R_9+R_{10}}. \tag{8}$$

With the circuit as shown at null balance, this expression may be equated to eq (7).

$$X_9=\frac{\dfrac{R_{4a}(R_9+R_{10})}{R_5R_9}}{\dfrac{R_v+R_7}{R_5}+X_3}\left[\frac{R_{6a}}{R_{4a}}+X_4+\frac{R_pR_2}{R_{4a}(R_1+R_2)}X_2X_3\right]. \tag{9}$$

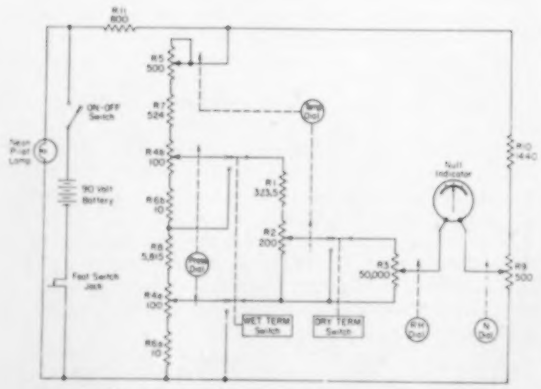

FIGURE 6. *Computer-circuit diagram.*

Both sides of this equation must be multiplied by 1,000 to permit solving for values of N up to 1,000. Investigation of the actual data disclosed that all the values of N will be between 0 and 1,000. The dial attached to R_9 must therefore be graduated from 0 to 1,000. Comparison of eq (6) and (9) requires that the following identities be satisfied in order to utilize the final circuit to solve the refractive-index equation:

$$1000\frac{R_{4a}(R_9+R_{10})}{R_5R_9}=10k_1=776. \tag{10}$$

$$\frac{(R_v+R_7)}{R_5}=2.23. \tag{11}$$

$$\frac{R_{6a}}{R_{4a}}=0.1. \tag{12}$$

$$\frac{R_pR_2}{R_{4a}(R_1+R_2)}=\frac{K_2}{1000}0.3820=1,8374. \tag{13}$$

also

$$R_p=\frac{(R_1+R_2)(R_{4a}+R'_8)}{R_1+R_2+R_{4a}+R'_8}. \tag{14}$$

$$R_v=R_p+R_{4a}+R_{6a}. \tag{15}$$

There exist several combinations of the above resistances that will satisfy the above identities. The variable resistances or potentiometers must first be chosen on the basis of commercially available values. In general, they were chosen as small as possible in order to keep the over-all internal resistance of the circuit low with regard to the internal impedance of the null indicator. Low circuit resistance is necessary in this case to maintain sufficient sensitivity of the null indicator.

R_{4a} and R_{4b} were chosen as 100 ohms each. This value, by eq (12), required that $R_{6a}=10$ ohms, which was still of a size that could be conveniently wound. R_1 and R_2 have already been determined as 323.5 and 200 ohms, respectively. These values and the value for R_{4a} when substituted in eq (13) give a value for R_p of 481.00 ohms. Substituting this value in eq (14), along with the values for R_1, R_2, and R_{4a}, gives a value of 5,825 ohms for R'_8. Solving eq (15) gives a value for R_v of 591.00 ohms. Equation (11) was next investigated in order to determine a value for R_5. As R_7 cannot have a negative value, R_5 must be at least 278 ohms. The closest commercially available value of 500 ohms was chosen for R_5. Using this value for R_5, eq (11) was solved, and R_7 was found to be 524.0 ohms.

Equation (10) was next used to determine the relative magnitude of R_9 and R_{10}. Solving this equation established the relationship

$$\frac{R_9}{R_9+R_{10}}=0.25773.$$

R_9+R_{10} was chosen to be approximately 2,000 ohms so that excessive current would not be drawn from

the voltage source and yet not be so great as to cause serious loss of sensitivity at the null indicator. This value for R_9+R_{10} would indicate a value for R_9 of about 515 ohms. A resistance of 500 ohms was chosen for R_9 because resistors of that value are commercially available. This choice for R_9 required that R_{10} equal 1,440 ohms. R_3 was selected as 50,000 ohms in order to satisfy the previously established relationship that R_3 be at least 200 times R_2.

Figure 6 shows a resistance R_{11} in series with the battery supply voltage. This resistor was used to reduce the bridge voltage to approximately 50 volts. At higher voltages a slight heating effect, along with corresponding resistance changes, was noted in some of the resistors.

6.3. Wet- and Dry-Term Switches

The refractive-index equation may be considered as being composed of two parts, a wet term equal to $K_1/T(K_2RHe_s/T)$ and a dry term equal to $(K_1/T)p$. Many of the applications that require the solution of the refractive-index equation also require the values for either the wet or dry contribution to N. Two switches were incorporated into the final circuit, which permit the computer to solve for either contribution and thereby greatly increase the usefulness of the computer.

In figure 6, R_8' has been divided to form R_8 and R_{8b}. R_{8b} has been made equal to 10 ohms and R_8 equal to 5,815 ohms, thereby keeping the total resistance the same. With the switch connection between R_{8b} and R_8 closed, the pressure term is effectively reduced to zero, and the computer, after rebalancing, reads the wet term. In a similar manner, closing the dry-term switch, effectively makes the wet term zero, and the computer solves for the dry term only.

7. Results and Discussion

The computer herein described was built under the author's supervision at the National Bureau of Standards, Boulder, Colo., and is at present being actively used by their Radio Meteorology Group. The use of the computer has resulted in considerable savings in time over previously used methods.

7.1. Accuracy

A complete test was run on the computer, and the results of this test are given in table 1. The table shows that the error is never greater than $\pm\frac{1}{2}$ N unit. This satisfies the original requirement. If greater accuracy were to be required, a greater number of tap points on the e_s/T potentiometer would permit a closer approximation to the desired curve and consequently increase the final accuracy. The need for greater accuracy would also necessitate the use of dials with finer graduations.

TABLE 1. *Final test data*

Temperature	Pressure	Relative humidity	N	
			Theoretical	Computer
° C	*Millibars*			
−50	100	0	34.80	34.6
−50	1,100	0	382.78	383.1
+50	100	0	24.02	24.0
+50	1,100	0	264.27	264.6
+50	100	100	465.51	465.7
+50	1,100	100	705.75	706.2
0	600	50	185.86	185.8
−14	600	50	185.53	185.5
−12	600	50	185.11	185.2
−10	600	50	184.77	184.9
+40	600	50	289.29	289.7
+42	600	50	302.27	302.6
+44	600	50	315.96	315.9
+46	600	50	331.00	330.7

7.2. Speed

The average operational time of the computer and operator was found to be approximately 10 sec, which is less than the original requirement of 12 sec. This time naturally varies with the individual operator. The shortest time of 8 sec was recorded for an experienced operator and the longest time of 13 sec was recorded for a relatively inexperienced operator. This time could be decreased somewhat by using an automatic balance system to rotate the N dial and thereby balance the bridge circuit more rapidly than can be done manually. This refinement was not deemed practical for the present computer due to the relatively longer time required to set in the variables.

7.3. Convenience

All of the original requirements on convenience have been incorporated in the final design. Figure 7 shows the computer. It is housed in a small sloping

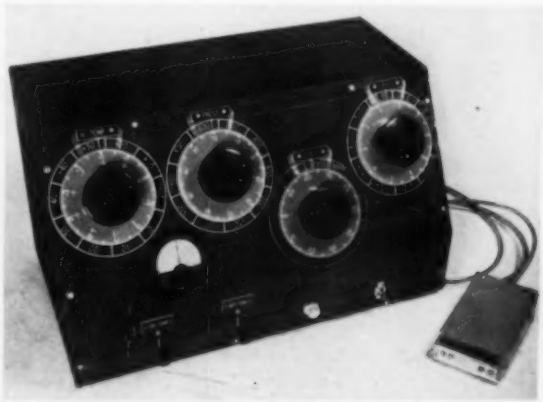

FIGURE 7. *Refractive-index computer.*

front cabinet that can be placed on a desk or table and used in the same manner as a standard calculating machine. Because of heating effects, it was found desirable not to leave the battery connected to the bridge circuit continuously. With this in mind, a foot switch was incorporated in the final design so that the operator could energize the circuit as needed and still have both hands free to operate the dials and record data.

In figure 7 the various dials are set up to solve for N, with the temperature, 32.0° C; pressure, 620 millibars; and RH, 62.5 percent. N is read as 277.0.

8. References

[1] P. Debye, Polar molecules, sec. 3.4 (Chemical Catalog Co., New York, N. Y., 1929).

[2] E. K. Smith, Jr., and S. Weintraub, The constants in the equation for atmospheric refractive index at radio frequencies, J. Research NBS **50,** 39 (January 1953) RP2385.

[3] D. M. Swingle, Nomograms for the computation of tropospheric refractive index, Proc. IRE [3] **41,** 385 (March 1953).

[4] S. Weintraub, Slide rule for the computation of the radio refractive index of air, Electronics [1] **26,** 182 (January 1953).

[5] Smithsonian meteorological tables, 6th revised ed., p. 351–352 (Smithsonian Inst., Washington, D. C., 1951).

Boulder, Colo., July 13, 1953.

Journal of Research of the National Bureau of Standards Vol. 51, No. 6. December 1953 Research Paper 2463

On the Accuracy of the Numerical Solution of the Dirichlet Problem by Finite Differences[1]

J. L. Walsh[2] and David Young[3]

This paper derives numerical bounds for the error, in certain closed regions, of the difference analog of the Dirichlet problem. It is concerned only with the difference between the exact solution of the difference equation and the solution of the Dirichlet problem. The error bounds obtained involve quantities which can actually be computed, such as the mesh size, and the oscillation and modulus of continuity of the given function on the boundary. So far as the method is concerned, the chief novelty is the use of the difference analogs of harmonic measure and the Schwarz Alternating Process.

1. Introduction

Although finite difference methods afford a powerful tool for obtaining numerical solutions of partial differential equations, little is known about the accuracy. It is the purpose of this paper to derive numerical bounds for the error, in certain closed regions, of the difference analog of the Dirichlet problem. We shall be concerned only with the difference between the exact solution of the difference equation and the solution of the Dirichlet problem. The error bounds that we obtain involve quantities that can actually be computed such as the mesh size, and the oscillation and modulus of continuity of the given function on the boundary. So far as method is concerned, the chief novelty is the use of the difference analogs of harmonic measure and the Schwarz Alternating Process.

Gerschgorin [4] [4] derived error bounds for boundary value problems associated with elliptic partial differential equations. These, and similar bounds derived by Collatz [2] and Mikeladze [10] involve bounds, in the closed region, of certain partial derivatives of the solution of the differential equation. However, the solution of the differential equation itself is not known, to say nothing of its derivatives, (although approximate values for the derivatives may sometimes be found by examining the corresponding difference quotients). Also, it may happen that although the derivatives in question are not bounded in the closed region, the solution of the difference equation may still converge to the solution of the differential equation.

Rosenbloom [13] presented an error bound for the Dirichlet problem which is closely related to Gerschgorin's but which utilizes special properties of harmonic functions. By use of well-known inequalities giving bounds for the partial derivatives of a harmonic function at an interior point in terms of the oscillation on the boundary and the distance from the boundary, he obtains upper bounds for the derivatives in closed subregions. Then, by solving the difference equation on subregions and, as the mesh size approaches zero, letting these subregions approach the given region, Rosenbloom obtains an error bound involving $\omega^*(\delta)$, the modulus of continuity in the closed region of the solution of the Dirichlet problem. However, Rosenbloom does not discuss the question of finding $\omega^*(\delta)$ in terms of $\omega(\delta)$, the known modulus of continuity of the given function on the boundary. Furthermore, in practical numerical work one would not wish to change the boundary of the network as the mesh size is decreased.

In section 3 we use the explicit solution of the difference analog of the Dirichlet problem for the rectangle, obtained by Le Roux [9] and by Phillips and Wiener [12], to derive an error bound involving bounds for the derivatives of the given function on the boundary. Wasow [15] has obtained error bounds for the rectangle which are applicable when the boundary values

[1] Presented to the American Mathematical Society, September 1951; abstract published in Bul. Am. Math. Soc. 57, 478 (1951). The paper was prepared in part while Professor Walsh was engaged as consultant on a National Bureau of Standards contract with the University of California at Los Angeles. The research was also supported by the Office of Naval Research under Contracts N5ori-07634 and N5ori-76, Project 22, with Harvard University, and later by the Office of Ordnance Research, U. S. Army, under Contract DA-36 034-ORD 966.

[2] Harvard University; consultant, National Bureau of Standards contract with the University of California at Los Angeles.

[3] University of Maryland.

[4] Figures in brackets indicate the literature references at the end of this paper.

have bounded third derivatives. Our results are somewhat more general in that we allow the second and third derivatives to fail to exist at a finite number of points. Also, we obtain error bounds for the case where only the second derivative is bounded, and we allow the first and second derivatives to fail to exist at a finite number of points. In sections 4 and 5 harmonic measure and its finite difference analog, discrete harmonic measure, are used to obtain bounds for the moduli of continuity of harmonic and discrete harmonic functions, respectively, in certain regions in terms of $\omega(\delta)$. Phillips and Wiener [12] showed the existence of such bounds, whereas we obtain suitable bounds in a precise numerical form. Then, in section 6 these upper bounds are used to yield a uniform error estimate for the closed rectangle in terms of the oscillation on the boundary and $\delta(\omega)$. In section 7 the extension to regions made up of two or more overlapping rectangles is discussed.

2. Discrete Harmonic Functions

Let h and k be arbitrary positive numbers, and let $L[h,k]$ denote the set of points (x, y) such that both x/h and y/k are integers. Let Ω be a simply connected closed region with interior R such that the boundary S of Ω consists of straight lines, each of which is parallel to a coordinate axis and contains a point of $L[h,k]$. Let Ω_L denote the subset of points of $L[h,k]$ contained in Ω. Two points (x_1,y_1) and (x_2,y_2) of $L[h,k]$ are *adjacent* if

$$[(x_1-x_2)/h]^2+[(y_1-y_2)/k]^2=1. \tag{2.1}$$

A point of Ω_L is an *interior* point of Ω_L if the four adjacent points belong to Ω_L. All other points of Ω_L are boundary points. We let R_L and S_L denote, respectively, the set of interior and boundary points of Ω_L. Evidently, we have $R_L \subseteq R$ and $S_L \subseteq S$.

A function $U(x,y)$ defined on Ω_L is said to be *discrete harmonic*,[5] (d. h.) in R_L if it satisfies the difference equation

$$\delta^2[U(x,y)]=[2\sigma^2/(1+\sigma^2)][U(x+h,y)+U(x-h,y)-2U(x,y)]$$
$$+[2/(1+\sigma^2)][U(x,y+k)+U(x,y-k)-2U(x,y)]=0, \tag{2.2}$$

where

$$\sigma=k/h. \tag{2.3}$$

The finite difference analog of the Dirichlet problem is the following problem: given a function $f(x,y)$ defined on S, to find a function $U(x,y)$ defined on Ω_L, d.h. in R_L and coinciding with $f(x,y)$ on S_L. The existence and uniqueness of a solution of this problem for bounded regions is easy to prove; see for instance Gerschgorin [4]. The convergence to the solution of the Dirichlet problem has been proved using nonconstructive methods by Le Roux [9], Phillips and Wiener [12], and others.

3. Error Estimate for the Rectangle Under Differentiability Assumptions

Let Ω be bounded by the lines $x=0$, $x=a$, $y=0$, and $y=b$, where $a=Ah$, $b=Bk$ and A and B are positive integers. Let $f(x,y)$ be defined and continuous on S and let $u(x,y)$ and $U(x,y)$ denote respectively the solution of the Dirichlet problem and its finite difference analog with boundary values determined by $f(x,y)$. In this section we shall derive an upper bound for the error $U(x,y)-u(x,y)$ in the region Ω_L, under certain assumptions about the derivatives of $f(x,y)$. If $f_i(x,y)$ is defined and continuous on S, we denote generically by $u_i(x,y)$ and $U_i(x,y)$ the solutions respectively of the Dirichlet problem and its finite difference analog with boundary values $f_i(x,y)$.

First, one can verify directly that the function $u_1(x,y)$ defined by

$$u_1(x,y)=f(0,0)+[f(a,0)-f(0,0)](x/a)+[f(0,b)-f(0,0)](y/b)$$
$$+[f(a,b)+f(0,0)-f(a,0)-f(0,b)](x/a)(y/b), \tag{3.1}$$

[5] Heilbronn [5] introduced the term *discrete harmonic function*, and studied the properties of these functions.

which is linear on every line parallel to either coordinate axis, is both harmonic in R and d.h. in R_L. Thus if $f_1(x,y)$ is defined on S and equal to $u_1(x,y)$ on S, then $u_1(x,y)=U_1(x,y)$ in Ω_L.

Next, if $f_2(x,y)=f(x,y)-f_1(x,y)$ on S, then we have by linearity of Laplace's equation and (3.1)

$$U(x,y)-u(x,y)=[U_2(x,y)+U_1(x,y)]-[u_2(x,y)+u_1(x,y)]$$

$$=U_2(x,y)-u_2(x,y). \tag{3.2}$$

Evidently both $U_2(x,y)$ and $u_2(x,y)$ vanish at all the corners of Ω.

We study arbitrary boundary values $f(x,y)$ by studying in turn four functions each of which has the boundary values $f_2(x,y)$ on one side of Ω and values identically zero on the other three sides. By the symmetry of the situation, it is sufficient to study in detail only one of the latter functions. Let us set $f_3(x,y)=f_2(x,0)$ when $y=0$ and $f_3(x,y)=0$ elsewhere on S. Since $f_2(x,y)$ is continuous and vanishes at the corners of Ω, $f_3(x,y)$ is continuous on S.

It can be verified directly [6] that if the Fourier series of $f_3(x,0)$ converges to $f_3(x,0)$, then we have

$$u_3(x,y)=\sum_{n=1}^{\infty} A_n \sin(n\pi x/a)\frac{\sinh[(n\pi b/a)(1-y/b)]}{\sinh(n\pi b/a)}, \tag{3.3}$$

where

$$A_n=(2/a)\int_0^a f_3(t,0)\sin(n\pi t/a)dt, \tag{3.4}$$

and that [7]

$$U_3(x,y)=\sum_{n=1}^{A} A_n^* \sin(n\pi x/a)\frac{\sinh[(m\pi b/a)(1-y/b)]}{\sinh(m\pi b/a)}, \tag{3.5}$$

where

$$A_n^*=(2h/a)\sum_{j=1}^{A-1}\sin(n\pi jh/a)f_3(jh,0), \tag{3.6}$$

and where m and n satisfy the relation

$$\sinh(m\pi k/2a)=\sigma\sin(n\pi h/2a). \tag{3.7}$$

Now let $g(x)\equiv f_3(x,0)$. We now prove the following theorem:

THEOREM 3.1 *Let $g(x)$ satisfy the following conditions:* (a) *$g(x)$ and its first $(s-2)$ derivatives are continuous, $0\leq x\leq a$;* (b) *$g^{(s-1)}(x)$ fails to exist or fails to be continuous for, at most, a finite number of points in the interval $0\leq x\leq a$, and $g^{(s-1)}(x)$ is uniformly continuous in each open interval in which it exists and is continuous;* (c) *$g^{(s)}(x)$ exists, except possibly for a finite number of points, and is bounded, $0\leq x\leq a$.*

Then uniformly for all $(x,y)\in\Omega_L$, we have

$$|U_3(x,y)-u_3(x,y)|\leq(2+C)D_2(h/a), \tag{3.8}$$

if $s=2$, and

$$|U_3(x,y)-u_3(x,y)|\leq(1+Ce)D_3(h/a)^2, \tag{3.9}$$

if $s=3$, where

$$C=(1/24)\pi^2(1+\sigma^2)\coth(\alpha\pi b/a)/\alpha e, \tag{3.10}$$

$$D_2=2(a/\pi)^2[2J_1M_1/a+M_2], \qquad D_3=2(a/\pi)^3[2(J_2+1)M_2/a+M_3] \tag{3.11}$$

$$\alpha=(2/\pi\sigma)\sinh^{-1}(\sigma), \tag{3.12}$$

[6] See, for instance [8], pages 95 and 96.

[7] See, for instance, Le Roux [9] or Phillips and Wiener [12].

and J_i, $i=1,2$, denotes the number of points in the open interval $0<x<a$ at which $g^{(i)}(x)$ does not exist or is not continuous. Here M_i, $i=1,2,3$, denotes the least upper bound of the modulus of $g^{(i)}(x)$.

PROOF.

LEMMA 3.1. *If m and n satisfy (3.7), then*

$$0\leq n-m\leq (1/24)(1+\sigma^2)\pi^2n^3(h/a)^2, \quad (n=1,2, \ldots, A). \tag{3.13}$$

PROOF. Let $p=m\pi k/2a$, $q=n\pi h/2a$. Then (3.7) takes the form

$$\sinh p=\sigma \sin q. \tag{3.14}$$

We now study the function $p(q)$ defined by (3.14) in the interval $0\leq q\leq \pi/2$. One can verify directly that $p(0)=0$, $p'(0)=\sigma$, and

$$p''(q)=\frac{-\sigma(1+\sigma^2)\sin q}{(1+\sigma^2\sin^2 q)^{3/2}}\leq 0,$$

$$p'''(q)=\frac{-\sigma(1+\sigma^2)(1-2\sigma^2\sin^2 q)\cos q}{(1+\sigma^2\sin^2 q)^{5/2}},$$

where primes denote differentiation with respect to q. By the extended mean value theorem, since $p''(q)\leq 0$, we have $p\leq \sigma q$. Therefore, $m\leq n$. On the other hand, we also have

$$|p'''(q)|\leq \frac{\sigma(1+\sigma^2)|1-2\sigma^2\sin^2 q|}{(1+\sigma^2\sin^2 q)^{5/2}}\leq \sigma(1+\sigma^2)$$

since $|(1-2\sigma^2\sin^2 q)(1+\sigma^2\sin^2 q)^{-5/2}|\leq 1$.

Again using the extended mean value theorem, we get

$$p(q)-\sigma q=(1/6)q^3p'''(\xi) \qquad (0<\xi<q)$$

and

$$|p(q)-\sigma q|\leq (1/6)q^3\sigma(1+\sigma^2),$$

and the lemma follows.

LEMMA 3.2. *If m and n satisfy (3.7), and if α is given by (3.12), then*

$$m\geq \alpha n, \qquad (n=1,2, \ldots, A). \tag{3.15}$$

PROOF. Defining p and q by (3.14), we have

$$\frac{d}{dq}(p(q)/q)=[p'(q)q-p(q)]/q^2.$$

By the mean value theorem, we have $p(q)=qp'(\xi)$ $(0<\xi<q)$. Since, as shown in the proof of lemma 3.1, $p''(q)\leq 0$, we have $p'(q)\leq p'(\xi)$ and $p'(q)q-p(q)\leq 0$. Therefore, the ratio $p(q)/q$ is a nonincreasing function of q, $(0\leq q\leq \pi/2)$. Its minimum value in the interval $0\leq q\leq \pi/2$ is assumed when $q=\pi/2$. Therefore, $p(q)/q\geq p(\pi/2)/(\pi/2)=(2/\pi)\sinh^{-1}(\sigma)$, and the lemma follows.

Now for convenience, let us define the function

$$\Gamma_m(y)=\frac{\sinh[(m\pi b/a)(1-y/b)]}{\sinh(m\pi b/a)}. \tag{3.16}$$

We shall study its behavior as a function of both m and y, where m is assumed to be a continuous variable.

LEMMA 3.3. *If $m\geq 0$, then for $0\leq y\leq b$ we have*

$$0\geq \frac{d}{dm}\Gamma_m(y)\geq -(\pi y/a)\coth(m\pi b/a)\exp[-m\pi y/a].$$

PROOF. Differentiating (3.16) with respect to m we obtain

$$\frac{d}{dm}\,\Gamma_m(y)=(\pi b/a)\{(1-y/b)\cosh[(m\pi b/a)(1-y/b)]\sinh(m\pi b/a)$$
$$-\cosh(m\pi b/a)\sinh[(m\pi b/a)(1-y/b)]\}\sinh^{-2}(m\pi b/a)$$
$$=(\pi b/a)\Gamma_m(y)\{(1-y/b)\coth[(m\pi b/a)(1-y/b)]-\coth(m\pi b/a)\}.$$

We note that for $K>0$, $x>0$,

$$\frac{d}{dx}\,(x\coth(Kx))=\coth(Kx)-Kx\,\operatorname{csch}^2(Kx)=\frac{1}{2}\,\frac{\sinh(2Kx)-2Kx}{\sinh^2(Kx)}.$$

But since $\sinh(2Kx)\geq 2Kx$, the last expression is nonnegative; therefore by the mean value theorem we have

$$(1-y/b)\coth[(m\pi b/a)(1-y/b)]\leq\coth(m\pi b/a),\qquad(0\leq y\leq b),$$

and

$$\frac{d}{dm}\,\Gamma_m(y)\leq 0.$$

On the other hand,

$$\frac{d}{dm}\,\Gamma_m(y)=(\pi b/a)\left\{(1-y/b)\,\frac{\cosh[(m\pi b/a)\,(1-y/b)]}{\sinh(m\pi b/a)}-\coth(m\pi b/a)\,\Gamma_m(y)\right\}$$
$$=(\pi b/a)\coth(m\pi b/a)\left\{(1-y/b)\,\frac{\cosh[(m\pi b/a)\,(1-y/b)]}{\cosh(m\pi b/a)}-\Gamma_m(y)\right\}$$
$$=(\pi b/a)\coth(m\pi b/a)\left\{(1-y/b)\,\frac{\sinh(m\pi y/a)}{\sinh(m\pi b/a)\cosh(m\pi b/a)}-(y/b)\,\Gamma_m(y)\right\}.$$

For $0\leq y\leq b$, the terms in the brackets are, respectively, nonnegative and nonpositive, whence

$$\frac{d}{dm}\,\Gamma_m(y)\geq-(\pi y/a)\coth(m\pi b/a)\,\Gamma_m(y).$$

Finally, we note that

$$\Gamma_m(y)=\exp(-m\pi y/a)\,\frac{1-\exp[-2(m\pi b/a)\,(1-y/b)]}{1-\exp[-2m\pi b/a]}\leq\exp(-m\pi y/a),$$

provided[8] $0\leq y\leq b$. The lemma now follows.

LEMMA 3.4. *If m and n satisfy* (3.7), *then*

$$\left|\left[\frac{d}{dm}\,\Gamma_m(y)\right]_{m=m_1}\right|\leq[\coth(\alpha\pi b/a)/\alpha e]\,n^{-1},\qquad(1\leq n\leq A),\quad(m\leq m_1\leq n,)\tag{3.17}$$

where α is given by (3.12).

PROOF. It is easily verified that if $0\leq t$, $0\leq K$, then $|te^{-Kt}|\leq(Ke)^{-1}$. Therefore, $y\exp(-m\pi y/a)\leq[(m\pi/a)e]^{-1}$. The lemma follows from lemmas 3.2 and 3.3, and from the fact that $\coth(x)$ is a decreasing function of x, for $x\geq 0$.

LEMMA 3.5. If m and n *satisfy* (3.7), *then*

$$|\Gamma_m(y)-\Gamma_n(y)|\leq C(h/a)^2n^2,\qquad(0\leq y\leq b),\quad(1\leq n\leq A),$$

where C and α are given by (3.10) *and* (3.12), *respectively.*

[8] This inequality was proved by Phillips and Wiener [12].

PROOF. By the mean value theorem we have

$$|\Gamma_m(y)-\Gamma_n(y)| \leq \mathrm{Max}_{m\leq m_1\leq n}\left|\left[\frac{d}{dm}\,\Gamma_m(y)\right]_{m=m_1}\right| \cdot |m-n|.$$

The lemma follows from (3.13) and (3.17).

LEMMA 3.6. *If A_n is defined by* (3.4), *then*

$$|A_n| \leq D_s/n^s, \qquad (n=2,3), \tag{3.18}$$

where D_s is defined by (3.11).

PROOF. The proof involves the use of repeated integration by parts of the integral expression for A_n, and is similar to that given by Jackson[8, p. 13–14] for the case $s=2$. We omit the details.

We now define the function $f_4(x,y)$:

$$f_4(x,y)=0 \text{ unless } y=0 \quad \text{and} \quad f_4(x,0)=\sum_{n=1}^{A} A_n \sin(n\pi x/a).$$

For $s=2,3$ and $0\leq x\leq a$, we have

$$|f_4(x,0)-g(x)|=\left|\sum_{n=A+1}^{\infty} A_n \sin(n\pi x/a)\right| \leq D_s \sum_{n=A+1}^{\infty} n^{-s} \leq D_s \int_A^{\infty} t^{-s}dt = D_s A^{1-s}/(s-1),$$

or

$$|f_4(x,0)-g(x)| \leq [D_s/(s-1)](h/a)^{s-1}. \tag{3.19}$$

On the other hand, if we replace $f_3(x,0)$ by $f_4(x,0)$ in (3.4) and (3.6), we get $A_n^*=A_n$, $(n=1,2,\ldots,A-1)$. Therefore, for $(x,y) \in L\,[h,k]$, we have, since $\sin(A\pi x/a)=0$,

$$U_4(x,y)-u_4(x,y)=\sum_{n=1}^{A-1} A_n \sin(n\pi x/a)[\Gamma_m(y)-\Gamma_n(y)], \tag{3.20}$$

and

$$|U_4(x,y)-u_4(x,y)| \leq \sum_{n=1}^{A-1} |A_n| \cdot |\Gamma_m(y)-\Gamma_n(y)| \leq CD_s(h/a)^2 \sum_{n=1}^{A-1} n^{2-s} \tag{3.21}$$

by lemma 3.5 and (3.18). It can be shown that

$$\sum_{n=1}^{A-1} n^{2-s} \leq 1+\int_1^A t^{2-s}dt \leq \begin{cases} A=(h/a)^{-1}, & (s=2) \\ 1+\log A = 1-\log(h/a), & (s=3). \end{cases} \tag{3.22}$$

Therefore, if $s=2$,

$$|U_4(x,y)-u_4(x,y)| \leq CD_2(h/a). \tag{3.23}$$

Evidently (3.22) could be used to obtain an error bound for the case $s=3$, and this was done in the original manuscript of the present paper. Since then, however, a paper by Wasow [15] has appeared which contains a stronger result for the case $s=3$ than the original form of theorem 3.1. A combination of his methods and the original ones now yields an improvement (the present theorem 3.1) of Wasow's result in this case since we allow $g^{(3)}(x)$ and $g^{(2)}(x)$ to fail to exist for a finite number of points.

Thus following [15], we obtain from lemmas 3.1, 3.2, 3.3, and the mean value theorem

$$|\Gamma_m(y)-\Gamma_n(y)| \leq C\alpha\epsilon(h/a)^2(\pi y/a)n^3\exp(-\alpha n\pi y/a).$$

By (3.20) and lemma 3.6 we have

$$|U_4(x,y)-u_4(x,y)| \leq CD_2\alpha e\,(h/a)^2(\pi y/a)\sum_{n=1}^{\infty}\exp(-\alpha n\pi y/a) \leq Ce\,D_2(h/a)^2, \tag{3.24}$$

since for $y>0$, $\sum_{n=1}^{\infty}\exp(-\alpha n\pi y/a)=[\exp(\alpha\pi y/a)-1]^{-1}\leq(\alpha\pi y/a)^{-1}$.

Since d.h. functions possess mean value properties, they assume their maximum and minimum values on the boundary as do harmonic functions. Since the functions $[u_3(x,y)-u_4(x,y)]$ and $[U_3(x,y)-U_4(x,y)]$ are harmonic and d.h., respectively, we have

$$|u_3(x,y)-u_4(x,y)| \leq \operatorname*{Max}_{0\leq x\leq a}|g(x)-f_4(x,0)|, \qquad |U_3(x,y)-U_4(x,y)| \leq \operatorname*{Max}_{0\leq x\leq a}|g(x)-f_4(x,0)|.$$

Therefore, in Ω_L

$$\begin{aligned}|U_3(x,y)-u_3(x,y)| &\leq |U_3(x,y)-U_4(x,y)|+|U_4(x,y)-u_4(x,y)|+|u_4(x,y)-u_3(x,y)| \\ &\leq |U_4(x,y)-u_4(x,y)|+2\operatorname*{Max}_{0\leq x\leq a}|g(x)-f_4(x,0)|.\end{aligned}$$

By (3.19), (3.23), and (3.24), the theorem follows.

4. Harmonic Measure

Let Ω denote a simply connected region with interior R and boundary S. Let S' denote a subset of S consisting of a finite number of connected subsets of S. We define the *harmonic measure*, (h.m.), $H[(x,y),S',\Omega]$ as the unique function which is harmonic and bounded in R, is continuous in Ω except perhaps at a finite number of points of S, and equals unity on S' and zero on $S-S'$. The properties of harmonic measure have been studied in considerable detail, see Nevanlinna [11], chapter III.

By analogy we define *discrete harmonic measure*, (d.h.m.), for regions of the type described in section 2, as follows: $H_L[(x,y),S',\Omega_L]$ is a function d.h. and bounded in R_L, equal to unity on $S_L\cap S'$ and to zero on $(S-S')\cap S_L$.

For bounded regions the existence and uniqueness of h.m. is well known, see [11]. The existence and uniqueness for the half plane can be proved by the use of conformal mapping.

The existence and uniqueness of d.h.m. for bounded regions follows from the existence and uniqueness of the solution of the difference analog of the Dirichlet problem. Later we shall prove existence and uniqueness of d.h.m. for a half plane and for certain other unbounded regions.

We list some elementary properties of d.h.m., which are analogs of well-known properties of h.m.

$$0\leq H_L[(x,y),S',\Omega_L]\leq 1 \quad \text{for all } S'\subseteq S. \tag{4.1}$$

If $S'\subseteq S''\subseteq S$, then

$$H_L[(x,y),S',\Omega_L]\leq H_L[(x,y),S'',\Omega_L]. \tag{4.2}$$

If S' is included in the boundary of both Ω_L and Ω_L^* where $\Omega_L\subseteq\Omega_L^*$ and if $(x,y)\epsilon\Omega_L$, then

$$H_L[(x,y),S',\Omega_L]\leq H_L[(x,y),S',\Omega_L^*]. \tag{4.3}$$

The first property follows at once from the fact that the maximum and minimum values of d.h. functions are assumed on the boundary. The second follows from this fact and from the fact that the expression $\{H_L[(x,y),S'',\Omega_L]-H_L[(x,y),S',\Omega_L]\}$ is nonnegative on S_L. The third follows since by the maximum and minimum principles $H_L[(x,y),S',\Omega_L^*]\geq 0$ and hence $\{H_L[(x,y),S',\Omega_L^*]-H_L[(x,y),S',\Omega_L]\}\geq 0$ for any point (x,y) on the boundary of Ω_L. This is the so-called principle of *gebietserweiterung*.

We shall use h.m. and d.h.m. for two purposes. In this section and in section 5 lower bounds will be derived to enable us to obtain upper bounds for the modulus of continuity of harmonic and d.h. functions in a closed region in terms of their moduli of continuity on the

boundary. In section 7, upper bounds will be derived which will enable us to use the Schwarz Alternating Process and its difference analog for overlapping rectangles.

Let Ω denote the rectangle of section 3, and let S' denote the side contained in the line $y=0$.

THEOREM 4.1. *If* $(x-a/2)^2+y^2\leq\delta^2$, *then*

$$H[(x,y),S',\Omega]\geq 1-\nu(b/a)(\delta/a), \tag{4.4}$$

$$H_L[(x,y),S',\Omega_L]\geq 1-\nu(b/a)(\delta/a), \tag{4.5}$$

where

$$\nu(b/a)=[4+\pi^2\coth^2(\pi b/a)]^{1/2}. \tag{4.6}$$

PROOF. Let $u(x,y)$, $U(x,y)$ be harmonic and d.h. functions respectively in R vanishing on $S-S'$ and equal to $\sin(\pi x/a)$ on S'. By (3.3) to (3.7) we have

$$u(x,y)=\sin(\pi x/a)\,\frac{\sinh[(\pi b/a)(1-y/b)]}{\sinh(\pi b/a)}, \quad \text{and} \quad U(x,y)=\sin(\pi x/a)\,\frac{\sinh[(m\pi b/a)(1-y/b)]}{\sinh(m\pi b/a)},$$

where $\sinh(m\pi k/2a)=\sigma\sin(\pi h/2a)$.

By lemma 3.1 we have $m\leq 1$. Also by lemma 3.3 we have $(d/dm)\,\Gamma_m(y)\leq 0$. Therefore, $\Gamma_m(y)\geq\Gamma_1(y)$, and we get

$$U(x,y)\geq u(x,y). \tag{4.7}$$

Now, for $0\leq\theta\leq\pi/2$ we have[9] $\sin\theta\geq(2/\pi)\theta$; and hence for $0\leq x\leq a/2$, we have $\sin(\pi x/a)\geq 2x/a=1-(2/a)\,(a/2-x)$. But since $\sin[(\pi/a)(a/2+\rho)]=\sin[(\pi/a)(a/2-\rho)]$ for all ρ it follows that $\sin(\pi x/a)\geq 1-(2/a)|a/2-x|$, $(0\leq x\leq a)$.

Also

$$\left|\frac{d}{dy}\sinh[(\pi b/a)(1-y/b)]\right|=|(\pi/a)\cosh[(\pi b/a)(1-y/b)]|\leq(\pi/a)\cosh(\pi b/a),$$

and by the mean value theorem

$$\sinh[(\pi b/a)(1-y/b)]\geq\sinh(\pi b/a)-(\pi y/a)\cosh(\pi b/a).$$

Therefore,

$$1-u(x,y)\leq 1-\{[1-(2/a)|a/2-x|][1-(\pi y/a)\coth(\pi b/a)]\}\leq(2/a)|a/2-x|+(\pi y/a)\coth(\pi b/a).$$

By the Schwarz inequality the last expression does not exceed

$$(1/a)[(a/2-x)^2+y^2]^{1/2}\nu(b/a)\leq(\delta/a)\nu(b/a),$$

provided $(x-a/2)^2+y^2\leq\delta^2$.

We now observe that $H[(x,y),S',\Omega]\geq u(x,y)$, $H_L[(x,y),S',\Omega_L]\geq U(x,y)$. The theorem now follows from (4.7).

Now let Ω_L denote the subset of $L[h,k]$ such that $y\geq 0$ and let R_L and S_L denote the interior and boundary of Ω_L, respectively.

THEOREM 4.2. *For the region* Ω_L, *d.h.m. exists and is unique.*

PROOF. Consider the sequence $\{H_L^{(n)}(x,y)\}$, where

$$H_L^{(n)}(x,y)=H_L[(x,y),S'\cap S_L^{(n)},\Omega_L^{(n)}],$$

and where $\Omega_L^{(n)}$ denotes the rectangle with vertices $(nh,0)$, $(-nh,0)$, (nh,nk) and $(-nh,nk)$. Evidently $H_L^{(n)}(x,y)$ exists, since d.h.m. exists for bounded regions. By (4.3) it follows that the sequence $\{H_L^{(n)}(x,y)\}$ is nondecreasing and bounded above by unity. Therefore, a unique limit exists which we denote by $H_L(x,y)$.

[9] This is Jordan's inequality; see Copson [3, p. 136].

Since $H_L^{(n)}(x,y)$ is d.h., it satisfies (2.2). Taking limits of both sides of (2.2), we find that $H_L(x,y)$ satisfies (2.2) and is therefore d.h. Evidently $H_L(x,y) \leq 1$, $H_L(x,y)=1$ on $S' \cap S_L$ and $H_L(x,y)=0$ on $S'-S_L$. Hence $H_L(x,y)$ has all the properties required for d.h.m.

In order to establish uniqueness, we prove

LEMMA 4.1. *If $U(x,y)$ is d.h., bounded in R_L and vanishes on S_L, then $U(x,y)$ vanishes in R_L.*

PROOF. By hypothesis there exists a constant P such that for $(x,y) \epsilon \Omega_L$, we have $|U(x,y)| \leq P$. Given any $(x,y) \epsilon \Omega_L$ and any $\epsilon > 0$, let a and b be chosen so that $(a,b) \epsilon L[h,k]$ and

$$a \geq P(x^2+y^2)^{1/2} \nu(1/2)/2\epsilon, \qquad b \geq a.$$

Let Ω^* denote the rectangle with vertices at (a,b), $(-a,b)$, $(a,0)$, and $(-a,0)$, and let I_a denote the interval $(-a<x<a)$. Since $|U(x,y)| \leq P$ on S^* and vanishes on I_a, we have

$$|U(x,y)| \leq P H_L[(x,y), S^* - I_a, \Omega_L^*].$$

By theorem 4.1 we have, replacing a by $2a$,

$$H_L[(x,y), I_a, \Omega_L^*] \geq 1 - \nu(b/2a)\,(\delta/2a),$$

provided $x^2+y^2 \leq \delta^2$. But by hypothesis, we have $(x^2+y^2)^{1/2} \leq 2\epsilon a / P\nu(1/2)$. Substituting, we get

$$H_L[(x,y), I_a, \Omega_L^*] \geq 1 - \nu(b/2a)\epsilon / P\nu(1/2).$$

Since $b \geq a$, we have $\nu(b/2a) \leq \nu(1/2)$; hence,

$$H_L[(x,y), I_a, \Omega_L^*] \geq 1 - \epsilon/P, \quad \text{and} \quad |U(x,y)| \leq \epsilon.$$

This proves the lemma.

The uniqueness can now be proved by assuming two d.h.m.'s and showing that their difference vanishes identically.

The proof of theorem 4.2 is complete.

We note that the existence of a unique bounded solution of the difference analog of the Dirichlet problem for Ω_L with bounded boundary values is almost immediate. If the boundary values are determined by $g(x)$, then the limit of the absolutely and uniformly convergent series $\sum_{\mu=-\infty}^{\infty} H_L[(x,y), \mu h, \Omega_L] g(\mu h)$ is d.h. in R_L, bounded in Ω_L and equals $g(x)$ on S_L. Thus a solution exists. The uniqueness follows at once from lemma 4.1.

We next consider the region $x \geq 0$, $y \geq 0$. To find d.h.m. for subsets of the line $y=0$ we perform a sign-changing reflection about the line $x=0$ and use theorem 4.2. Since the d.h.m. is zero on the line $x=0$, this can be done in such a way that the new function will be d.h. in R_L. Similarly to find d.h.m. for subsets of the line $y=0$ we reflect in the line $x=0$.

By similar methods the existence and uniqueness of d.h.m. can be established for other regions such as the semi-infinite strip $0 \leq x \leq a$, $y \geq 0$.

5. Modulus of Continuity

The modulus of continuity of a function $f(x,y)$ in a closed region Ω is defined by

$$\omega(\delta) = LUB |f(x_1,y_1) - f(x_2,y_2)|,$$

where $(x_1,y_1), (x_2,y_2) \epsilon \Omega$ and $(x_1-x_2)^2+(y_1-y_2)^2 \leq \delta^2$. Evidently if δ is not less than the diameter of Ω then $\omega(\delta)$ equals the oscillation of $f(x,y)$ in Ω.

For harmonic functions we prove the following theorem:

THEOREM 5.1. *Let Ω denote a bounded simply connected closed region with interior R and whose boundary S is a closed Jordan curve with the following property: there exist constants $r_0 > 0$ and $\theta \geq 0$ such that for any point P of S there exists a circular sector with vertex at P, with*

radius r_0 and included angle θ containing no point of R. Let $u(x,y)$ be harmonic in R, continuous in Ω with modulus of continuity $\omega(\delta)$ on S. If for some positive number D we have

$$\delta \leq \mathrm{Max}\{r_0, D, D(r_0/D)^{(\pi+\psi)/\pi}\}$$

then the modulus of continuity of $u(x,y)$ in Ω satisfies the inequality

$$\omega^*(\delta) \leq \omega[D(\delta/D)^{\pi/(\pi+\psi)}] + (4M/\pi)(\delta/D)^{\pi/(\pi+\psi)}, \tag{5.1}$$

where $\psi = \mathrm{Max}(2\pi-\theta, \pi)$ and

$$M = \underset{(x,y)\in S}{\mathrm{Max}}[u(x,y)] - \underset{(x,y)\in S}{\mathrm{Min}}[u(x,y)] \tag{5.2}$$

is the oscillation of $u(x,y)$ on S.

PROOF.

LEMMA 5.1. *Let I_r denote the interval $-r \leq x \leq r$, $y=0$ and let C_ρ denote the region $x^2+y^2 \leq \rho^2$, $y \geq 0$. If $(x,y) \in C_\rho$, then*

$$H[(x,y), I_r, y \geq 0] \geq 1 - 2\rho/\pi r.$$

PROOF. It is easy to show that if ϕ is the angle at $(-r,0)$ from I_r to the circle C through the points $(-r,0)$, $(r,0)$ and (x,y), then $H[(x,y), I_r, y \geq 0] = 1 - \phi/\pi$.

Now if $\rho/r = (1-\cos\phi)/\sin\phi$, then C_ρ is contained in the region bounded by C and the line $y=0$. Hence, by the minimum principle for harmonic functions we have for $(x,y) \in C_\rho$

$$H[(x,y), I_r, y \geq 0] \geq 1 - (2/\pi)\tan^{-1}(\rho/r) \geq 1 - 2\rho/\pi r,$$

and the lemma is proved.

LEMMA 5.2. *Let $C_{r,\psi}$ denote the region $x^2+y^2 \leq r^2$, $0 \leq \tan^{-1}(y/x) \leq \psi \leq 2\pi$ and let $B_{r,\psi}$ denote the bounding radii of $C_{r,\psi}$. (If $\psi = 2\pi$, then $B_{r,\psi}$ denotes the line $0 \leq x \leq r$, $y=0$). If $\rho \leq r$ and if $(x,y) \in C_{\rho,\psi}$, then*

$$H[(x,y), B_{r,\psi}, C_{r,\psi}] \geq 1 - (4/\pi)(\rho/r)^{\pi/\psi}.$$

PROOF. We first consider the case $\psi = \pi$. If $x^2+y^2=r^2$ and $y>0$, then as in lemma 5.1 we have $H[(x,y), I_r, y \geq 0] = 1/2$. Hence, as we verify at once,

$$H[(x,y), I_r, C_r] = 2H[(x,y), I_r, y \geq 0] - 1.$$

If $(x,y) \in C_{\rho,\pi}$, then by lemma 5.1 we have

$$H[(x,y), I_r, C_r] \geq 1 - (4/\pi)(\rho/r).$$

The lemma can now be verified for the general case by mapping $C_{r,\pi}$ onto $C_{r,\psi}$ by means of the conformal transformation $(w/r) = (z/r)^{\psi/\pi}$. We omit the details.

Now by the maximum principle for harmonic functions, for given δ the maximum value of $|U(x_1,y_1) - U(x_2,y_2)|$ for $(x_1-x_2)^2 + (y_1-y_2)^2 \leq \delta^2$ occurs when either (x_1,y_1) or (x_2,y_2) belongs to S. If $(x_1,y_1) \in S$, then for all r such that $0 < r \leq r_0$ there exists a circular sector $C_{r,\psi}$ containing at least one point of R with vertex at (x_1,y_1) with radius $r \geq \delta$ and angle ψ, such that $B_{r,\psi}$ the union of the bounding radii is disjoint from R. Since the theorem is trivially true if $(x_2,y_2) \in S$, we assume $(x_2,y_2) \in R$. Let Ω_1 denote the closure of the connected component of (x_2,y_2) for the region $\Omega \cap C_{r,\psi}$. Evidently $\Omega_1 \subset C_{r,\psi}$. Since for $(x,y) \in \Omega_1 \cap S$, we have

$$H[(x,y), B_{r,\psi}, C_{r,\psi}] \leq 1 = H[(x,y), \Omega_1 \cap S, \Omega_1]$$

and for (x,y) contained in Ω_1 and on the arc of $C_{r,\psi}$, we have

$$H[(x,y), B_{r,\psi}, C_{r,\psi}] = 0,$$

then for all $(x,y)\epsilon\Omega_1$ it follows that

$$H[(x,y),B_{r,\psi},C_{r,\psi}]\leq H[(x,y),\Omega_1\cap S,\Omega_1].$$

But by lemma 5.2 we have

$$H[(x_2,y_2),B_{r,\psi},C_{r,\psi}]\geq 1-(4/\pi)(\delta/r)^{\pi/\psi}$$

since the lemma is obviously true if we rotate the sector.

Therefore, we have

$$|u(x_2,y_2)-u(x_1,y_1)|\leq\omega(r)H[(x_2,y_2),C_{r,\psi}\cap S,\Omega]+MH[(x_2,y_2),S-C_{r,\psi},\Omega]\leq\omega(r)+(4M/\pi)(\delta/r)^{\pi/\psi}.$$

Now by the assumptions on δ we have $D(\delta/D)^{\pi/(\pi+\psi)}\leq D(r_0/D)=r_0$. Hence, we can choose $r=D(\delta/D)^{\pi/(\pi+\psi)}\leq r_0$, and the theorem follows.

We now consider the case where Ω is an arbitrary simply connected region. We first prove the following general theorem, which is essentially a formulation for harmonic functions which is equivalent to Carathéodory's form of the theorem of Milloux for analytic functions:

THEOREM 5.2. *Let G be a Jordan subregion of $|z|<1$, whose boundary consists of a Jordan arc α_1 which passes through $z=0$ plus an arc α_2 of $\Gamma:|z|=1$. Let $u(z)$ be harmonic and bounded in G, continuous in the corresponding closed region except at the end points of α_1 and α_2, equal to unity in the interior points of α_1 and to zero in the interior points of α_2. Then in every point z of G we have*

$$u(z)\geq 1-(4/\pi)\tan^{-1}|z|^{1/2}. \tag{5.3}$$

PROOF. Let $v(z)$ be conjugate to $u(z)$ in G, and let $f(z)\equiv\exp[-u(z)-iv(z)]$. Except perhaps at the end points of the arcs, on α_1 we have $|f(z)|=e^{-1}$, and on α_2 we have $|f(z)|=1$; on these open arcs $|f(z)|$ is continuous in the two-dimensional sense. Then by the form of Milloux's theorem presented by Carathéodory, [1], 354, we have for $z\epsilon G$

$$\log|f(z)|=-u(z)\leq-1+(4/\pi)\tan^{-1}|z|^{1/2}$$

as we were to prove.

THEOREM 5.3. *Let Ω denote a bounded simply connected closed region with interior R and boundary S. Let $u(x,y)$ be harmonic in R, continuous in Ω and having modulus of continuity $\omega(\delta)$ on S. If D is any positive constant, then the modulus of continuity of $u(x,y)$ in Ω satisfies the inequality*

$$\omega^*(\delta)\leq\omega[D(\delta/D)^{1/3}]+(4M/\pi)(\delta/D)^{1/3}$$

for all $\delta\leq D$.

PROOF. As in the proof of theorem 5.1, it is sufficient to show that if C_r is a circle with center (x_1,y_1) on S and radius r and if $(x_2,y_2)\epsilon\Omega$ and $(x_1-x_2)^2+(y_1-y_2)^2\leq\delta^2\leq r^2$, then

$$H[(x_2,y_2),C_r\cap S,\Omega]\geq 1-(4/\pi)(\delta/r)^{1/2}. \tag{5.4}$$

The theorem then follows if we let $r=D(\delta/D)^{1/3}$ since $\delta\leq D$ and hence $D(\delta/D)^{1/3}\geq\delta$.

Now, if Ω is a Jordan region, (5.4) follows at once from theorem 5.2, since $\tan^{-1}|z|^{1/2}\leq|z|^{1/2}$ for $|z|\leq 1$. We indicate the modifications necessary to include the case where Ω is an arbitrary simply connected region.

Let O be a boundary point of Ω, let C_r be the circle $|z|=r$, and let z_0 be a point interior to Ω and to C_r. If no point of Ω lies exterior to C_r, then a function $v(z)$ harmonic in R and continuous in Ω equal to unity on S is identically unity in Ω so we have $v(z_0)=1$. We proceed to study the contrary case. If points of R lie exterior to C_r, such points can be joined to z_0 by a Jordan arc lying wholly in R, so at least one arc of C_r lies in R. Let the totality of mutually disjoint arcs of C_r in R be $A_1, A_2, \ldots$. Denote by R_0 the subregion of R interior to C_r containing z_0 and by R_1 the sum of R_0, its reflection (inverse) in C_r, and the arcs A_k which form part of the boundary of R_0; if an arc of C_r is part of the boundary of R, it does not belong to R_1. We modify R_1 by

adjoining to R_1 the interior of each Jordan curve that can be drawn in R_1 and to which O and z_0 are exterior. Denote this new region by R_2. Then R_2 contains z_0, is simply connected, and has O as either an exterior or a boundary point. The subregion R_3 of R_2 interior to C_r is also simply connected, and part of its boundary is an open arc A_0 of C_r of which every point is accessible; we choose A_0 as the largest such arc, so that every boundary point of R_3 not on A_0 is either a boundary point of R interior to C_r or is a point of C_r not contained in an arc of C_r consisting wholly of accessible boundary points of R_3. By a conformal map of R_3 onto the interior of a circle γ (in which A_0 necessarily corresponds to an arc of γ) it is clear that $H(z,A_0,R_3)$ exists and is unique; this function takes the boundary value unity at every point of A_0 and the boundary value zero at every boundary point of R_3 not on the closure of A_0. Carathéodory's proof of Milloux's theorem is valid for the region R_3, the distance from z_0 to the boundary of R_3 is not greater than $|z_0|$, so (5.4) is valid for an arbitrary simply connected region, and the theorem follows.

The modulus of continuity of a function $F(x,y)$ on any subset Ω_L of $L[h,k]$ is defined by

$$\omega_L(\delta) = LUB|F(x_1,y_1) - F(x_2,y_2)|,$$

where (x_1,y_1), $(x_2,y_2)\,\epsilon\Omega_L$, and where $(x_1-x_2)^2+(y_1-y_2)^2 \leq \delta^2$.

For d.h. functions in a rectangle we prove the following theorem:

THEOREM 5.4. *Let Ω denote the rectangle $0\leq x\leq a$, $0\leq y\leq b$, where $(a,b)\epsilon L[h,k]$. Let Ω_L denote the subset of $L[h,k]$ contained in Ω. If $U(x,y)$ is d.h. in R_L, the interior of Ω_L, and has modulus of continuity $\omega(\delta)$ on S_L, the boundary of Ω_L, then for $\delta\leq r=(ab)^{1/2}$ the modulus of continuity of $U(x,y)$ in Ω_L satisfies the inequality*

$$\omega_L^*(\delta) \leq \omega[2^{1/2}\{(r\delta)^{1/2}+h+k\}] + (M/2)\nu(1/2)(\delta/r)^{1/2} \tag{5.5}$$

where M and $\nu(1/2)$ are defined by (5.2) and (4.6), respectively.

PROOF. As in the proof of theorem 5.1 the maximum value of $|U(x_1,y_1)-U(x_2,y_2)|$ for $(x_1-x_2)^2+(y_1-y_2)^2\leq\delta^2$ is assumed when either (x_1,y_1) or (x_2,y_2) belongs to S_L. Let us assume that $(x_1,y_1)\epsilon S_L$. Now if (x_2,y_2) also belongs to S_L the theorem is trivial, since $\delta\leq r$. We therefore assume $(x_2,y_2)\epsilon R_L$.

Let p denote a straight line containing (x_1,y_1) and including one of the sides of the rectangle. Let C denote the closed interior of a semicircle with center at (x_1,y_1), with radius $\delta_1=2^{1/2}\{(\delta r)^{1/2}+h+k\}$, with bounding diameter included in p and containing at least one point of R_L. Since $\delta\leq r$ we have $\delta_1\geq 2^{1/2}\delta$. Evidently there exists a rectangle T included in C with one side contained in p and with vertices contained in $L[h,k]$ such that the sides perpendicular to p are at least half as long as those parallel to p and such that the latter sides have length at least $2(\delta r)^{1/2}$.

By (4.2) and (4.3) we have

$$H_L[(x,y),C\cap S_L,\Omega_L] \geq H_L[(x,y),T\cap S_L,\Omega_L] \geq H_L[(x,y),T\cap S_L,\Omega_L\cap T].$$

Now, for $(x,y)\epsilon S_L\cap T$ we have

$$H_L[(x,y),T\cap p,T] \leq 1 = H_L[(x,y),\ T\cap S_L,\Omega_L\cap T].$$

Moreover, since the intersection of p and the boundary of $T\cap\Omega_L$ is contained in $T\cap S_L$ we have $H_L[(\lambda,y),\ T\cap p,T]=0$ for all points of the boundary of $\Omega_L\cap T$ not contained in $S_L\cap T$. Therefore, for all points of the boundary of $T\cap\Omega_L$ we have

$$H_L[(x,y),T\cap S_L,\Omega_L\cap T] \geq H_L[(x,y),T\cap p,T].$$

It follows that for all $(x,y)\epsilon T\cap\Omega_L$ we have

$$H_L[(x,y),T\cap S_L,\Omega_L\cap T] \geq H_L[(x,y),T\cap p,T].$$

Now since $(x_2,y_2)\epsilon T\cap\Omega_L$, we have by theorem 4.1

$$H_L[(x_2,y_2),T\cap p,T]\geq 1-(1/2)\nu(1/2)(\delta/r)^{1/2}.$$

Hence,

$$H_L[(x_2,y_2),S_L-(S_L\cap C),\Omega_L]\leq(1/2)\nu(1/2)(\delta/r)^{1/2}.$$

Therefore,

$$|U(x_1,y_1)-U(x_2,y_2)|\leq\omega[2^{1/2}\{(r\delta)^{1/2}+h+k\}]+(M/2)\nu(1/2)(\overset{*}{\delta}/r)^{1/2},$$

and the theorem follows.

In the above proof if $h=k$, one could have obtained a rectangle with the desired properties by letting C have radius $2^{1/2}[(r\delta)^{1/2}+h]$. Therefore, we have

COROLLARY: *If $h=k$, then*

$$\omega_L{}^*(\delta)\leq\omega[2^{1/2}\{(r\delta)^{1/2}+h\}]+(M/2)\nu(1/2)(\delta/r)^{1/2}.$$

6. Error Estimate for the Rectangle In Terms of the Modulus of Continuity on the Boundary

In this section we obtain an error bound for the rectangle of section 3 under the assumption that the function $f(x,y)$, which determines the boundary values, has modulus of continuity $\omega(\delta)$ on S. The function $f_3(x,y)$ defined in section 3 is also continuous, and we denote by $\omega_3(\delta)$ its modulus of continuity for $0\leq x\leq a$, $y=0$.

Let $U_3(x,y)$ and $u_3(x,y)$ be given by (3.3) and (3.5), respectively. We define the function $t_3(x)$ by the partial sum

$$t_3(x)=\sum_{n=1}^{A} d_{A,n}A_n\sin(n\pi x/a), \tag{6.1}$$

where the A_n are the Fourier coefficients for $f_3(x,0)=g(x)$ as defined by (3.4) and where the coefficients $d_{A,n}$ are summation coefficients defined by Jackson [7, p. 9]. Let $u_5(x,y)$ and $U_5(x,y)$ denote respectively the solutions of the Dirichlet problem and its difference analog vanishing on S except for $y=0$. If $y=0$, the values are determined by $f_5(x)$. We now prove

THEOREM 6.1. *If $(x,y)\epsilon\Omega_L$ and $0\leq x\leq a$, $\epsilon\leq y\leq b$, then*

$$|U_5(x,y)-u_5(x,y)|\leq 8M^*C\lambda(h/a)^2(\epsilon/a)^{-3}, \tag{6.2}$$

where

$$\lambda=\frac{6\epsilon}{\alpha^3\pi^3}+\frac{27\epsilon/a}{\alpha^2\pi^2\epsilon^2},\qquad M^*=\operatorname*{Max}_{0\leq x\leq a}|g(x)| \tag{6.3}$$

and where C and α are determined by (3.10) *and* (3.12), *respectively.*

PROOF. It can be verified that

$$u_5(x,y)=\sum_{n=1}^{A} d_{A,n}A_n\sin(n\pi x/a)\Gamma_n(y), \tag{6.4}$$

$$U_5(x,y)=\sum_{n=1}^{A} d_{A,n}A_n\sin(n\pi x/a)\Gamma_m(y), \tag{6.5}$$

where m and n are related by (3.7), and where $\Gamma_m(y)$ is defined by (3.16). Evidently we have

$$|U_5(x,y)-u_5(x,y)|\leq\sum_{n=1}^{A}|d_{A,n}A_n|\cdot|\Gamma_m(y)-\Gamma_n(y)|. \tag{6.6}$$

By lemma 3.3 we have

$$\left|\frac{d}{dm}\Gamma_m(y)\right|\leq(\pi y/a)\coth(m\pi b/a)\exp(-m\pi y/a),\qquad(0\leq y\leq b),\quad(m\geq 0). \tag{6.7}$$

By lemma 3.2 we have $m \geq \alpha n$ for $1 \leq n \leq A$, and

$$\left|\frac{d}{dm}\,\Gamma_m(y)\right| \leq (\pi y/a)\coth(\alpha\pi b/a)\exp(-\alpha n\pi y/a). \tag{6.8}$$

Using lemma 3.1 we get, as in the proof of lemma 3.5,

$$|\Gamma_m(y)-\Gamma_n(y)| \leq C\alpha\epsilon(h/a)^2(\pi y/a)n^3\exp(-\alpha n\pi y/a).$$

Therefore, we have

$$\sum_{n=1}^{A}|\Gamma_m(y)-\Gamma_n(y)| \leq \sum_{n=1}^{\infty}|\Gamma_m(y)-\Gamma_n(y)| \leq C\alpha\epsilon(h/a)^2(\pi y/a)\sum_{n=1}^{\infty}n^3\exp(-\alpha n\pi y/a),$$

which is convergent for $y>0$.

Now the following statement can be verified easily: if $G(x)$ is a continuous nonnegative function for $x \geq 0$, nondecreasing for $0 \leq x \leq X$, and nonincreasing for $X \leq x$, then

$$\sum_{n=1}^{\infty}G(n) \leq \int_0^{\infty}G(t)dt+G(X).$$

Therefore, since for $\nu>0$ we have

$$\operatorname*{Max}_{x\geq 0}[x^3\exp(-\nu x)] = (3/\nu\epsilon)^3,$$

it follows that

$$\sum_{n=1}^{\infty}n^3\exp(-\alpha n\pi y/a) \leq \int_0^{\infty}t^3\exp(-\alpha\pi yt/a)\,dt+(3a/\alpha\pi y\epsilon)^3 \leq 6(a/\alpha\pi y)^4+(3a/\alpha\pi y\epsilon)^3.$$

Therefore, we get

$$\sum_{n=1}^{A}|\Gamma_m(y)-\Gamma_n(y)| \leq \lambda C(h/a)^2(y/a)^{-3} \leq \lambda C(h/a)^2(\epsilon/a)^{-3}, \tag{6.9}$$

since $y \geq \epsilon$.

For the Fourier coefficients, since $|g(t)| \leq M^*$, we have

$$|A_n| = |(2/a)\int_0^a g(t)\sin(n\pi t/a)\,dt| \leq (2/a)\int_0^a |g(t)|dt \leq 2M^*. \tag{6.10}$$

Jackson [6] proved that $|1-d_{A,n}| \leq 3n/A \leq 3$. Hence

$$|d_{A,n}| \leq 4. \tag{6.11}$$

From (6.6), (6.9), (6.10), and (6.11) the theorem now follows.

COROLLARY. *For $(x,y)\epsilon\Omega_L$ and $0 \leq x \leq a$, $\epsilon \leq y \leq b$ we have*

$$|U_3(x,y)-u_3(x,y)| \leq 8M^*C\lambda(h/a)^2(\epsilon/a)^{-3}+2K\omega_3(2h), \tag{6.12}$$

where K is a positive absolute constant less than [10] 3.

PROOF.

$$|U_3(x,y)-u_3(x,y)| \leq |U_3(x,y)-U_5(x,y)|+|U_5(x,y)-u_5(x,y)|+|u_5(x,y)-u_3(x,y)|.$$

By the maximum and minimum principles for harmonic and d.h. functions, we have for $(x,y)\epsilon\Omega_L$

$$|U_3(x,y)-U_5(x,y)|, |u_3(x,y)-u_3(x,y)| \leq \operatorname*{Max}_{0\leq x\leq a}|f_5(x)-g(x)|.$$

Using a theorem of Jackson [7, p. 7], we obtain

$$\operatorname*{Max}_{0\leq x\leq a}|f_5(x)-g(x)| \leq K\omega_3(2a/A),$$

[10] See Jackson [7, p. 7].

where K is a positive absolute constant less than 3. The corollary now follows from the theorem.

We shall now derive an error bound for the original problem where we no longer assume that the boundary values vanish at the corners or along the sides of the given rectangle.

THEOREM 6.2. *For all* $(x,y)\epsilon\Omega_L$, *we have*

$$|U(x,y)-u(x,y)| \leq \operatorname{Max}\left\{I; 2\omega_L^*\left[r\left(\frac{hk}{r^2}\right)^{2/7}\right]\right\}, \tag{6.13}$$

where

$$I=16M[\lambda_a C_a \sigma^{-6/7}(a/b)^{9/14}(h/a)^{2/7}+\lambda_b C_b \sigma^{6/7}(b/a)^{9/14}(k/b)^{2/7}]+ 4K\{\omega(2h)+\omega(2k)+2M[h/a+k/b]\},$$

$$r=(ab)^{1/2} \tag{6.14}$$

$$C_a=\frac{\pi^2(1+\sigma^2)}{24\alpha e}\coth(\alpha\pi b/a), \quad C_b=\frac{\pi^2(1+\sigma^{-2})}{24\beta e}\coth(\beta\pi a/b) \tag{6.15}$$

$$\alpha=(2/\pi\sigma)\sinh^{-1}(\sigma), \quad \beta=(2\sigma/\pi)\sinh^{-1}(\sigma^{-1}) \tag{6.16}$$

$$\left.\begin{aligned}\lambda_a&=\frac{6e}{\alpha^3\pi^3}+\frac{27/2}{\alpha^2\pi^2e^2}\\ \lambda_b&=\frac{6e}{\beta^3\pi^3}+\frac{27/2}{\beta^2\pi^2e^2}\end{aligned}\right\} \tag{6.17}$$

$$M=\operatorname*{Max}_{(x,y)\epsilon S} u(x,y)-\operatorname*{Min}_{(x,y)\epsilon S} u(x,y) \tag{6.18}$$

$$\omega_L^*(\delta)=\omega[2^{1/2}[(r\delta)^{1/2}+h+k]]+(M/2)\nu(1/2)(\delta/r)^{1/2} \tag{6.19}$$

and $\omega(\delta)$ *is the modulus of continuity of* $u(x,y)$ *on* S. *The function* $\nu(b/a)$ *is defined by* (4.6) *and* $\nu(1/2)$ *equals* 3.97, *approximately.*

PROOF.

LEMMA 6.1. *If* $u_1(x,y)$ *is defined by* (3.1), *then for all* $(x,y)\epsilon\Omega$ *we have* $|u(x,y)-u_1(x,y)|\leq M$.

PROOF. Since $u(x,y)$ and $u_1(x,y)$ are harmonic, the maximum of $|u(x,y)-u_1(x,y)|$ is assumed on S. We can assume, without loss of generality that the maximum occurs at a point whose ordinate is zero. By (3.1) we have

$$u_1(x,0)=(1-x/a)u(0,0)+(x/a)u(a,0),$$

and

$$|u(x,0)-u_1(x,0)|\leq|1-x/a|\cdot|u(x,0)-u(0,0)|+|x/a|\cdot|u(x,0)-u(a,0)|.$$

But,

$$|u(x,0)-u(0,0)|,|u(x,0)-u(a,0)|\leq\operatorname*{Max}_{0\leq x\leq a} u(x,0)-\operatorname*{Min}_{0\leq x\leq a} u(x,0)\leq M,$$

and the lemma follows.

The above result cannot be improved as one can show by considering the case where $u_1(x,y)$ is identically zero and $u(x,y)\geq 0$.

From lemma 6.1 we conclude that $|u_3(x,y)|\leq M$. In particular we have $|g(x)|\leq M$; hence,

$$M^*\leq M. \tag{6.20}$$

LEMMA 6.2.

$$\omega_3(\delta)\leq\omega(\delta)+\delta M/a. \tag{6.21}$$

PROOF. Evidently we have $\omega_3(\delta)\leq\omega(\delta)+\omega_1(\delta)$, where $\omega_1(\delta)$ denotes the modulus of con-

tinuity of $u_1(x,0)$ considered as a function of x. But since

$$u_1(x+\delta,0)-u_1(x,0)=(\delta/a)[u(a,0)-u(0,0)],$$

we have $\omega_1(\delta)\leq\delta M/a$, and the lemma follows.

LEMMA 6.3. *If* $\epsilon\leq x\leq a-\epsilon, \epsilon\leq y\leq b-\epsilon, (x,y)\in\Omega_L$, *then*

$$|U(x,y)-u(x,y)|\leq 16M\{\lambda_a C_a(h/a)^2(\epsilon/a)^{-3}+\lambda_b C_b(k/b)^2(\epsilon/b)^{-3}\}+4K[\omega(2h)+\omega(2k)+2M(h/a+k/b)]. \tag{6.22}$$

PROOF. We observe that $|U(x,y)-u(x,y)|=|U_2(x,y)-u_2(x,y)|$. The function $[U_2(x,y)-u_2(x,y)]$ is the sum of $[U_3(x,y)-u_3(x,y)]$ and three other terms of similar type. The lemma follows from (6.12), from (6.20) and from lemma 6.2. (We note that from the hypothesis we have $\epsilon/a, \epsilon/b\leq\frac{1}{2}$.)

Lemma 6.3 affords us an error bound for those points of Ω_L which are at a distance of not less than ϵ from the boundary. In order to obtain a uniform error bound we now consider those points which are within ϵ of the boundary.

Since $4/\pi<\nu(1/2)/2$ it follows from theorem 5.1, (with $D=r$), and theorem 5.4 that the moduli of continuity of $U(x,y)$ and $u(x,y)$ do not exceed the upper bound for $\omega_L^*(\delta)$ given by theorem 5.4, provided $\delta\leq(ab)^{1/2}$. If $(x,y)\epsilon\Omega_L$ and if (x,y) is within ϵ of a point of S, then there exists a point of S_L at a distance not greater than ϵ from (x,y). We remark that every point of Ω_L is within $(ab)^{1/2}$ of some point of S_L. Since $U(x,y)=u(x,y)$ on S_L we have

$$|U(x,y)-u(x,y)|\leq 2\omega_L^*(\epsilon).$$

If I denotes the right member of (6.22), then we have

$$|U(x,y)-u(x,y)|\leq \operatorname{Max}\{I;2\omega_L^*(\epsilon)\}. \tag{6.23}$$

In order that the error in Ω_L should approach zero with the highest power of $\gamma=(hk)^{1/2}$ whenever $\omega(\delta)/\delta$ is bounded as a function of δ, we choose $\epsilon=r(hk/r^2)^{2/7}$. Evidently we have

$$\epsilon/a=\sigma^{2/7}(h/a)^{4/7}(b/a)^{3/14}, \qquad \epsilon/b=\sigma^{-2/7}(k/b)^{4/7}(a/b)^{3/14}.$$

The theorem now follows from (6.23), lemma 6.3, and theorem 5.4.

For the special case of the unit square theorem 6.2 and theorem 5.4, corollary, give

COROLLARY. *If* $a=b=\sigma=1$, *then we have*

$$|U(x,y)-u(x,y)|\leq \operatorname{Max}\{J_1;J_2\},$$

where

$$J_1=32M\lambda Ch^{2/7}+8K[\omega(2h)+2Mh], \qquad C=(\pi^2/12\alpha e)\coth(\alpha\pi)\sim.572,$$

$$J_2=2\omega[2^{1/2}(h^{2/7}+h)]+M\nu(1/2)h^{2/7}, \qquad \alpha=(2/\pi)\sinh^{-1}(1)\sim.561,$$

$$\lambda=\frac{6e}{\alpha^3\pi^3}+\frac{27/2}{\alpha^2\pi^2e^2}\sim 3.566.$$

Substituting numerical values, we obtain

$$J_1\leq 66Mh^{2/7}+24\omega(2h)+48Mh, \qquad J_2\leq 2\omega[2^{1/2}(h^{2/7}+h)]+4Mh^{2/7}.$$

The above expressions for J_1 and J_2 represent a slight improvement in the formulas previously given by the authors [14].

7. Other Regions

In this section we consider regions of the type described in section 2 other than rectangles. The case of two overlapping rectangles is studied in detail as an illustration of the method

which can be extended to more complicated regions. We first prove a theorem valid for two overlapping regions whether rectangles or not.

THEOREM 7.1. *Let $\Omega=\Omega'\cup\Omega''$, where $R'\cap R''$ is not empty, and where neither region includes the other. Let $u(x,y)$ and $U(x,y)$ denote, respectively, the solution of the Dirichlet problem and its finite difference analog for Ω. Let Ω_L, Ω_L', and Ω_L'' denote the points of $L[h,k]$ belonging to Ω, Ω', and Ω'', respectively. Let $T_L'=S_L'\cap R_L''$, $T_L''=S_L''\cap R_L'$, and let*

$$\mu_1=\operatorname*{Max}_{(x,y)\in T_L'} H_L[(x,y),T_L'',\Omega_L''], \qquad \mu_2=\operatorname*{Max}_{(x,y)\in T_L''} H_L[(x,y),T_L',\Omega_L'].$$

Next, let U' and U'' denote functions d.h. in Ω_L' and Ω_L'', respectively, and equal to u on S_L' and S_L'', respectively. Then for $(x,y)\in\Omega_L$, we have

$$|U(x,y)-u(x,y)|\leq \operatorname{Max}(A,B),$$

where

$$A=\frac{E'(1+\mu_1-\mu_1\mu_2)+E''}{1-\mu_1\mu_2}, \qquad E'=\operatorname*{Max}_{(x,y)\in R_L'} |U'(x,y)-u(x,y)|,$$

$$B=\frac{E''(1+\mu_2-\mu_1\mu_2)+E'}{1-\mu_1\mu_2}, \qquad E''=\operatorname*{Max}_{(x,y)\in R_L''} |U''(x,y)-u(x,y)|.$$

PROOF. Let

$$F'=\operatorname*{Max}_{(x,y)\in T_L'} |U(x,y)-u(x,y)|, \qquad F''=\operatorname*{Max}_{(x,y)\in T_L''} |U(x,y)-u(x,y)|.$$

Clearly, for $(x,y)\in T_L'$

$$|U(x,y)-u(x,y)|\leq |U(x,y)-U''(x,y)|+|U''(x,y)-u(x,y)|$$

$$\leq \mu_1 \operatorname*{Max}_{(x,y)\in T_L''} |U(x,y)-U''(x,y)|+|U''(x,y)-u(x,y)|.$$

Hence, by the maximum and minimum principles for d.h. functions $F'\leq\mu_1F''+E''$. Similarly, $F''\leq\mu_2F'+E'$. Therefore,

$$F'\leq\frac{\mu_1E'+E''}{1-\mu_1\mu_2}, \qquad F''\leq\frac{\mu_2E''+E'}{1-\mu_1\mu_2}.$$

By the maximum and minimum principles,

$$\operatorname*{Max}_{(x,y)\in\Omega_L'} |U(x,y)-u(x,y)|\leq E'+F', \qquad \operatorname*{Max}_{(x,y)\in\Omega_L''} |U(x,y)-u(x,y)|\leq E''+F'',$$

and the theorem follows.

The proof of this theorem was, of course, motivated by consideration of the difference analog of the Schwarz Alternating Process. Indeed, in order to solve the difference equation for Ω_L, one might guess values for $U(x,y)$ on $S_L'\cap R_L''$ and then solve the difference equation in R_L' obtaining in particular values on $S_L''\cap R_L'$. Next one solves the difference equation for R_L'', using the computed values on $S_L''\cap R_L'$, and obtains new values for $S_L'\cap R_L''$. This process can be repeated and the successive values thus obtained converge to the exact solution of the *difference* equation. Moreover, the rapidity of convergence can be estimated if μ_1 and μ_2 are known. In fact, one can show that after a complete iteration the maximum error is reduced by a factor of $(1-\mu_1\mu_2)$.

If for Ω' and Ω'' the quantities E' and E'' are known whenever the modulus of continuity and oscillation of $u(x,y)$ are known on S' and S'', then by using theorem 5.1 or theorem 5.3, E' and E'' can be computed, provided the modulus of continuity of $u(x,y)$ on S is known. If, moreover, μ_1 and/or μ_2 are known, an error bound for the composite region can be obtained.

We consider now the case of two overlapping rectangles Ω_1 and Ω_2 with sides parallel to the coordinate axes. If the intersection of the interiors is not empty, and if neither region is a

subset of the other, then the cases A through F shown in figure 1 occur.

FIGURE 1.

The composite regions of cases C and D are of the same type as those of cases A and B, respectively. The problem of determining μ_1 and μ_2 become problems in d.h.m. for the rectangle of the types shown in figure 2.

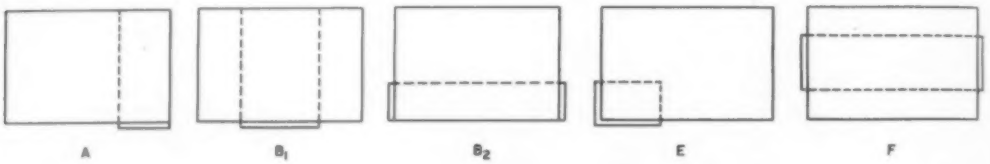

FIGURE 2.

Upper bounds for d.h.m. are required in points on the closed dotted lines for the open arcs on the boundary indicated by heavy lines.

By (4.3), these upper bounds are not greater than the upper bounds for the problems shown in figure 3.

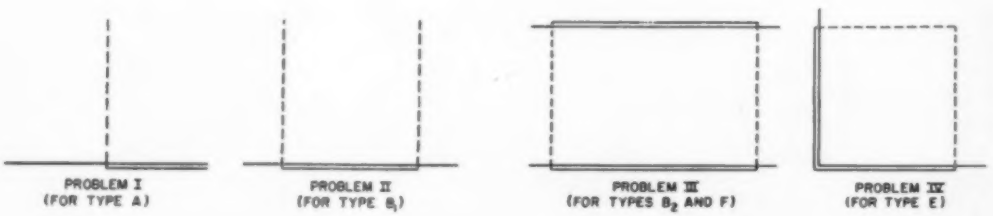

FIGURE 3.

For problem I, since the harmonic measure of the open arc is required, $\frac{1}{2}$ is an upper bound on the dotted line, by symmetry.

THEOREM 7.2. *Let Ω_L be bounded in part by a segment of a line l. Let R_L contain no point of l. Let l' denote a line perpendicular to l and containing a point of $l \cap S_L$. Let S' denote any subset of $l \cap S_L$ contained in one of the open half planes bounded by l'. If (x,y) is any point of $R_L \cap l'$, then*

$$H_L[(x,y),S',\Omega_L] \leq \tfrac{1}{2}.$$

PROOF. The theorem follows easily by (4.2), (4.3), and problem I.

As a corollary we have an upper bound of $\frac{1}{2}$ for problem II. Also, for problem III if we extend the lines whose harmonic measure is required to the right, we get by symmetry as in

problem I, $\frac{1}{2}$ as an upper bound for the d.h.m. on the left dotted line. Similarly $\frac{1}{2}$ is an upper bound for the d.h.m. on the right dotted line.

For problem IV the situation is somewhat more complicated. We prove

THEOREM 7.3: *Let Ω denote the region: $x \geq 0$, $y \geq 0$, and let Ω_L denote the subset of $L[h,k]$ contained in Ω. Let I_a, I_b denote respectively the intervals $0<x<a$, $y=0$ and $0<y<b$, $x=0$, where the point (a,b) belongs to $L[h,k]$. We have*

$$H_L[(x,b),I_a \cup I_b,\Omega_L] \leq \mathrm{Max}\left[\frac{1+w}{2}; 1-\frac{(1-w)b}{2y_0}\right], \tag{7.1}$$

where

$$w=(2/\pi)\log\frac{1+\exp(-\pi/2)}{1-\exp(-\pi/2)}. \tag{7.2}$$

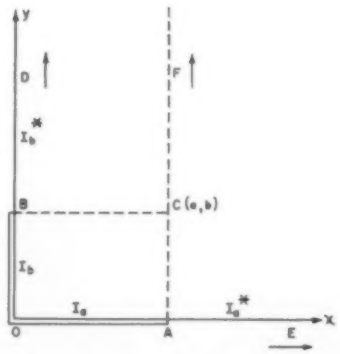

FIGURE 4.

Here y_0 is the smallest number not less than $a/2\alpha$ such that y_0/k is an integer. The quantities α and σ are defined by (3.12) *and* (2.3), *respectively.*

PROOF. Let I_a^*, I_b^* denote respectively the intervals $x \geq a$, $y=0$, and $y \geq b$, $x=0$. We first prove

LEMMA 7.1. *If $0 \leq x$, $0 \leq y$, then*

$$H_L[(x,b),I_b^*,\Omega_L] \geq H_L[(x,b),I_b,\Omega_L], \tag{7.3}$$

and

$$H_L[(a,y),I_a^*,\Omega_L] \geq H_L[(a,y),I_a,\Omega_L]. \tag{7.4}$$

PROOF: By theorem 7.2, we have

$$H_L[(x,b),y \geq b \cap x=0, x \geq 0] \geq H_L[(x,b),y<b \cap x=0, x \geq 0].$$

Hence, we certainly have

$$H_L[(x,b),\{y \geq b \cap x=0\} \cup \{-b<y<0 \cap x=0\},x \geq 0] \geq H_L[(x,b),\{0<y<b \cap x=0\} \cup \{y \leq -b \cap x=0\},x \geq 0].$$

But by a sign-changing reflection about the line $y=0$, we can show that the left member of the above expression minus the right member equals $H_L[(x,b),I_b^*,\Omega_L]-H_L[(x,b),I_b,\Omega_L] \geq 0$.

This proves (7.3). Evidently (7.4) can be proved by the same method.

From lemma 7.1, we conclude that

$$H_L[(x,b),I_a \cup I_b,\Omega_L] \leq H_L[(x,b),I_a,\Omega_L]+(1/2)H_L[(x,b),0<y \cap x=0,\Omega_L]. \tag{7.5}$$

But by (7.4) we have

$$(1/2)H_L[(a,y),0<y\cap x=0,\Omega_L]+H_L[(a,y),I_a,\Omega_L]\leq 1/2.$$

Therefore, the d.h. function

$$W(x,y)=H_L[(x,y),I_a,\Omega_L]+(1/2)H_L[(x,y),0<y\cap x=0,\Omega_L] \tag{7.6}$$

satisfies the conditions

$$W(x,0)=1, \quad (0<x<b); \qquad W(0,y)=1/2, \quad (0<y); \qquad W(a,y)\leq 1/2, \quad (0\leq y). \tag{7.7}$$

Let Ω^* denote the region $0\leq x\leq a\cap y\geq 0$, and let Ω_L^* denote the corresponding subset of $L[h,k]$. Evidently,

$$W(x,y)\leq U_1(x,y), \tag{7.8}$$

where

$$\left.\begin{array}{ll} \text{(a)} & U_1(x,y) \text{ is d.h. and bounded in } R_L^* \\ \text{(b)} & U_1(x,0)=1, \quad (0<x<a) \\ \text{(c)} & U_1(0,y)=U_1(a,y)=1/2, \quad (y\geq 0). \end{array}\right\} \tag{7.9}$$

We now prove

Lemma 7.2. Let $U_2(x,y)$ be d.h. and bounded for $(x,y)\epsilon R_L^*$ and such that

$$U_2(x,0)=1, \quad (0<x<1); \qquad U_2(0,y)=U_2(a,y)=0, \quad (y\geq 0).$$

We have

$$U_2(x,c)\leq \text{Max } [w;1-(1-w)c/y_0]. \tag{7.10}$$

Proof. Substituting in (3.5) and (3.6) and taking the limit as b becomes infinite we get

$$U_2(x,y)=\sum_{\substack{n=1\\ n \text{ odd}}}^{A}(2/A)\cot(n\pi/2A)\sin(n\pi x/a)\exp(-m\pi y/a),$$

where $Ah=a$.

By lemma 3.2, we have $m\geq \alpha n$. Also, since $\cot[n\pi/2A]\leq 2A/n\pi$ for $n\leq A$ we have

$$U_2(x,y)\leq \sum_{\substack{n=1\\ n \text{ odd}}}^{A}(4/\pi n)\exp(-\pi\alpha yn/a)\leq \sum_{\substack{n=1\\ n \text{ odd}}}^{\infty}(4/\pi n)\exp(-\pi\alpha yn/a)=(2/\pi)\log\frac{1+\exp(-\pi\alpha y/a)}{1-\exp(-\pi\alpha y/a)}.$$

Evidently if $y\geq a/2\alpha$, we have

$$U_2(x,y)\leq w. \tag{7.11}$$

Now since $0<w<1$, the function

$$U_3(x,y)=1-(1-w)y/y_0 \tag{7.12}$$

is d.h in R_L^* and is not less than $U_2(x,y)$ for $S_L^*\cap y\leq y_0$ and for $y=y_0$. Therefore, for $y\leq y_0$ we have

$$U_2(x,y)\leq 1-(1-w)y/y_0, \tag{7.13}$$

and the lemma follows.

Now $U_2(x,y)=2U_1(x,y)-1$. We also have by (7.5), (7.6), and (7.8).

$$H_L[(x,b),I_a \cup I_b,\Omega_L] \leq W(x,b) \leq U_1(x,b),$$

and the theorem now follows.

In applying the theorem to problem IV, we note that we can assume the value zero at the point (0,0) without changing the d.h.m.

Thus, an error bound can be obtained for the case of two overlapping rectangles. The above methods can also be used to find error bounds for other regions of the type considered in section 2.

8. References

[1] C. Carathéodory, Funktionentheorie, II (Verlag Birkhäuser Basel, 1950).

[2] L. Collatz, Bemerkungen zur Fehlerabschätzung für das Differenzenverfahren bei partiellen Differentialgleichungen, Z. angew. Math. u. Mech. **13**, 56–57 (1933).

[3] E. Copson, Functions of a complex variable (Oxford Press, Cambridge 1935).

[4] S. Gerschgorin, Fehlerabschätzung für das Differenzenverfahren zur Lösung partieller Differentialgleichungen, Z. angew. Math. u. Mech. **10,** 373–382 (1930).

[5] H. Heilbronn, On discrete harmonic functions, Proc. Cambridge Phil. Soc. **45,** 194–206 (1949).

[6] D. Jackson, On the degree of convergence of Sturm-Liouville series, Trans. Am. Math. Soc. **15,** 439–466 (1914).

[7] D. Jackson, The theory of approximation, Am. Math. Soc. Coll. Pub. **XI** (1930).

[8] D. Jackson, Fourier series and orthogonal polynomials, Mathematical Association of America Carus Monograph No. 6 (1941).

[9] J. Le Roux, Sur le problème de Dirichlet, J. Math. **10,** 189–230 (1914).

[10] S. Mikeladze, Über die numerische Lösung der Differentialgleichungen von Laplace und Poisson, Bul. acad. sci. U. S. S. R. (Ser. Math.) No. **2,** 271–290 (1938).

[11] R. Nevanlinna, Eindeutige analytische Funktionen (Berlin, 1936).

[12] H. Phillips and N. Wiener, Nets and the Dirichlet problem, J. Math. Phys. **2,** 105–124 (1923).

[13] P. C. Rosenbloom, On the difference equation method for solving the Dirichlet problem, Construction and applications of conformal maps, NBS AMS **18,** 231 (1952).

[14] J. L. Walsh and D. Young, On the accuracy of the numerical solution of the Dirichlet problem by finite differences, Bul. Am. Math. Soc. **57,** Abstract 500t, p. 478 (1951).

[15] W. Wasow, On the truncation error in the solution of Laplace's equation by finite differences, J. Research NBS **48,** 345–348 (1952) RP2321.

Washington, January 6, 1953.

INDEX TO VOLUME 51

TA
1
.U58

A

Page

Ackhammer, B. G., M. J. Reiney, M. Tryon, Study of degradation of polystyrene, using ultraviolet spectrophotometry, RP2445 155
Airborne microwave refractometer, measurement of refractive index of atmosphere with, RP2447 171
Air elutriation, particle-size determination of metal powder by, RP2428 17
D-Arabinose-1-C^{14} and D-ribose-1-C^{14}, synthesis, RP2458 307
D-Arabinose-5-C^{14}, preparation of, RP2446 167
Atmosphere, refractive index of, measurement with airborne microwave refractometer, RP2447 171
Atomic-energy states of chromium, Cr I, RP2457 247

B

Barium-oxide–boric-oxide–silica, system, RP2430 37
Bates, R. G., V. E. Bower, E. Smith, pH of solutions of potassium tetroxalate from 0° to 60° C, RP2450 189
Becker value of manila rope by photoelectric reflectometry, RP2443 141
Behrent, L. F., Fabrication of radio-frequency micropotentiometer resistance elements, RP2426 1
Bers, L., On mildly nonlinear partial difference equations of elliptic type, RP2455 229
Birnbaum, G., H. E. Bussey, Measurement of variations in atmospheric refractive index with an airborne refractometer, RP2447 171
Blaine, R. L., D. N. Evans, A. Litvin, A. C. Figlia, Properties of some masonry cement, RP2427 11
Boric-oxide–barium-oxide–silica, system, RP2430 37
Bower, V. E., R. G. Bates, E. Smith, pH of solutions of potassium tetroxalate from 0° to 60° C, RP2450 189
Buffers, standard tetroxalate, RP2450 189
Bussey, H. E., G. Birnbaum, Measurement of variations in atmospheric refractive index with an airborne refractometer, RP2447 171

C

Calorimetric properties of polybutadienes, RP2460 321
Carbohydrates, C^{14} labeled, RP2458 307
Carbon 14, determination of, in terminal positions of sugars, RP2446 167
Carbon 14, sugars position-labeled with, RP2458 307
Carlson, E. T., R. B. Peppler, L. S. Wells, Studies in the system magnesia-silica-water at elevated temperatures and pressures, RP2448 179
—, *L. S. Wells,* Hydrothermal preparation of some strontium silicates, RP2433 73
Cast irons, nickel, soil corrosion, RP2459 313
Cements, masonry, properties of some, RP2427 11
Cesium bromide, refractive index, for ultraviolet, visible, and infrared wavelengths, RP2440 123
Chromium spectrum, Cr I, RP2457 247
Chrysotile, synthesis, RP2448 179
Circuit bandwidth, effective, for noise with a power-law spectrum, RP2438 93
Computation, dynamic response, errors introduced by finite space and time increments in, RP2431 57
Computer, analogue, for solution of radio refractive-index equation, RP2462 335
Computers, metal ultrasonic delay lines, RP2453 209
Copolymer, styrene-acrylonitrile, dielectric relaxation during and after polymerization, RP2444 145
Corrosion, soil, of nickel cast irons, RP2459 313
Couette flow, small disturbances of plain, RP2451 195
Coughanour, L. W., V. A. DeProsse, Phase equilibria in the system MgO-TiO_2, RP2435 25
Crystallization effects in polybutadienes, RP2460 321

D

Darr, J. H., R. W. Mebs, J. D. Grimsley, Metal ultrasonic delay lines, RP2453 209
Degradation of polystyrene, using ultraviolet spectrophotometry, RP2445 155
Degradation, thermal, of tetrafluoroethylene and hydrofluoroethylene polymers in a vacuum, RP2461 327
DeJuren, J. A., H. Rosenwasser, Diffusion length of thermal neutrons in water, RP2452 203
Delay lines, metal ultrasonic, RP2453 209
DeLollis, N. J., P. Ehrlich, Dielectric relaxation in a styrene-acrylonitrile copolymer during and after its polymerization, RP2444 145
Denison, I. A., M. Romanoff, Corrosion of nickel cast irons in soils, RP2459 313
DeProsse, V. A., L. W. Coughanour, Phase equilibria in the system MgO-TiO_2, RP2435 85
Dielectric properties of Teflon, RP2449 185
Dielectric relaxation in a styrene-acrylonitrile copolymer during and after polymerization, RP2444 145
Differential equations, expansion method for parabolic, RP2441 127
Diffusion length of thermal neutrons in water, RP2452 203
Dirichlet problem, error of the difference analogue of, RP2463 343
Dynamic response computation, errors introduced by finite space and time increments in, RP2431 57

E

Ehrlich, P., Dielectric properties of Teflon from room temperature to 314° C and from frequencies of 10^2 to 10^5 c/s, RP2449 185
—, *N. J. DeLollis,* Dielectric relaxation in a styrene-acrylonitrile copolymer during and after its polymerization, RP2444 145
Eigenvectors of matrix polynomials, RP2429 33
Electron configuration of chromium, Cr I, RP2457 247
Entropy of tetrafluoroethylene, RP2432 69
Equations, nonlinear elliptic, solution, RP2455 229
Errors introduced by finite space and time increments in dynamic response computation, RP2431 57
Evans, D. N., A. Litvin, A. C. Figlia, R. L. Blaine, Properties of some masonry cement, RP2427 11

F

Fano, U., Penetration of X- and gamma rays to extremely great depths, RP2439 95
Figlia, A. C., D. N. Evans, A. Litvin, R. L. Blaine, Properties of some masonry cement, RP2427 11
Flieger, Jr., H. W., J. S. Wicklund, J. F. Masi, Heat capacity of gaseous hexafluoroethane, RP2437 91
Flynn, J. H., H. F. Launer, W. K. Wilson, Determination of glucose by means of sodium chlorite, RP2456 237
D-Fructose-1,6-C^{14}, preparation and radio assay of, RP2446 167
Frush, H. L., H. S. Isbell, Determination of carbon^{14} in the terminal positions of sugars: Preparation of D-arabinose-5-C^{14} from D-fructose-1,6-C^{14}, RP2446 167
—, —, Preparation of D-arabinose-1-C^{14} and D-ribose-1-C^{14}, RP2458 307
Furukawa, G. T., R. E. McCoskey, Calorimetric properties of 41° and 122° F polybutadienes, RP2460 321
—, —, *M. L. Reilly,* Heat capacity, heats of fusion and vaporization, and vapor pressure of tetrafluoroethylene, RP2432 69

G

Gamma rays and X-rays, penetration, RP2439 95
Glass, optical, system barium-oxide–boric-oxide–silica, RP2430 37
Glass, transformation in polybutadienes, RP2460 321
Glucose, determination by means of sodium chlorite, RP2456 237
Green, J. W., An expansion method for parabolic partial differential equations, RP2441 127
Grimsley, J. D., R. W. Mebs, J. H. Darr, Metal ultrasonic delay lines, RP2453 209

H

Haas, P. H., A radio-frequency permeameter, RP2454 221
Hammond, III, H. K., S. B. Newman, H. F. Piddell, Becker values of manila rope by photoelectric reflectometry, RP2443 141
Hart, V. E., S. L. Madorsky, S. Straus, V. A. Sedlak, Thermal degradation of tetrafluoroethylene and hydrofluoroethylene polymers in a vacuum, RP2461 327
Heat capacities of polybutadienes, RP2460 321
Heat capacity, heats of fusion and vaporization, and vapor pressure of tetrafluoroethylene, RP2432 69
Heat capacity of gaseous hexafluoroethane, RP2437 91
Heat of fusion, heat capacity, heat of vaporization and vapor pressure of tetrafluoroethylene, RP2432 69
Hexafluoroethane, gaseous, heat capacity, RP2437 91
Hydrated strontium silicates, preparation, RP2433 73
Hydrofluoroethylene and tetrafluoroethylene polymers, thermal degradation, RP2461 327
Hydrothermal preparation of some strontium silicates, RP2433 73
Hyperbolic equations, RP2441 127

I

Internal waves, characteristics, RP2442 133
Ionization potential of chromium, Cr I, RP2457 247
Isbell, H. S., H. L. Frush, Determination of carbon^{14} in the terminal positions of sugars: Preparation of D-arabinose-5-C^{14} from D-fructose-1,6-C^{14}, RP2446 167
—, —, Preparation of D-arabinose-1-C^{14} and D-ribose-1-C^{14}, RP2458 307

J

Johnson, A. E., An analogue computer for the solution of the radio refractive index equation, RP2462 335
Johnston, R., R. Stair, Ultraviolet spectral radiant energy reflected from the moon, RP2434 81

K

Karr, P. R., Effective circuit bandwidth for noise with a power-law spectrum, RP2438 93
Keulegan, G. H., Characteristics of internal solitary waves, RP2442 133
Kiess, C. C., Description and analysis of the first spectrum of chromium, Cr I, RP2457 247
Kroll, W. D., S. Levy, Errors introduced by finite space and time increments in dynamic response computation, RP2431 57

L

Launer, H. F., W. K. Wilson, J. H. Flynn, Determination of glucose by means of sodium chlorite, RP2456 237
Levin, E. M., G. M. Ugrinic, The system barium-oxide–boric-oxide–silica, RP2430 37
Levy, S., W. D. Kroll, Errors introduced by finite space and time increments in dynamic response computation, RP2431 57
Litvin, A., D. N. Evans, A. C. Figlia, R. L. Blaine, Properties of some masonry cement, RP2427 11

M

Page

Madorsky, S. L., V. E. Hart, S. Straus, V. A. Sedlak, Thermal degradation of tetrafluoroethylene and hydrofluoroethylene polymers in a vacuum, RP2461 327
Magnesia-silica-water system, studies at elevated temperatures and pressures, RP2448 179
Magnesia, solubility of, RP2448 179
Magnesium-oxide–titanium-dioxide system, phase equilibria, RP2435 85
Magnesium silicates, hydrothermal synthesis, RP2448 179
Mannes, M., Eigenvectors of matric polynomials, RP2429 33
Masi, J. F., J. S. Wicklund, H. W. Flieger, Jr., Heat capacity of gaseous hexafluoroethane, RP2437 91
Masonry cements, properties of some, RP2427 11
Matrices, pairs of normal, RP2436 89
McCoskey, R. E., G. T. Furukawa, Calorimetric properties of 41° and 122° F polybutadienes, RP2460 321
—, —, *M. L. Reilly*, Heat capacity, heats of fusion and vaporization, and vapor pressure of tetrafluoroethylene, RP2432 69
Mebs, R. W., J. H. Darr, J. D. Grimsley, Metal ultrasonic delay lines, RP2453 209
Metal powders, particle-size measurement by air elutriation, RP2428 17
Metal ultrasonic delay lines, RP2453 209
Micropotentiometer resistance elements, radio frequency, fabrication, RP2426 1
Moon, ultraviolet spectral radiant energy reflected from, RP2434 81

N

Neutrons in water, thermal, diffusion length, RP2452 203
Newman, S. B., H. K. Hammond, III, H. F. Riddell, Becker value of manila rope by photoelectric reflectometry, RP2443 141
Nickel cast irons, soil corrosion, RP2459 313
Noise with a power-law spectrum, effective circuit bandwidth for, RP2438 93
Numerical analysis:
RP2441 127
RP2451 195
RP2455 229
RP2463 343
Numerical analysis, matrices, RP2436 89

P

Pairs of normal matrices with property L, RP2436 89
Particle size of metal powders, measurement by air elutriation, RP2428 17
Penetration of X- and gamma rays to extremely great depths, RP2439 95
Peppler, P. B., E. T. Carlson, L. S. Wells, Studies in the system magnesia-silica-water at elevated temperatures and pressures, RP2448 179
Permeameter, radio-frequency, RP2454 221
pH of potassium tetroxalate solutions, RP2450 189
Phase equilibria in the system magnesium oxide–titanium dioxide, RP2435 85
Phase equilibrium, the system barium-oxide–boric-oxide–silica, RP2430 37
Pollard, F. E. Subsieve particle-size measurement of metal powders by air elutriation, RP2428 17
Polybutadienes, calorimetric properties, RP2460 321
Polymerization of styrene-acrylonitrile copolymer, dielectric relaxation, RP2444 145
Polymers, tetrafluoroethylene and hydrofluoroethylene, thermal degradation, RP2461 327
Polynomials, matric, eigenvectors of, RP2429 33
Polystyrene, degradation, determination by ultraviolet spectrophotometry, RP2445 155
Potassium tetroxalate, pH of, RP2450 189
Powders, metal, particle-size measurements, RP2428 17
Power-law spectrum, effective circuit bandwidth for noise with, RP2438 93
Pyrolysis of fluoroethylene polymers, RP2461 327

R

Radiant energy, ultraviolet spectral, reflected from the moon, RP2434 81
Radioactive sugars, synthesis, RP2458 307
Radioactivity of labeled sugars, determination, RP2446 167
Radio-frequency micropotentiometer resistance elements, fabrication, RP2426 1
Radio-frequency permeameter, RP2454 221
Radio-propagation, computer for calculating radio refractive index, RP2462 375
Radio refractive-index equation, analogue computer for solution of, RP2462 335
Reflectometry, photoelectric, determination of Becker value of manila rope by, RP2443 141
Refractive-index equation, radio, analogue computer for solution of, RP2462 335
Refractive index of cesium bromide for ultraviolet, visible, and infrared wavelengths, RP2440 123
Refractive index of the atmosphere, measurement with airborne microwave refractometer, RP2447 171
Refractometer, airborne microwave, measurement of refractive index of the atmosphere with, RP2447 171
Reilly, M. L., G. T. Furukawa, R. E. McCoskey, Heat capacity, heats of fusion and vaporization, and vapor pressure of tetrafluoroethylene, RP2432 69
Reiney, M. J., M. Tryon, B. G. Achhammer, Study of degradation of polystyrene, using ultraviolet spectrophotometry, RP2445 155
Resistance elements for radio-frequency micropotentiometer, fabrication, RP2426 1
D Ribose-1-C^{14} and D-arabinose-1-C^{14}, synthesis, RP2458 307
Riddell, H. F., S. B. Newman, H. K. Hammond, III, Becker value of manila rope by photoelectric reflectometry, RP2443 141
Rodney, W. S., R. J. Spindler, Refractive index of cesium bromide for ultraviolet, visible, and infrared wavelengths, RP2440 123
Romaneff, M., I. A. Denison, Corrosion of nickel cast irons in soils, RP2459 313
Rope, manila, determination of Becker value by photoelectric reflectometry, RP2443 141
Rosenwasser, H., J. A. DeJuren, Diffusion length of thermal neutrons in water, RP2452 203

S

Page

Sedlak, V. A., S. L. Madorsky, V. E. Hart, S. Straus, Thermal degradation of tetrafluoroethylene and hydrofluoroethylene polymers in a vacuum, RP2461 327
Silica-barium-oxide–boric-oxide, system, RP2430 37
Silica transport in aqueous vapor phase, RP2448 178
Size, particle, of metal powder, RP2428 17
Smith, E., V. E. Bower, R. G. Bates, pH of solutions of potassium tetroxalate from 0° to 60° C, RP2450 189
Sodium chlorite, determination of glucose by means of, RP2456 237
Soil corrosion of nickel cast irons, RP2459 313
Solitary waves, internal, characteristics, RP2442 133
Specific heat of gaseous hexafluoroethane, RP2437 91
Spectral radiant energy, ultraviolet, reflected from the moon, RP2434 81
Spectrophotometry, ultraviolet, study of degradation of polystyrene by, RP2445 155
Spectrum, first, of chromium, Cr I, RP2457 247
Spindler, R. J., W. S. Rodney, Refractive index of cesium bromide for ultraviolet, visible, and infrared wavelengths, RP2440 123
Stair, R., R. Johnston, Ultraviolet spectral radiant energy reflected from the moon, RP2434 81
Standards for pH, tetroxalate, RP2450 189
Straus, S., S. L. Madorsky, V. E. Hart, V. A. Sedlak, Thermal degradation of tetrafluoroethylene and hydrofluoroethylene polymers in a vacuum, RP2461 327
Stront'um silicates, formation and X-ray diffraction patterns, RP2433 73
Styrene-acrylonitrile copolymer, dielectric relaxation during and after polymerization, RP2444 145
Sugars, determination of carbon 14 in terminal positions of, RP2446 167
Sugars, position-labeled with carbon 14, RP2458 307
System barium-oxide–boric-oxide–silica, RP2430 37
System magnesia-silica-water at elevated temperatures and pressures, studies of, RP2448 179
System magnesium oxide–titanium dioxide, phase equilibria, RP2435 85

T

Teflon, dielectric properties, RP2449 185
Tetrafluoroethylene and hydrofluoroethylene polymers, thermal degradation, RP2461 327
Tetrafluoroethylene, heat capacity, heats of fusion and vaporization and vapor pressure, RP2432 69
Tetroxalate buffers, pH of, RP2450 189
Thermal degradation of tetrafluoroethylene and hydrofluoroethylene polymers in a vacuum, RP2461 327
Titanium dioxide–magnesium oxide, phase equilibria, RP2435 85
Tryon, M., M. J. Reiney, B. G. Achhammer, Study of degradation of polystyrene, using ultraviolet spectrophometry, RP2445 155

U

Ugrinic, G. M., E. M. Levin, The system barium-oxide–boric-oxide–silica, RP2430 37
Ultrasonic delay lines, metal, RP2453 209
Ultraviolet spectral radiant energy reflected from the moon, RP2434 81
Ultraviolet spectrophotometry, study of degradation of polystyrene by, RP2445 155
Ultraviolet, visible, and infrared wavelengths, refractive index of cesium bromide for, RP2440 123

V

Vapor pressure, heat capacity, and heats of fusion and vaporization of tetrafluoroethylene, RP2432 69

W

Walsh, J. L., D. Young, On the accuracy of the numerical solution of the Dirichlet problem by finite differences, RP2463 343
Wasow, W., On small disturbances of plane Couette flow, RP2451 195
Water, thermal neutrons in, diffusion length of, RP2452 203
Wavelengths and estimated intensities of chromium, Cr I, RP2457 247
Wavelength's, ultraviolet, visible, and infrared, refractive index of cesium bromide for, RP2440 123
Waves, internal solitary, characteristics, RP2442 133
Wells, L. S., E. T. Carlson, Hydrothermal preparation of some strontium silicates, RP2433 73
—, —, *R. B. Peppler*, Studies in the system magnesia-silica-water at elevated temperatures and pressures, RP2448 179
Wicklund, J. S., H. W. Flieger, Jr., F. Masi, Heat capacity of gaseous hexafluoroethane, RP2437 91
Wielandt, H. W., Pairs of normal matrices with property L, RP2436 89
Wilson, W. K., H. F. Launer, J. H. Flynn, Determination of glucose by means of sodium chlorite, RP2456 237

X

X-ray diffraction patterns of strontium silicate hydrates, RP2433 73
X-rays and gamma rays, penetration, RP2439 95

Y

Young, D., J. L. Walsh, On the accuracy of the numerical solution of the Dirichlet problem by finite differences, RP2463 343

Z

Zeeman effect of chromium, Cr I, RP2457 247

U. S. GOVERNMENT PRINTING OFFICE: 1954

UNITED STATES
GOVERNMENT PRINTING OFFICE
DIVISION OF PUBLIC DOCUMENTS
WASHINGTON 25, D. C.
OFFICIAL BUSINESS

UNIVERSITY OF MICHIGAN
GENERAL LIBRARY
DOCUMENTS DIVISION
1276 ANN ARBOR MICH

Journal of Research of the National Bureau of Standards Vol. 51, No. 6 December 195

Contents

		Page
Preparation of D-arabinose-1-C^{14} and D-ribose-1-C^{14}. Harriet L. Frush and Horace S. Isbell.	RP2458	307
Corrosion of nickel cast irons in soils. Irving A. Denison and Melvin Romanoff.	RP2459	313
Calorimetric properties of 41° and 122° F Polybutadienes. George T. Furukawa and Robert E. McCoskey.	RP2460	321
Thermal degradation of tetrafluoroethylene and hydrofluoroethylene polymers in a vacuum. S. L. Madorsky, V. E. Hart, S. Straus, and V. A. Sedlak.	RP2461	327
An analogue computer for the solution of the radio refractive-index equation. Walter E. Johnson.	RP2462	335
On the accuracy of the numerical solution of the Dirichlet problem by finite differences. J. L. Walsh and David Young.	RP2463	343

Single copies of the above Research Papers are not available for sale, but the Superintendent of Documents, U. S. Government Printing Office, Washington 25, D. C., will reprint 100 or more copies, and request for the purchase price should be mailed promptly to that Office.

For sale by the Superintendent of Documents, U. S. Government Printing Office, Washington 25, D. C. Price 60 cents (single copy). Subscription Price: $5.50 a year; $1.25 additional for foreign mailings. Single copies vary in price.

UNITED STATES GOVERNMENT PRINTING OFFICE, WASHINGTON : 1953